UNIVERSIDADE DA BEIRA INTERIOR
Engenharia

Robust H_∞ Control for Rendezvous in Near-Circular Orbit

Pedro Henrique Oliveira Barros

Dissertação para obtenção do Grau de Mestre em
Engenharia Aeronáutica
(ciclo de estudos integrado)

Orientador: Prof. Doutor Kouamana Bousson

Covilhã, outubro de 2018

Acknowledgements

It is with a pleasant feeling that i thank Prof. Doutor Kouamana Bousson for agreeing to be my research supervisor and for proposing the present problem to me. His efforts towards the completion of this work, from the numerous discussions, guidance and counsel to the final proof-reading are gratefully acknowledged.
A special heartfelt thanks to all my friends, my lab co-workers, and everyone else that in some way influenced me in this period of strife and ordeal. All the support was greatly appreciated.

Resumo

Rendezvous em órbita representa um encontro previamente meditado entre dois veiculos espaciais que se encontra a orbitrar um corpo celestial. A tecnologia que permita a aplicação de rendezvous em órbitra para realizar montagens, manutenção ou troca de tripulação serve de exemplo para demonstrar a importância de rendezvous em orbita para continuar com uma presença forte na exploração espacial.
O foco principal desta dissertação encontra-se em desenvolver um controlador robusto para obter rendezvous óptimo entre um veículo espacial activo, denominado como o "chaser", capaz de realizar as manobras necessárias para ir de encontro ao veiculo espacial passivo, denominado como o "target", que se assume estar num estado de "thrust-free".
Todos os resultados obtidos recorrem ao algoritmo de quinta ordem de Runge-Kutta para simular o modelo dinâmico que descreve o movimento relativo entre os dois veículos espaciais diferentes, num sistema de coordenadas orbitais centrado no veiculo espacial denominado de "target", em que são aplicados parámetros de incertezas para descrever com maior precisão um órbitra quase circular com pequena excentricidade. Para além disso, foi aplicado um controlador linear quadrático regulador e um controlador H_∞ em todos os casos de estudo para guiar e garantir que o veiculo espacial denominado como "chaser" convergia assimptoticamente até se encontrar com o veiculo espacial denominado como "target" com posição e velocidade relativa aproximadamente igual a zero.
O controlador robusto H_∞ apresenta melhores resultados, quando comparado com o controlador linear quadrático regulador, para resolver problemas na presença de parametros de incerteza e perturbações. Esta disparidade entre o comportamento apresentados pelos dois controladores é agravada consoante o crescimento da distância incial entre os dois veículos espaciais, em que o controlador robusto H_∞ sendo o controlador mais adequado para o problema de rendezvous em órbitra.
Os resultados presentes na dissertação actual indicam que o controlador H_∞ é o mais apropriado para guiar e orientar o veículo espacial denominado como "chaser" na realização de rendezvous em órbitra com um veículo espacial denominado como "target". O uso deste controlador pode, potencialmente, levar a obter rendezvous num espaço de tempo mais curto, com menor consumo de combustível e menos risco de saturação dos atuadores para problemas de rendezvous em órbita sujeito a perturbações e incertezas.

Palavras-chave

Rendezvous em órbita; Optimização; Órbita quase circular; Controlador H_∞

Abstract

Orbital Rendezvous entails a pre-arranged meeting between two spacecraft orbiting around a celestial body. A technology that enables its application in assembly, maintenance and crew exchange serve as example of the importance of orbital rendezvous towards maintaining a stronghold and sustained presence in space exploration. The main focus of this dissertation leans towards the development of a robust controller for optimal rendezvous between an active spacecraft, designated as the chaser, capable of performing any necessary manoeuvres to reach a passive spacecraft, known as the target, that is assumed to thrust-free.
All results are obtained resorting to the fifth-order Runge-Kutta algorithm to simulate the dynamic model, describing the relative motion between the two different spacecraft on a target-centred orbital coordinate system, employing uncertain parameters to more accurately describe a near-circular orbit with small eccentricity. Furthermore, the linear quadratic regulator controller as well as the H_∞ controller are employed for all examples to guide and guarantee that the chaser spacecraft asymptotically converge to the target spacecraft with relative position and velocity equal to zero.
The robust H_∞ controller presents overall better results when compared to the linear quadratic regulator controller for problems in the presence of uncertain parameters and disturbances. This behaviour disparity displayed when comparing both controllers become more apparent as the initial distance between the chaser and target spacecraft increases with the H_∞ controller responding better to the orbital rendezvous problem.
The results portrayed in the present dissertation indicate that the H_∞ controller is appropriate to guide and orient a chaser spacecraft when performing rendezvous with a target spacecraft. Also, the use of this controller could potentially lead to smaller rendezvous time, less fuel usage and less risk from actuators saturation when the rendezvous is subject to disturbances and uncertain parameters.

Keywords

Orbital Rendezvous; Optimal; Near-circular orbit; H_∞ controller

Contents

List of Figures

List of Tables

Nomenclature

Symbols	Description	System of Units
Δ	Controllability matrix	$[-]$
ΔA	Uncertain matrix	$[-]$
Θ	Observability matrix	$[-]$
η	Control input in the absence of feedback	$[-]$
μ	Gravitational parameter	$[m^3 \cdot s^{-2}]$
π	Pi	$[-]$
γ	Disturbance attenuation	$[-]$
A	State matrix	$[-]$
B	Control matrix	$[-]$
C	Output matrix	$[-]$
D	Disturbance matrix	$[-]$
E	Eccentric anomaly	$[Rad]$
F	Control input force	$[N]$
G	Universal Gravitational Constant	$[m \cdot Kg^{-1} \cdot s^{-2}]$
J	Quadratic performance index	$[-]$
K	Feedback gain matrix	$[-]$
L	Quadratic function	$[-]$
L	Gramian	$[-]$
M	Mean anomaly	$[Rad]$
P	Algebraic Ricatti equation solution	$[-]$
P	Periapsis	$[Km]$
Q	State weighting matrix	$[-]$
R	Control weighting matrix	$[-]$
Re	Real part	$[-]$
T	Time of rendezvous	$[-]$
$\|T\|_\infty$	Closed-loop transfer function	$[-]$
U	Input Constraint	$[-]$
V	Lyapunov's function	$[-]$
a	Thrust acceleration	$[m \cdot s^{-2}]$
a	Apogee	$[Km]$
c	Chord	$[m]$
dt	Time step	$[s]$
e	Eccentricity	$[-]$
k	Feedback gain vector	$[-]$
m	Mass	$[Kg]$
n	Mean motion	$[rad \cdot s^{-1}]$
r	Position along a keplerian orbit	$[m]$
$\ddot{r}$	Vetor acceleration of the mass measured	$[m \cdot s^{-2}]$
t	Time	$[s]$
$u(t)$	Control input vector	$[-]$
v	Separation velocity	$[m \cdot s^{-1}]$

Symbols	Description	System of Units
$\dot{v}$	Separation acceleration	$[m \cdot s^{-2}]$
w	Disturbance vector	$[-]$
$x(t)$	State vector	$[-]$
$\dot{x(t)}$	State differential equation	$[-]$
$y(t)$	Output variable	$[-]$
x, y, z	Relative position components	$[m]$
$\dot{x}$, $\dot{y}$, $\dot{z}$	Relative velocity components	$[m \cdot s^{-1}]$
$\ddot{x}$, $\ddot{y}$, $\ddot{z}$	Relative acceleration components	$[m \cdot s^{-2}]$

Subscripts

0	Initial
1	Random point along a keplerian orbit
2	Random point along a keplerian orbit
c	Controllability
f	Final
g	Gravitational
max	Maximum
min	Minimum
o	Observability
p	Periapsis
x	Component along the x-axis
y	Component along the y-axis
z	Component along the z-axis

List of Acronyms

ARE	Algebraic Ricatti Equation
ASTRO	Autonomous Space Transport Robotic Operations
ATV	Automated Transfer Vehicle
C-W	Clohessy-Wiltshire equations
DART	Demonstration of Autonomous Rendezvous Technology
ESA	European Space Agency
ETS-VII	Engineering Test Satellite VII
HTV	H-II Transfer Vehicle
ISS	International Space Station
LEO	Low Earth Orbits
LQE	Linear Quadratic Estimator
LQG	Linear Quadratic Gaussian
LQR	Linear Quadratic Regulator
LVLH	Local Vertical, Local Horizontal
MIMO	Multi Input Multi Output
ODE	Ordinary Differential Equation
PID	Proportional Integral Derivative
RODC	Rendezvous Orbital Dynamics and Control
RVD	Rendezvous and Docking Technology
SDM	Sliding Mode Control
SISO	Single Input Single Output
XSS-11	Experimental Satellite System-11

Chapter 1

Introduction

Space exploration has been a dream of humanity for the paste century with men trying to soar through the skies and conquer space.
Beginning with Gemini, we started to take definitive steps towards this shared dream, proving that it is indeed possible to explore beyond the Planet Earth and discover the unknown. Decades of study and implementation of numerous space programs began to take place all over the world. Starting with the Gemini and Apollo programs which developed the initial concepts for rendezvous and docking technology (RVD), followed by the space shuttle that demonstrated that these capabilities can be performed for various Low Earth Orbits (LEO) missions, as well as recent programs such as Experimental Satellite System-11 (XSS-11), Demonstration of Autonomous Rendezvous Technology (DART), Autonomous Space Transport Robotic Operations(ASTRO) from the United States of America, the Soyus and Progress spacecraft from Russia or the former Soviet Union, the Automated Transfer Vehicle (ATV) from the European Space Agency (ESA), the Engineering Test Satellite VII (ETS-VII) and H-II Transfer Vehicle (HTV) from Japan, the Shenzou spaceship from China and the most recent Orion program, all led to one very important conclusion. All these programmes have relied heavily on Rendezvous Orbital Dynamics and Control (RODC) as a key technology of RVD , with more than half a century of study and research, and yet, it is still a long way to go until it becomes a completely autonomous and human independent procedure. A completely autonomous and human independent procedure refers to having the capacity of planning the trajectory and generating guidance commands to be performed live and on-board without requiring a large operational burden on the flight crew and ground operators, which would lead to an increase in the probability of success and also, more safety, more security, less human risk involved and more overall control of the mission as well as many other benefits.
The International Space Station (ISS) program, a joint project among five participating space agencies, in particular, the National Aeronautics Space Station (NASA), the Roscosmos State Corporation for space activities, the Japan Aerospace Exploration Agency (JAXA), the ESA and the Canadian Space Agency (CSA), is one of the main beneficiaries form RODC demonstrating the common desire to develop this technology and the many benefits to be obtained from it. Fig.1.1 shows an illustrated picture of the ISS.
This artificial satellite had its first component launched into space in 1998 and has since then been a part of many missions involving procedures such as crew exchange, spacecraft intercepting, repairing and maintenance, saving, docking, large scale structure assembling and satellite networking. All these procedures are dependent on RODC. As a primary factor which determines the success of the mission, rendezvous has been and remains to be an important area of research. A large structure such as this one requires constant maintenance in order to sustain activity, using materials transported from Earth, which means that subsequent visits will continue to be performed as to transport equipment, astronauts, scientists and their support systems and other eventualities. Eugene I. Butikov [1] considered and compared several possibilities to launch a space vehicle from the orbital space station and investigated the relative motion of orbiting bodies as examples of spacecraft rendezvous with the ISS which stays in a

near circular orbit around the Earth. With plans to continue fully operational in the years to

Figure 1.1: International Space Station

come, we can expect that the interest and demand for research and development in this field of study will be maintained with the possibility to grow even further.
Howard Hu and Tim Straube [2] provided an overview of the Orion guidance, navigation and control system, its functional capabilities in the context of constellation architecture and its plans for the future. This and many other programmes incited the development of RODC as a key technology with high importance and demand for improvements and new ideas to solve the many issues that have become known in the early space programmes.
With sights set on the future, several researchers studied the past in order to search for answers to current dilemmas and issues. Douglas Zimpfer [3] provided a technical and historical perspective on autonomous rendezvous and capture missions, from the earlier programmes until 2005 as well as the needs for the future exploration missions, presenting an overview for autonomous rendezvous technology future requirements, Luo Yazhong [4] surveyed several studies on RODC, evaluating the relative dynamics equations, studies on rendezvous trajectory optimization and relative navigation and, most recently, Christopher D'Souza [5] described the design and analysis which has been performed to date to allow a space vehicle to perform its mission, addressing each of its problems and requirements.

1.1 Orbital Rendezvous and Operation

Orbital Rendezvous refers to a sequence of manoeuvres between two space vehicles, a chaser spacecraft and a target spacecraft, to meet in space and time. This means that in some instant in time, the relative position and velocity between the chaser and the target spacecraft will be approximately zero. Such a meeting is provided by the spacecraft thrusters, the chaser

being denominated as ”active” and the target as ”passive”, in the case that the target does not use the thrusters, and as ”active” in the opposite case. The case study with relation to this dissertation represent rendezvous in space where only the chaser spacecraft performs the required manoeuvres to encounter the target spacecraft.

Most space exploration missions apply a rendezvous and docking process. This can be further divided in several different phases. The first phase being the launch where the spacecraft is sent to space, followed by the phasing phase with the chaser executing several manoeuvres under guidance from the ground telemetry tracking and command network until the chaser navigation sensors manage to lock the target. This phase typically ends when the phase angle between the two spacecraft is adjusted, reducing the orbital plane differences, increasing orbital height and initiating the relative navigation.

The next phase is the homing phase. In this phase, the chaser has autonomous control performing the required manoeuvres until the chaser arrives to a station-keeping point located a couple of kilometres away from the target, whilst acquiring the target orbit.

The closing phase together with the homing phase represent what is known as Close-Range Rendezvous. Here the chaser reduces the relative distance to the target to a location a few hundred of meters away.

Lastly, the final approach end with the chaser arriving to its intended destination whilst approaching the target along a straight line as much as possible, in order to satisfy the docking requirements of relative position, velocity, attitude and angular rate. All these procedures are represented in Figure 1.2

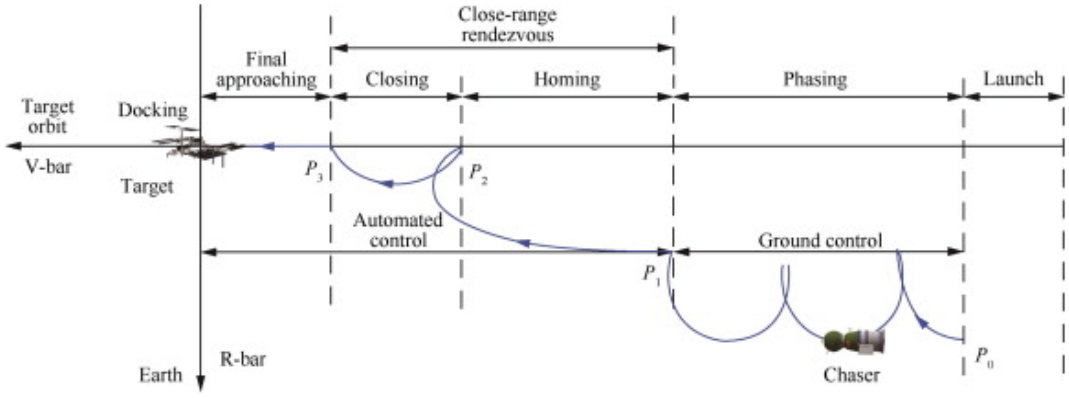

Figure 1.2: Spacecraft Rendezvous and Docking process [4].

1.2 Guidance and Control

Successful Rendezvous is a precondition of many astronautic missions involving more than one spacecraft. However, to this day, successful rendezvous remains a challenge. Behind each space exploration mission, there are always many interests and resources invested from several entities, being the success of each mission crucial, and so, since the Apollo Lunar program of 1960, many studies were performed to ensure the success of every implemented program.

Although there are many benefits to be obtained from a circular orbit, the reality is that it is nearly impossible to achieve and maintain throughout the course of the entire mission. This resulted in the early studies on this subject to be relevant only to closed-range rendezvous, where the target orbit has a small but non-zero eccentricity, as can be seen in the work of Oscar

W. Olszewski [6] where he proposed an automated, terminal guidance algorithm for a shuttle to rendezvous with the space station from mid course through docking.
Later, Zhanhua Ma [7] presented an optimal control strategy for a servicing spacecraft to perform rendezvous in close range with a tumbling satellite by applying Pontryagin's maximum principle to generate near-optimal trajectories of proximity manoeuvres of a chaser spacecraft required to dock a target, with predetermined thrust history along a master direction. R. Bevilacqua [8] also applied Pontryagin's maximum principle for rapid generation of combined time-propellant near-optimal trajectories of proximity manoeuvres of a chaser spacecraft required to dock a target one, with a predetermined thrust history along a master direction. This new direct method was based on high-order polynomials as reference functions, pre-set on-off sequence of a master control, and reduction of the optimization problem to the determination of a small set of parameters.
The trend between these different approaches is to achieve a simple, with quick response and ease of mechanization guidance scheme for it to be feasible to apply when there are limitations of hardware and available time to complete manoeuvres. However, these methods do not attempt to address issues relating to optimization of fuel consumption during rendezvous, which means that they only have practical utility during the close-range rendezvous phase due to the fact that having a quick response and manoeuvrability takes precedence to fuel cost in these specific situations.
This situation changed in 2005 when NASA initiated the DART program which, unfortunately, experienced some failures due to fuel shortage, inaccurate position and velocity readings leading to a premature ending without meeting more than half of the predefined mission objectives.
From this point onwards, fuel expenditure was no longer ignored, with special attention being given for long distance and duration rendezvous. A. Miele [9, 10] employed several numerical investigations of the thrust function required to minimize either the time, the fuel required or both for the terminal phase of the rendezvous between two spacecraft in a planar circular orbit by applying either a single or multiple sub-arc sequential gradient restoration algorithm to generate the guidance trajectory. Denis Arzelier [11] also developed a numerical approach that focuses on the fixed-time minimum-fuel rendezvous between close elliptic orbits of an active spacecraft and a passive spacecraft, assuming linear impulsive setting and a keplerian relative motion.
As the linear relative dynamic equations, used to represent the relative motion between two spacecraft, is in most cases described by the Clohessy-Wiltshire (C-W) or Hill equations, these are only precise enough for perfect circular orbits and do not take into consideration external factors like J_2 perturbations, aerodynamic drag and Earth oblateness.
Many authors tried to solve this issue, using several different methods, in order to achieve acceptable results. Jong-Uk Park [12] introduced a two-step sliding mode control method, in the presence of the Earth's gravitational perturbation, to solve the rendezvous problem with finite-thrust, including unmodeled dynamics. Christian Tournes [13] proposed a second order sliding mode control. By including second order terms, he made it possible to improve the precision of the relative dynamics, providing a quasi-optimal robust solution to the automatic space rendezvous and docking problem. Gang Zhang and Di Zhou [14] also presented a new second order solution to the two point boundary value problem for relative motion about orbital rendezvous using nonlinear differential equations to describe the relative motion, considering J_2 perturbation effects in the state transition equations and later Gang Zhang [15] studied the tangent-impulse coplanar orbit rendezvous problem based on linear relative motion for J_2 perturbed elliptic orbits.

A different method was devised by Mathieu Claeys [16] to find lower bounds on large class nonlinear optimal control problems with impulsive controls using semi-definite programming, by relaxing an optimal control problem into a measure differential problem, and, recently, Joshua Sullivan [17] introduced a new strategy to improve angle-only relative navigation for distributed space systems by utilizing a rigorous state comparison and an observability assessment conducted to provide new insight into the benefits gained from improved dynamic and measurement modelling. This work describes a new method to derive J_2 perturbed state transition matrix in mean quasi-nonsingular relative orbit elements.
By then, autonomous rendezvous became a well known problem with many parameters that need control and optimization, which led to studies to achieve rendezvous whilst being efficient and robust. Daero Lee and Henry Pernicka [18] proposed an optimal control technique for determining translational and rotational manoeuvres to facilitate proximity operations and docking using either a state dependent Riccati equation formulated from nonlinear relative motion dynamics or a linear quadratic equation formulated from linearised relative motion equations as a tracking controller, Ping Lu and Xinfu Lu [19] presented an algorithmic procedure to achieve autonomous rendezvous and proximity operations, formulated as a nonlinear optimal control problem subject to various state and control inequality constraints and equality constraints on interior and terminal points, with the capacity to plan onboard and execute highly constrained trajectories between two different spacecraft without ground support. Jin Zhang and Geoffrey Parks [20] developed a multi objective algorithm for multiphase orbital rendezvous mission's analysis.

1.2.1 Rendezvous Robust Control

It is to our benefit to take information from noise and an uncertain macrocosm, conventing such observations into useful knowledge about a process of our interest. Following that, comes the task of controlling a fundamental uncooperative world to do our bidding. These two perspectives of interchange are core fundamentals of modern automatic control as the dual notions of estimation theory and control theory.
As man faced new challenges, new approaches were made to achieve progress in new projects. From the general theory of systems advent of mass communication and the telephones long lines and the classical theory of control, developed to control gunnery, aircraft and missile systems during the world wars, came the modern theory of control systems to handle the appearance of satellites and aerospace systems. The frequency domain approach that had been suitable so far no longer was capable to control advanced non-linear multi-variable systems that were arising in aerospace applications. So came the need to resort to differential equation techniques couched in the time domain.
Orbital rendezvous and docking is, in essence, a planned collision between two spacecraft. As such, the presence of trajectory errors might deviate the chaser from the planned trajectory leading to a serious accident if the two spacecraft, which are planned to approach each other, suddenly collide out of the docking point with a high relative velocity. Through the years, many attempts were made to increase trajectory safety and robustness, as a critical factor in rendezvous missions.
The earlier orbital rendezvous missions, often relied on the solution of the two-point, boundary-value problem, commonly known as Lambert's problem, one of the remarkable theorems in astrodynamics, to act as a passive control in order to solve orbital transfers and rendezvous problems in astrodynamics. This method is concerned with the determination of an orbit from

two position vectors and the time of flight, determining a preliminary orbit prior to the mission. Lambert's problem [21, 22, 23] states that the time of flight, t, to travel along a keplerian orbit from r_1 to r_2 is only a function of the orbit semi-major axis, a, of the sum $r_1 + r_2$ and of the chord c of the triangle having r_1 and r_2 as sides. The eccentric anomaly E is defined via the corresponding Sundmann transformation $rdE = ndt$ and the mean motion through $n = \sqrt{\frac{\mu}{a^3}}$, where μ is the gravitational parameter and a is the apogee. The following relation is then valid for an elliptic orbit ($a > 0$):

$$r = a(1 - e \cdot cosE) \quad \textbf{(1.1)}$$

Equation 1.1 is valid along a Keplerian orbit, including r_1 and r_2 and the time of flight can thus be written as:

$$\sqrt{\mu}(t_2 - t_1) = a^{\frac{3}{2}}(E_2 - E_1 + e \cdot cosE_1 - e \cdot cosE_2 + 2M\pi) \quad \textbf{(1.2)}$$

where e is the orbit eccentricity and $M = \tilde{M}_2 - \tilde{M}_1$ is the number of complete revolutions performed during the transfer from r_1 to r_2.

This passive control method benefited from allowing rendezvous to be performed for all kinds of orbital rendezvous, namely rendezvous performed in elliptic and hyperbolic orbits. However, this method was not capable to deal with the presence of perturbations and uncertainties.

The purpose of obtaining more robust controllers led to the study and application of active controllers with the Sliding Mode Control (SDM) method [12, 24] as an example of the earlier attempts at robust active control. This method is a type of variable structure control utilizing a high-speed switching control law to drive a non-linear system state trajectory onto a user-chosen surface, know as the sliding surface, allowing for system parameter uncertainty and unmodeled dynamics.

The H_∞ control method is another approach to robust active control that appeared in the second half of the 20^{th} century that promised to solve these issues but did not see much action due to the technology limitations of the time. Nowadays, the risk of saturation of the actuators and sensors has decreased significantly, leading to the possibility of the H_∞ control method to be applied in the newer programs.

Pramod P. Khargonekar [25] studied a H_∞ control problem, where the measured outputs are the states of the plant, to compare the infimum of the norm of the closed-loop transfer function using linear state-feedback with the infimum norm of the closed-loop transfer function over all stabillizing dynamic state feedback controllers and later [26] offered a solution to the quadratic stabilization problem with uncertainty between the state and input matrices given, exploring the relations between robust stabilization problems and H_∞ control theory. Yeih J. Wang and Leang S. Shieh [27] presented a simple, flexible method for designing full-order observer-based robust H_∞ control laws for linear systems with structured parameter uncertainty, obtaining it by solving three augmented algebraic Riccati equations to provide both robust stability and disturbance attenuation with H_∞ norm bound for the closed-loop uncertain linear system .

Recently, studies have been developed where researchers have tried to solve the rendezvous problem by applying these control laws. Huijun Gao [28] investigated the problem of robust H_∞ control for a class of spacecraft rendezvous systems based on the relative motion dynamic model illustrated by C-W equations, which contain parametric uncertainties, external disturbances and input constraints, and design a H_∞ state-feedback controller via a Lyapunov approach, which guarantees the closed-loop system to meet the multi-objective design requirements, followed

by Neng Wan's work [29] where he proposes an observer based robust guaranteed cost control method for thrust-limited rendezvous in near circular orbits, treating the non-circularity of the target as a parametric uncertainty and adopting a linearised model derived from the two body problem as the controlled plant.

1.3 Focus of the Dissertation

An inspection of the most recent developments in the field of Rendezvous Orbital Dynamics and Control displays what appears to be an emerging trend towards the development of robust controllers. These controllers have a central dogma to guarantee that the chaser spacecraft goes through a predefined trajectory until it finds the target spacecraft.

The present dissertation seeks to propose a robust controller with state-feedback for optimal rendezvous between two different spacecraft in a near-circular orbit around the planet Earth. As the chaser and the target spacecraft are in relatively close proximity during the rendezvous, a linearised Clohessy-Wiltshire equation model of motion with the addition of uncertain parameters is employed, assuming that the target orbit has low eccentricity. For reasons of fuel consumption and time limiter, two different controllers, applying a state feedback system, are developed and compared, a linear quadratic regulator and a H_∞ controller, with each performance evaluated. Butcher's method is implemented to estimate the state in an initial value problem.

A brief description of the organization of the present dissertation is presented next.

1.4 Layout of the Dissertation

This dissertation is divided in a total of five chapters in order to provide a better reading and comprehension of the contents described and explained to the reader.

The current chapter presents an introduction of the rendezvous and orbital dynamics control problem. The main motivators to the pursue of the thematic by different entities is shown and an overall review of the many studies and projects performed, as well as, the most relevant theorems and methods developed are revealed. The focus of the present thesis is also briefly displayed.

Chapter 2 describes the motion model used to describe the rendezvous performed between the two spacecraft, introducing a brief explanation of the Clohessy-Whiltshire equations followed by a description of uncertain parameters.

Chapter 3 studies the properties of a linear system, describing the main concerns when devising a controller. A state feedback system is introduced and its core properties are described, and its benefits to the present thesis are presented. This is followed by the description of two optimal controllers, the linear quadratic regulator and the H_∞ and its main properties are exposed and explained in the context of the present thesis.

Chapter 4 is composed of all simulations performed together with an analysis of the results. The results are discussed with rendezvous problem in consideration.

Chapter 5 is composed of the principal remarks and conclusions relating to the present, followed by suggestions for further development to complement the work presented in the current dissertation.

Lastly, some appendix containing relevant information are presented to complement the information that is described in the previous chapters.

Chapter 2

Dynamic Model

From dozens of kilometres in Earth's atmosphere to hundreds and thousands of kilometres in outer space, two different situations can occur. Either the relative distance between the two spacecraft is considerably large and in this case their movements can be described in a planet-centred coordinate system, or both spacecraft are close to each other, allowing the relative motion to be presented in a target-centred orbital coordinate system.
In the later, the coordinate system used is of the LVLH type (local vertical, local horizontal), located in the target's center of mass, with the x-axis, also known as R-bar, being directed radially outward along the local vertical, the y-axis, also called V-bar, along the direction of motion or velocity direction and the z-axis normal to the reference orbit plane and completes the right-handed system as can be seen in Fig.2.1.

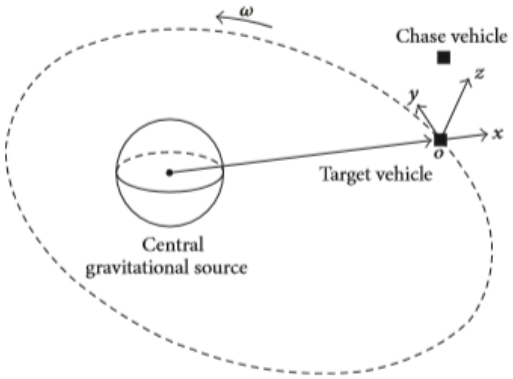

Figure 2.1: Relative cartesian coordinate system for spacecraft rendezvous (LVLH type) [29].

2.1 Clohessy-Whiltshire equations

The fundamentals of astrodynamics known today stand on the work done by Newton and Kepler. Through Kepler's and Newton's law it was possible to understand the physics behind deeply complex phenomenons, namely orbital rendezvous.
Kepler three laws, that are now know as the Kepler's Laws that marked an epoch in the history of mathematical science, describe the orbit of each planet as an ellipse, with a sun at a focus; the line joining the planet to the sun sweeps out equal areas at equal times; and the square of the period of a planet is proportional to the cube of its mean distance from the sun [30, 31].
Newton was then capable to derive important physical laws based on Kepler's earlier description of the orbits motion, and as such came Newton's second law that can be expressed mathematically as follows [30, 31]:

$$\sum F = m \cdot \ddot{r} \quad (2.1)$$

where $\sum F$ is the vector sum of all forces acting on the mass, m, and $\ddot{r}$ is the vetor acceleration of the mass measured in figure 2.2. Newton also stated that any two bodies attract one another

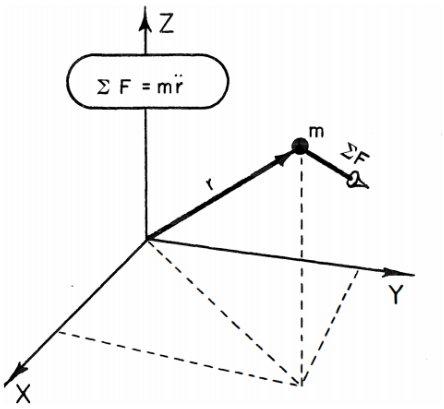

Figure 2.2: Newton's Law of Motion [30].

with a force proportional to the product of their masses and inversely proportional to the square distance between them as seen in the next equation [30, 31].

$$F_g = -\frac{GMm}{r^2} \cdot \frac{\mathbf{r}}{r} \quad (2.2)$$

where F_g is the force on mass m due to mass M and **r** is the vector from M to m. G is the universal gravitational constant.

Clohessy and Whiltshire could later developed a set of linear dynamic equations, based on Kepler's and the Gravitational Law, to effectively describe the relative motion between two different spacecraft as presented below [32]:

$$\begin{cases} \ddot{x} - 2n\dot{y} - 3n^2x = a_x \\ \ddot{y} + 2n\dot{x} = a_y \\ \ddot{z} + n^2z = a_z \end{cases} \quad (2.3)$$

where x, y and z represent the relative position components, the $\dot{x}$, $\dot{y}$ and $\dot{z}$ compose the relative velocity components and the $\ddot{x}$, $\ddot{y}$ and $\ddot{z}$ are the components of the relative acceleration; n is the mean motion of the target vehicle and $a_i(i = x, y, z)$ is the i^{th} component of the thrusts acceleration components on the directions described in figure 2.2.

The thrusts components might also go as follows:

$$\begin{cases} a_x = \frac{1}{m}F_x \\ a_y = \frac{1}{m}F_y \\ a_z = \frac{1}{m}F_z \end{cases} \quad (2.4)$$

with m being the mass of the chaser and $F_i(i = x, y, z)$ being the i^{th} component of the control input force acting on the relative motion dynamics.

This set of equations, also referred as C-W or Hill equations, has a closed-form analytical solution, thus allowing the relative motion to be divided in two different and independent parts, the first being the in-plane motion (the x-y plane) and the second being the out-of-plane motion (the z direction), which means that only the motions of x and y are coupled with each other.

In the event that the control forces disappear, the out-of-plane trajectory behaves as a trigonometric function, meaning that the in-plane trajectory closely relates to its initial state. These equations proved to be a great asset in many programmes and studies even though it assumed that the two spacecraft performed the rendezvous on neighbouring circular orbits, where the relative distance between each other was much shorter then the spacecraft's geocentric distance, as well as the fact that orbital perturbations, eccentricity as well as second and higher order terms of relative position and velocities were all ignored. All these assumptions did not permit to accurately represent the relative motion of both spacecraft performing rendezvous, which meant that they could only be used for relative trajectories with close distance and short time duration with zero eccentricity.

2.2 Relative dynamics equations with uncertain parameters

The majority of control designs are based on the use of a design model and the relation between these models and the reality they represent is subtle and incredibly complex. Usually, a mathematical model is devised to provide a relation between the inputs and its responses with the quality of the model being dependent from how closely its responses match the reality of the physical system. However, the modelling process is much more deep and complex due to the fact that a model set which includes the true physical plant cannot ever be constructed. A good model must, then, be simple enough to facilitate design whilst being reasonably complex to give acceptable accuracy, meaning that the model will work on the real plant.
The addition of uncertain parameters in the C-W equations accomplishes a more accurate description of the dynamics present in the rendezvous problem. The resultant equations go as follows [33]:

$$\begin{cases} \ddot{x} - 2n\dot{y} - 3n^2x + [-10en^2\cos(M)x + 2en^2\sin(M)y - 4en\cos(M)\dot{y}] = a_x \\ \ddot{y} + 2n\dot{x} + [-2en^2\sin(M)x - en^2\cos(M)y + 4en\cos(M)\dot{x}] = a_y \\ \ddot{z} + n^2z + [3en^2\cos(M)z] = a_z \end{cases} \tag{2.5}$$

where m is the mass of the chase vehicle, e is the eccentricity of the target orbit and $M = n(t-t_p)$ is the mean anomaly with t_p being the time of the periapsis passage. In these equations the dot superscript denotes derivative with respect to the actual time t, which ranges in the interval $0 \leq t \leq t_f$, t_f being the time when rendezvous is achieved.
In equation 2.5 the n terms are present due to the Coriolis acceleration, the n^2 terms are due in part to the transport acceleration and also due to the fact that the gravitational attractions on the chaser differ in magnitude and direction from the acceleration of gravity at the target.
Equation 2.5 can then be transformed from a second order form to a first order form, resulting in the following system of equations:

$$\begin{cases} \dot{x} = v_x \\ \dot{y} = v_y \\ \dot{z} = v_z \\ \dot{v_x} - 2nv_y - 3n^2x + [-10en^2\cos(M)x + 2en^2\sin(M)y - 4en\cos(M)v_y] = a_x \\ \dot{v_y} + 2nv_x + [-2en^2\sin(M)x - en^2\cos(M)y + 4en\cos(M)v_x] = a_y \\ \dot{v_z} + n^2z + [3en^2\cos(M)z] = a_z \end{cases} \tag{2.6}$$

where $v_i(i = x, y, z)$ are the separation velocities in the downrange, radial and out-of-plane directions and the dot superscript denotes derivative with relation to the actual time t.
By forming the state vector as

$$x(t) = [x, y, z, \dot{x}, \dot{y}, \dot{z}]^T \quad \textbf{(2.7)}$$

which contains the position and velocity states of the chase vehicle, the input vector as

$$u(t) = [F_x(t), F_y(t), F_z(t)]^T \quad \textbf{(2.8)}$$

and rewriting the system of equations 2.6 into a matrix form, the relative motion model for rendezvous in near circular orbit yields the following form:

$$\dot{x}(t) = (A + \Delta A(t))x(t) + Bu(t) \quad \textbf{(2.9)}$$

$$A = \begin{bmatrix} 0 & 0 & 0 & 1 & 0 & 0 \\ 0 & 0 & 0 & 0 & 1 & 0 \\ 0 & 0 & 0 & 0 & 0 & 1 \\ 3n^2 & 0 & 0 & 0 & 2n & 0 \\ 0 & 0 & 0 & -2n & 0 & 0 \\ 0 & 0 & -n^2 & 0 & 0 & 0 \end{bmatrix} \quad \textbf{(2.10)}$$

$$B = \frac{1}{m} \begin{bmatrix} 0 & 0 & 0 \\ 0 & 0 & 0 \\ 0 & 0 & 0 \\ 1 & 0 & 0 \\ 0 & 1 & 0 \\ 0 & 0 & 1 \end{bmatrix} \quad \textbf{(2.11)}$$

$$\Delta A(t) = \begin{bmatrix} 0 & 0 & 0 & 0 & 0 & 0 \\ 0 & 0 & 0 & 0 & 0 & 0 \\ 0 & 0 & 0 & 0 & 0 & 0 \\ 10en^2\cos(M) & -2en^2\sin(M) & 0 & 0 & 4en\cos(M) & 0 \\ 2en^2\sin(M) & en^2\cos(M) & 0 & -4en\cos(M) & 0 & 0 \\ 0 & 0 & -3en^2\cos(M) & 0 & 0 & 0 \end{bmatrix} \quad \textbf{(2.12)}$$

The uncertain matrix ΔA is bounded by the presence of the mean motion and the $\cos M$ as $n \in [n_{min}; n_{max}]$ and $\cos M \in [-1; 1]$, so we have $\|\Delta A\| \leq \alpha$, where α is positive and can be determined by the mean anomaly, M. By adding the norm-bounded uncertain matrix ΔA, which determines the shape of the target orbit, it is possible to more accurately represent the rendezvous problem, seeing as it contains the target orbit's eccentricity. Normal plant models for elliptical are, usually, nonlinear in contrast to 2.9 which is a linearised model, making it more designer friendly and easier to implement. Most of the rendezvous missions, the current case study included, are accomplished in near circular orbits, implying that this control plat is practical and precise enough to represent the regular spacecraft rendezvous of the present dissertation.

Chapter 3

Control Law Based Rendezvous

Classical control theory was naturally couched in the frequency domain, relying on transformation methods to apply primarily to linear time-invariant systems. This methodology was acceptable when the physical problem could be described by simple dynamic models as the Single Input Single Output (SISO), through the use of simple compensators like the Proportional Integral Derivative (PID), lead-lag or wash-out in the control structure.
However, these methods were not suitable to Multi Input Multi Output (MIMO) or multi-loop systems that emerged from the satellites and aerospace systems problematic. The modern control theory with methods such as the H_∞ couched in the time domain tried to solve this issues by defining an objective and validating a controller gain that is more adequate to the problem.
The current chapter is further divided into several sub chapters. The first sub chapter describes the notions of a linear system, followed by the second sub chapter elucidating on the primary system properties. The third sub chapter enunciates the state feedback design and its benefits to control systems. The last two sub chapters go into detail on the two controllers employed in the current dissertation, namely the LQR and the H_∞ controller.

3.1 Linear System

Typically, most systems can be described by a set of simultaneous differential equations in the following form:

$$\dot{x}(t) = f[x(t), u(t), t] \quad (3.1)$$

where t representes the time variable, $x(t)$, the state of the system, is a real time varying column vector with $x(t) \in \mathbb{R}^n$ and $u(t)$ is a real column vector of dimension $u(t) \in \mathbb{R}^m$, denoting the input or control variable [34]. The function f is real and vector valued. The choice of the state follows naturally from the physical structure, and 3.1, known as the state differential equation, usually abides directly from the elementary physical laws that govern the system.
Let $y(t)$ be a real l-dimensional system that can be observed or through which the system influences its environment. This variable is known as the output variable of the system and can be expressed with the equation below:

$$y(t) = g[x(t), u(t), t] \quad (3.2)$$

The system described with 3.1 and 3.2 is known as a finite-dimensional linear differential system, being usually represented in the following form:

$$\begin{aligned} \dot{x} &= Ax(t) + Bu(t) \\ \dot{y} &= Cx(t) + Du(t) \end{aligned} \quad (3.3)$$

where A, B, C and D are constant matrices of appropriate dimensions, making the system time-invariant.

3.2 Stability, Controllability and Observability

3.2.1 Stability

When analysing a linear time-invariant system, it is of the utmost importance to verify and guarantee the existence of stability. One way to find out if a system is stable is to know its eigenvalues. A dynamic system, $\dot{x} = Ax$, is stable if the eigenvalues of the state matrix, A, have all real parts below zero, $Re(\lambda) < 0$.

3.2.2 Controlability

Controllability and Observability are dual aspects of the same problem. The first characteristic verifying the capacity of the state to be controlled by the input variables.

A system is said to be controllable if it is possible by means of an unconstrained controller to transfer the physical system between any two arbitrarily specified states in a finite time [35].

Let the dynamic system be described by the following equation:

$$\dot{x} = Ax(t) + Bu(t) \quad \textbf{(3.4)}$$

$x(t = 0) = x_0$ or the par (A, B) is controllable if for any given $x(0) = x_0$, $t_1 > 0$ and final state x_1, there is a control input $u(t)$ that the solution of the above equation satisfies the condition $x(t_1) = x_1$ [36].

This property means that no information on the past of a system is needed to predict its future, if the state at the current time and all control variables are known [36].

It is possible to find if a dynamic system is controllable though the controllability matrix, Δ, with:

$$\Delta = [B, AB, A^2B, \cdots, A^{n-1}B] \quad \textbf{(3.5)}$$

The system is controllable if $rank(\Delta) = n$.

3.2.3 Observability

A dynamic system is observable, if for any sequence of state and control vectors, the current state can be determined in finite time, using only outputs.

A dynamic system 3.3 or the par (C, A) is said to be observable, if for any $t > 0$, the initial state $x(0) = x_0$ can be determined by the control input behaviour and the output variable in the interval $[0, t]$ [35].

This can be found through the observability matrix, Θ.

$$\Theta = \begin{bmatrix} C \\ CA \\ CA^2 \\ \vdots \\ CA^{n-1} \end{bmatrix} \quad (3.6)$$

The dynamic system is observable when $rank(\Theta) = n$.
When a dynamic system is observable, it is possible to determine the behaviour of the entire system from knowing the system outputs [36].

3.2.4 Lyapunov Theory

The analysis of the three properties mentioned previously is a crucial step in the evaluation of a dynamic linear system. However, not always is it possible and easy to directly evaluate each of these properties. Instead we can resort to Lyapunov's equation [37].

$$A^T P + PA + Q = 0 \quad (3.7)$$

where A and Q are known matrices.
If A is stable, then:

1. $P = \int e^{At} Q e^{At} dt$
2. $P > 0, if\ Q > 0\ and\ P \geq 0, if\ Q \geq 0$
3. $If\ Q \geq 0, then\ (Q, A)\ is\ observable\ if\ P > 0$

The par (C, A) is observable, with the matrix A stable, if and only if, there is a definitive positive solution from the following equation:

$$A^T L_o + L_o A + C^T C = 0 \quad (3.8)$$

with L_o being the observability gramian [37].
The same approach can be aplied to determine if the par (A, B) is controllable, with the par being controllable, if and only if, there is a definitive solution for :

$$AL_c + L_c A^T + BB^T = 0 \quad (3.9)$$

where L_c being the controllability gramian [37].
If P is a solution for Lyapunov's equation then:

1. $Re(\lambda_i) \leq 0, if\ P > 0\ and\ Q \geq 0$
2. $A\ is\ stable\ if\ P > 0\ and\ Q > 0$
3. $A\ is\ stable\ if\ P \geq 0, Q \geq 0$

The par (Q, A) is such that a system with a dynamic matrix given by $A + LQ$ is stable for any given value of L [37].

3.3 State Feedback

There are several fundamental issues, when designing control systems, that transcend the boundaries of specific applications whilst being generic in their relationship to control design and procedures. One crucial issue is the requirement to provide good overall performance in the presence of uncertainty parameters, systems variation and modelling errors, which became the original motivation for the development of state feedback systems.

A feedback control system can be designed within the state-variable framework to provide a specific desired eigenvalue structure for a closed-loop plant matrix, when it can not be achieved in the system performance due to the presence of too weighty model uncertainties making it harder to obtain the desired accuracy of response. Essentially, the state feedback design problem centers around the trade-off involved in reducing the overall impact of the uncertain parameters.

Considering the following system:

$$\begin{aligned} \dot{x} &= Ax + B\eta \\ y &= Cx \end{aligned} \quad (3.10)$$

It is possible to infer that, if the system is controllable, then it is possible to define a linear control law to achieve any desired closed-loop eigenvalue structure [35]. For a single-input system, a linear control law is given by:

$$\eta = -k^T x + \eta' \quad (3.11)$$

where η' is the control input in the absence of feedback, and k is the feedback gain vector as can be seen in Fig. 3.1. Introducing the control law into the state equation system allows to

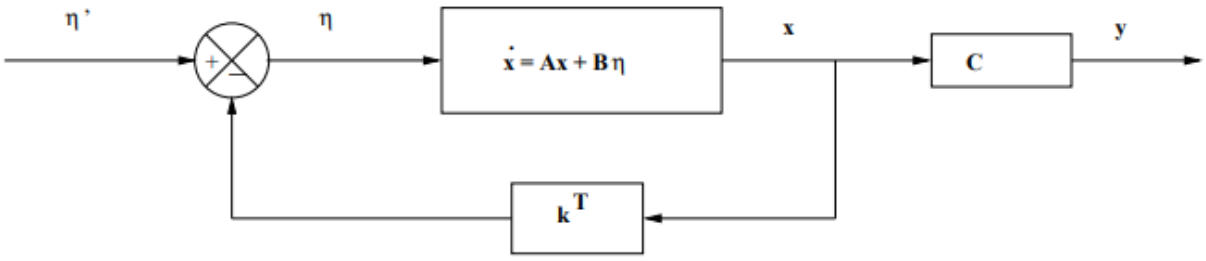

Figure 3.1: Block diagram for a system with state-variable feedback.

derive the following form of the state equation:

$$\begin{aligned} \dot{x} &= Ax + B[\eta' - k^T x] \\ &= [A - Bk^T]x + B\eta' \\ &= A^* x + B\eta' \end{aligned} \quad (3.12)$$

where the plant matrix describing the behaviour of the closed-loop system is:

$$A^* = A - Bk^T \quad (3.13)$$

3.4 Linear Quadratic Regulator

It is important to obtain a balance over several factors as state stabilization and regulation, when trying to achieve an optimal control over a trajectory, and control of the system's output. With that in mind, it is crucial to find a control that allows to maximize or minimize a criteria that constitutes the optimization problem [36].

Considering the following linear dynamic system:

$$\dot{x} = Ax + Bu \quad (3.14)$$

with $x \in \mathbb{R}^n$, $u \in \mathbb{R}^m$, $A \in \mathbb{R}^{nxn}$ and $B \in \mathbb{R}^{mxm}$, being, respectively, the state vector, the control vector, the state matrix and the control matrix.

It is necessary to carefully choose the control input vector $u(t)$ that can minimize the quadratic performance index J defined by:

$$J(u) = \int_0^\infty L(x,u)dt \quad (3.15)$$

where $L(x,u)$ is a quadratic function of x and u.

One controller has been widely accepted among researchers of this particular field of study due to its relatively easy implementation and acceptable results. The Linear Quadratic Regulator (LQR) is a quadratic linear regulator whose control vector can be described as a linear function of the state vector as follows:

$$u = -Kx \quad (3.16)$$

with $K \in \mathbb{R}^{mxn}$

The main objective of a controller lies in finding the matrix K that minimizes the performance index J with the control defined in 3.16 [36].

$L(x,u)$ in its quadratic form can be expressed as:

$$L(x,u) = x^T Qx + u^T Ru \quad (3.17)$$

where the state weighting matrix $Q \in \mathbb{R}^{nxn}$ is a positive symmetric matrix related to the convergence rate of the relative motion states and the smoothness of the rendezvous trajectory, and the control weighting matrix $R \in \mathbb{R}^{mxm}$ is a positive symmetric matrix related to the fuel cost of the chase vehicle.

The weight of both these matrices should not be chosen arbitrarily as they have a great effect on the performance of the controller, so its final values should be carefully evaluated through simulation and iteration. One method to obtain fairly good weighting matrices is Bryson's method that relates the matrix diagonal with the maximum acceptable value for each state as can be seen below:

$$Q = \begin{bmatrix} \frac{1}{x_{1max}^2} & 0 & \dots & 0 \\ 0 & \frac{1}{x_{2max}^2} & \dots & 0 \\ \vdots & \vdots & \ddots & \vdots \\ 0 & 0 & \dots & \frac{1}{x_{nmax}^2} \end{bmatrix} \quad (3.18)$$

$$R = \begin{bmatrix} \frac{1}{u_{1max}^2} & 0 & \dots & 0 \\ 0 & \frac{1}{u_{2max}^2} & \dots & 0 \\ \vdots & \vdots & \ddots & \vdots \\ 0 & 0 & \dots & \frac{1}{u_{nmax}^2} \end{bmatrix} \quad (3.19)$$

Another alteration can further develop this method in order to obtain rendezvous with less amplitude of each cycle and even fewer cycles with the changes seen in 3.20 and 3.21.

$$Q = \begin{bmatrix} \frac{\eta_1}{x_{1max}^2} & 0 & \dots & 0 \\ 0 & \frac{\eta_2}{x_{2max}^2} & \dots & 0 \\ \vdots & \vdots & \ddots & \vdots \\ 0 & 0 & \dots & \frac{\eta_n}{x_{nmax}^2} \end{bmatrix} \quad (3.20)$$

$$R = \begin{bmatrix} \frac{\lambda_1}{u_{1max}^2} & 0 & \dots & 0 \\ 0 & \frac{\lambda_2}{u_{2max}^2} & \dots & 0 \\ \vdots & \vdots & \ddots & \vdots \\ 0 & 0 & \dots & \frac{\lambda_n}{u_{nmax}^2} \end{bmatrix} \quad (3.21)$$

where $\forall_i \, \eta_i \geq 1$ and $\forall_i \, 0 < \lambda_i \leq 1$. Adjusting these matrices will improve the overall performance of the plant with values of λ_i closer to 0 obtaining better performance with relation to fuel usage and values closer to 1 obtaining shorter duration to achieve rendezvous.

Combining equations 3.15 and 3.17 yields the following form of the performance index :

$$J(u) = \int_0^\infty (x^T Q x + u^T R u) dt \quad (3.22)$$

Then, by adding equations 3.14, 3.16 and 3.22, we obtain equations 3.23 and y3.24, respectively.

$$\dot{x} = Ax - BKx = (A - BK)x \quad (3.23)$$

$$J(u) = \int_0^\infty (x^T (Q + K^T R K) x dt \quad (3.24)$$

To find the appropriate control law is necessary to find a Lyapunov function V for the closed-loop dynamic system as:

$$V(x) = x^T P x \quad (3.25)$$

with P being a positive symmetric matrix.

Then, the derivative with relation to the actual time of Lyapunov's function should yield the same function to be integrated in 3.24

$$\dot{V}(x) \equiv \frac{d}{dt}(x^T P x) = -x^T (Q + K^T R K) x \quad (3.26)$$

However, we have:

$$\frac{d}{dt}(x^T P x) = \dot{x}^T P x) + x^T P \dot{x} \quad (3.27)$$

So, by adding 3.26 and 3.27 we obtain:

$$x^T[(A - BK)^T P + P(A - BK)]x = -x^T(Q + K^T R K)x \quad (3.28)$$

For this equation to be stable, it is necessary that the matrix K satisfies the following Lyapunov's equation:

$$(A - BK)^T P + P(A - BK) = -(Q + K^T R K) \quad (3.29)$$

K being the unknown value and its solution achieved by:

$$K = R^{-1} B^T P \quad (3.30)$$

The matrix P is the solution of the Algebraic Ricatti Equation (ARE). ARE is a more general equation than the Lyapunov equation in control theory, with the main difference being that Lyapunov's equation is most useful in system analysis while ARE is better suited to control system synthesis, playing a central role in LQR and H_∞ optimal control.
Then, through 3.16 and 3.30 we obtain:

$$u = -R^{-1} B^T P x \quad (3.31)$$

Relating to the rendezvous problem, ARE has been extensively used when looking for control laws for closed-loop dynamic systems. For the usage of ARE to be valid and possible, it is necessary to guarantee the conditions mentioned previously in section 3.2. The par (A, B) must be stable and controllable, the par (C, A) must be observable and the matrices Q and R must be positive and definitive. Then, we have the Riccati equation in the following form:

$$A^T P + PA - PBR^{-1} B^T P + Q = 0 \quad (3.32)$$

Applying ARE-based control laws on the controllers design, guarantees the existence of a quadratic Lyaunov function, and hence, stability for a closed-loop uncertain dynamic system, and these robust controllers are not only able to stabilize linear systems with uncertain parameters but are also capable to reduce the effect of disturbances on the controlled output to a pre-specified level.

3.5 H_∞ Robust Controller

Rendezvous is, essentially, a planned collision between two spacecraft and, as such, leaves little room for deviations and trajectory errors. No system is perfect, so it is always subject to interference and uncertainties that can take the chaser off from the planned trajectory, which can lead to the collision out of the docking point with a high relative velocity of the two spacecraft, and therefore lead to a serious accident. Consequentially, it means that the implementation of a robust control is a crucial step in a rendezvous problem.
Even though the Linear Quadratic Gaussian (LQG), that is essentially the combination of a Lin-

ear Quadratic Estimator (LQE) and a LQR, can be a meaningful performance measure and LQG theory can give efficient design compromises under certain disturbance and plant assumptions, its trade-off between disturbance error reduction and noise error reduction, as well as the limitations on high loop gains are issues that cannot be ignored in the robust controller design. For this dissertation, the robust H_∞ control was chosen to guarantee that the chaser spacecraft follows the destined trajectory and achieves rendezvous.

The norm H_∞, is essentially, a measure of the worst possible performance for many classes of input signals, which means that its minimization implies the attenuation of the relation between the inputs and outputs of the system. In other words, it is the attenuation of the disturbances in the controlled outputs, making the main focus of an H_∞ robust control to find the gain matrix K that minimizes the closed-loop transfer function $\|T\|_\infty$ [38].

Considering the following linear dynamic uncertain system:

$$\begin{aligned} \dot{x}(t) &= Ax(t) + Bu(t) + Dw(t) \\ y(t) &= Cx(t) \\ x(t_0) &= x_0 \end{aligned} \tag{3.33}$$

where x_0 is given but arbitrary, $w \in \mathbb{R}^p$ and D is a matrix of appropriate size. The matrix A is a time varying matrix which contains uncertain parameters and the measured state is assumed to be available for feedback which means that the measured output is the state $x(t)$. The main objective being to find a control function $u(t)$ defined on the interval $[t_0, T]$, T defining the time of rendezvous, which can be a function of the state $x(t)$, such that the state $x(t)$ is driven to close enough to the target at a predefined time T. Theoretically, such a problem might me solvable for any $T > 0$ if the system is controllable, however any physical system will always have energy limitation, meaning that one cannot construct any one control function that will drive the state to zero in an arbitrarily short time without taking into consideration the possibility of actuator saturation, as well as the fact that large control action can easily drive the system out of the region where the given linear model is valid.

It is possible to have two classes of controller for a system as the one described previously, namely, a static or a dynamic linear state feedback. However, [25] proves that the disturbance attenuations in both cases is equal, $\gamma_{static} = \gamma_{dynamic}$. The value of the norm γ should be evaluated with the minimization of the disturbances affecting the plant states [38]. So, the static state feedback was chosen due to being easier to design and implement as well as the fact that a static state feedback has lower times of computation.

It goes as follows:

$$u = -kx \tag{3.34}$$

Let,

$$T(s) := E[sI - (A - BK)]^{-1}D \tag{3.35}$$

denote the closed-loop transfer function from the input w to the output y with the static state feedback control law 3.34.

Then we can define γ as:

$$\gamma := inf\{\|T\|_\infty : K \in S\} \tag{3.36}$$

where

$$S = \{K \in \mathbb{R}^{mxn} : A - BK \; is \; a \; stability \; matrix\} \quad (3.37)$$

The disturbance attenuation described previously with the plant states available for feedback, allows the norm of the closed-loop transfer function to be reduced as desired to the H_∞ optimum control using state feedback.
Let P be a positive definite solution of the Ricatti equation

$$PA + A^T P - \frac{1}{\varepsilon} PBR^{-1}B^T P + \frac{1}{\gamma} PDD^T + \frac{1}{\gamma} C^T C + \varepsilon Q = 0 \quad (3.38)$$

with disturbance attenuation, γ, constant for some $\varepsilon > 0$, where

$$K = \frac{R^{-1}B^T P}{2\varepsilon} \quad (3.39)$$

Chapter 4

Numerical Results and Discussion

This chapter main purpose is to present the simulations performed and the results obtained to validate the concepts mentioned and described in the previous chapters, alongside a detailed analysis and discussion of all notable features and details. All simulations are obtained through the use of the programming language $Python^{TM}$. The present chapter is further divided in several sub chapters to provide better understanding and a sense of ease to the reader.

In sub chapter 1 the dynamic model is presented with discrimination of every parameter and how they were obtained through all simulations thereafter. All matrices are presented and a table with the orbital parameters for this dissertation is displayed.

Sub chapter 2 displays an analysis of the dynamic system properties followed by an explanation of the method used for simulating the rendezvous problem as well as a comparison of the behaviour generated through the employment of the LQR controller and the robust H_∞ controller.

Lastly, sub chapter 3 presents the results of the optimization whilst exposing and discussing the benefits and main differences between the LQR controller and the robust H_∞ controller.

4.1 Dynamic Model

The first process is the description of the dynamic model used to represent the movement of the chaser and target spacecraft whilst performing the rendezvous manoeuvres. This model is described in chapter 2 with the state vector, representing the relative position and velocity in all three directions, and the control vector, containing the thrust force components in all three directions, goes as follows:

$$\dot{x}(t) = [x, y, z, \dot{x}, \dot{y}, \dot{z}]^T \quad (4.1)$$

$$u(t) = [F_x(t), F_y(t), F_z(t)]^T \quad (4.2)$$

with the matrices A, ΔA, B and C described in equations 4.3, 4.4, 4.5 and 4.6.

$$A = \begin{bmatrix} 0 & 0 & 0 & 1 & 0 & 0 \\ 0 & 0 & 0 & 0 & 1 & 0 \\ 0 & 0 & 0 & 0 & 0 & 1 \\ 3n^2 & 0 & 0 & 0 & 2n & 0 \\ 0 & 0 & 0 & -2n & 0 & 0 \\ 0 & 0 & -n^2 & 0 & 0 & 0 \end{bmatrix} \quad (4.3)$$

$$\Delta A = \begin{bmatrix} 0 & 0 & 0 & 0 & 0 & 0 \\ 0 & 0 & 0 & 0 & 0 & 0 \\ 0 & 0 & 0 & 0 & 0 & 0 \\ 10en^2\cos(M) & -2en^2\sin(M) & 0 & 0 & 4en\cos(M) & 0 \\ 2en^2\sin(M) & en^2\cos(M) & 0 & -4en\cos(M) & 0 & 0 \\ 0 & 0 & -3en^2\cos(M) & 0 & 0 & 0 \end{bmatrix} \quad (4.4)$$

$$B = \frac{1}{m}\begin{bmatrix} 0 & 0 & 0 \\ 0 & 0 & 0 \\ 0 & 0 & 0 \\ 1 & 0 & 0 \\ 0 & 1 & 0 \\ 0 & 0 & 1 \end{bmatrix} \quad (4.5)$$

$$C = \begin{bmatrix} 1 & 0 & 0 & 0 & 0 & 0 \\ 0 & 1 & 0 & 0 & 0 & 0 \\ 0 & 0 & 1 & 0 & 0 & 0 \end{bmatrix} \quad (4.6)$$

Matrices A, B, ΔA, and C are applied for the LQR controller case and in the instance of the H_∞ controller, the further addition of the matrix D, as follows, is necessary.

$$D = \frac{1}{m}\begin{bmatrix} 0 & 0 & 0 \\ 0 & 0 & 0 \\ 0 & 0 & 0 \\ 1 & 0 & 0 \\ 0 & 1 & 0 \\ 0 & 0 & 1 \end{bmatrix} \quad (4.7)$$

All cases of study were assumed to be between two relatively close spacecraft where the target vehicle is assumed to be moving on a Low Earth Orbit (LEO) with eccentricity $e = 0.01$, gravitational parameter $\mu = 3.99 \cdot 10^{14} m^3 \cdot s^{-2}$ and mean motion $n = 1.130 \cdot 10^{-3}\ rad \cdot s^{-1}$. The chase vehicle mass is set for $m = 200Kg$. The mean anomaly M can be obtained with the following equations:

$$\begin{aligned} P &= \frac{1}{n} \\ a &= \frac{P}{1-e^2} \\ t_p &= 2\Pi\sqrt{\frac{a^3}{\mu}} \\ M &= n(t - t_p) \end{aligned} \quad (4.8)$$

where P is the perigee, a is the apogee and μ is the contant gravitational parameter. The parameters mentioned are stated in the following table. The perigee and apogee show similar value due to the low eccentricity value, meaning that the apogee and perigee are approximately equal.

Table 4.1: Orbital Parameters.

Parameter	Value	Units
e	$10.00 \cdot 10^{-3}$	Rad
n	$1.130 \cdot 10^{-3}$	$Rad \cdot s^{-1}$
μ	$3.99 \cdot 10^{14}$	$m^3 \cdot s^{-2}$
P	$885 \cdot 10^3$	Km
a	$885 \cdot 10^3$	Km
t_p	$8.29 \cdot 10^{-3}$	s
$M(t=0)$	$-9.36 \cdot 10^{-6}$	Rad

The matrices A, ΔA, B and D can now be given as seen below:

$$A = \begin{bmatrix} 0 & 0 & 0 & 1.000 \cdot 10^0 & 0 & 0 \\ 0 & 0 & 0 & 0 & 1.000 \cdot 10^0 & 0 \\ 0 & 0 & 0 & 0 & 0 & 1.000 \cdot 10^0 \\ 3.83 \cdot 10^{-6} & 0 & 0 & 0 & 2.26 \cdot 10^{-3} & 0 \\ 0 & 0 & 0 & -2.26 \cdot 10^{-3} & 0 & 0 \\ 0 & 0 & -1.277 \cdot 10^{-6} & 0 & 0 & 0 \end{bmatrix} \quad (4.9)$$

$$\Delta A = \begin{bmatrix} 0 & 0 & 0 & 1.000 \cdot 10^0 & 0 & 0 \\ 0 & 0 & 0 & 0 & 1.000 \cdot 10^0 & 0 \\ 0 & 0 & 0 & 0 & 0 & 1.000 \cdot 10^0 \\ 127.7 \cdot 10^{-9} & 239 \cdot 10^{-15} & 0 & 0 & 45.2 \cdot 10^{-6} & 0 \\ -239 \cdot 10^{-15} & 12.77 \cdot 10^{-9} & 0 & -45.2 \cdot 10^{-6} & 0 & 0 \\ 0 & 0 & -38.3 \cdot 10^{-9} & 0 & 0 & 0 \end{bmatrix} \quad (4.10)$$

$$B = \begin{bmatrix} 0 & 0 & 0 \\ 0 & 0 & 0 \\ 0 & 0 & 0 \\ 5.00 \cdot 10^{-3} & 0 & 0 \\ 0 & 5.00 \cdot 10^{-3} & 0 \\ 0 & 0 & 5.00 \cdot 10^{-3} \end{bmatrix} \quad (4.11)$$

$$D = \begin{bmatrix} 0 & 0 & 0 \\ 0 & 0 & 0 \\ 0 & 0 & 0 \\ 5.00 \cdot 10^{-3} & 0 & 0 \\ 0 & 5.00 \cdot 10^{-3} & 0 \\ 0 & 0 & 5.00 \cdot 10^{-3} \end{bmatrix} \quad (4.12)$$

and the final matrix A together with the uncertain matrix ΔA yields:

$$A + \Delta A = \begin{bmatrix} 0 & 0 & 0 & 1.000 \cdot 10^{0} & 0 & 0 \\ 0 & 0 & 0 & 0 & 1.000 \cdot 10^{0} & 0 \\ 0 & 0 & 0 & 0 & 0 & 1.000 \cdot 10^{0} \\ 3.96 \cdot 10^{-6} & 239 \cdot 10^{-15} & 0 & 0 & 2.30 \cdot 10^{-3} & 0 \\ -239 \cdot 10^{-15} & 12.77 \cdot 10^{-9} & 0 & -2.30 \cdot 10^{-3} & 0 & 0 \\ 0 & 0 & -1.315 \cdot 10^{-6} & 0 & 0 & 0 \end{bmatrix} \quad (4.13)$$

4.2 First Analysis

An initial analysis is now possible to perform in order to validate the existence of the primary characteristics of the dynamic model previously described, such as stability, controllability and observability.

As mentioned in section 3.2, it is possible to verify if a system is stable by knowing its eigenvalues. From matrix 4.9 we obtain the following eigenvalue vector:

$$\begin{bmatrix} 0.00 \cdot 10^{0} + 0.00 \cdot 10^{0} j \\ -6.47 \cdot 10^{-60} + 0.00 \cdot 10^{0} j \\ -101.6 \cdot 10^{-21} + 1.130 \cdot 10^{-3} j \\ -101.6 \cdot 10^{-21} + 1.130 \cdot 10^{-3} j \\ 0.00 \cdot 10^{0} + 1.130 \cdot 10^{-3} j \\ 0.00 \cdot 10^{0} + 1.130 \cdot 10^{-3} j \end{bmatrix}^{T} \quad (4.14)$$

It is possible to see through matrix 4.14 that all real parts are bellow or equal to zero, $Re(\lambda) < 0$, which means that the system is stable, and as some real parts are negative the system will tend to equilibrium.

The programming language, $Python^{TM}$, has a library named analysis which contains three useful commands. Through the use of the commands, $is\_stabilisable(A, B)$, $is\_controllable(A, B)$ and $is\_observable(C, A)$, it was possible to evaluate the presence of stability, controllability and observability in the system.

Before starting the simulation of the dynamic model to represent the rendezvous, two aspects of great importance to the project need proper and careful study in order to validate the results to be obtained.

Firstly, we need to chose a numerical method to obtain a numerical approximate to the solution of the Ordinary Differential Equation (ODE) problem of the form described in chapter 3. Through these methods it is possible to obtain the solution x_{n+1} to the initial value problem with nothing more than its state x and the differential equation $\dot{x}$.

For the purpose of this dissertation, the fifth order Runge-Kutta algorithm [39], also known as Butcher's method, was chosen due to its precise approximations and wide use overall in the science community.

Butcher's method is capable of solving ordinary differential equations of the form:

$$\dot{x} = f(x, u);\ x(t) \in \mathbb{R}^{n};\ u \in \mathbb{R}^{m} \quad (4.15)$$

The initial value problem is then solved, having in consideration the initial contritions (t_0, x_0), using the following equation:

$$x_{n+1} = x_n + \frac{1}{90}(7k_1 + 32k_3 + 12k_4 + 32k_5 + 7k_6) \quad \textbf{(4.16)}$$

where $k_i (i = 1, 2, 3, 4, 5, 6)$ are obtained at each iteration with the formulas listed below:

$$\begin{aligned}
k_1 =& dt * f(x_k, u_k) \\
k_2 =& dt * f(x_k + \frac{1}{4}k_1, u_k) \\
k_3 =& dt * f(x_k + \frac{1}{8}k_1 + \frac{1}{8}k_2, u_k) \\
k_4 =& dt * f(x_k - \frac{1}{2}k_2 + k_3, u_k) \\
k_5 =& dt * f(x_k + \frac{3}{16}k_1 + \frac{9}{16}k_4, u_k) \\
k_6 =& dt * f(x_k - \frac{3}{7}k_1 + \frac{2}{7}k_2 + \frac{12}{7}k_3 - \frac{12}{7}k_4 + \frac{8}{7}k_5, u_k)
\end{aligned} \quad \textbf{(4.17)}$$

In equation 4.17, dt, represents the time step used to iterate every calculation through the simulation and also the second important consideration to study in order to obtain good proximate results.

The time step, dt has the importance of being sufficiently small as to obtain an proximate solution that is as close as possible to the reality, though not too small as to increase the computation time to impractical standards.

A convergence study was made to determine the appropriate value of time step for the simulation of the rendezvous and the following results were obtained: The results displayed in

Table 4.2: Time step study.

Time Step [s]	Iterations	Computation Time [s]	x [m]	error
$102.4 \cdot 10^0$	$88.0 \cdot 10^0$	$58.7 \cdot 10^{-3}$	$55.4 \cdot 10^3$	$311 \cdot 10^{-3}$
$51.2 \cdot 10^0$	$176.0 \cdot 10^0$	$117.3 \cdot 10^{-3}$	$38.1 \cdot 10^3$	$180.8 \cdot 10^{-3}$
$25.6 \cdot 10^0$	$352 \cdot 10^0$	$235 \cdot 10^{-3}$	$31.2 \cdot 10^3$	$129.4 \cdot 10^{-3}$
$12.80 \cdot 10^0$	$703 \cdot 10^0$	$469 \cdot 10^{-3}$	$27.2 \cdot 10^3$	$55.5 \cdot 10^{-3}$
$6.40 \cdot 10^0$	$1.406 \cdot 10^3$	$937 \cdot 10^{-3}$	$25.7 \cdot 10^3$	$79.8 \cdot 10^{-3}$
$3.20 \cdot 10^0$	$2.81 \cdot 10^3$	$1.873 \cdot 10^0$	$23.6 \cdot 10^3$	$13.94 \cdot 10^{-3}$
$1.600 \cdot 10^0$	$5.62 \cdot 10^3$	$3.75 \cdot 10^0$	$23.3 \cdot 10^3$	$12.74 \cdot 10^{-3}$
$800 \cdot 10^{-3}$	$11.25 \cdot 10^3$	$7.50 \cdot 10^0$	$23.0 \cdot 10^3$	$5.66 \cdot 10^{-3}$
$400 \cdot 10^{-3}$	$22.5 \cdot 10^3$	$15.00 \cdot 10^0$	$22.9 \cdot 10^3$	$2.89 \cdot 10^{-3}$
$200.0 \cdot 10^{-3}$	$45.0 \cdot 10^3$	$30.0 \cdot 10^0$	$22.8 \cdot 10^3$	$1.447 \cdot 10^{-3}$
$100.0 \cdot 10^{-3}$	$90.0 \cdot 10^3$	$60.0 \cdot 10^0$	$22.8 \cdot 10^3$	$720 \cdot 10^{-6}$
$50.00 \cdot 10^{-3}$	$180.0 \cdot 10^3$	$120 \cdot 10^0$	$22.8 \cdot 10^3$	$311 \cdot 10^{-6}$

table 4.2 represent the deviation of the relative position, x, at $t = 1000s$ that represent a critical point in the rendezvous, making it appropriate for the convergence study due to the fact that the simulation needs to be precise enough to accurately represent the oscillations of the movement. The computation time was calculated for a time of rendezvous $t_f = 9000s$ with an average computation speed of 1500 iterations per second. As can be seen through figures 4.1 and 4.2 the precision of the results converge as the time step decreases. For the purpose of this dissertation the time step was set as $dt = 0.1s$ for all simulations due to the relative error being considerably small and also the fact that the decrease in time step from 0.1 no longer provides sufficient improvement for the increase in computation time.

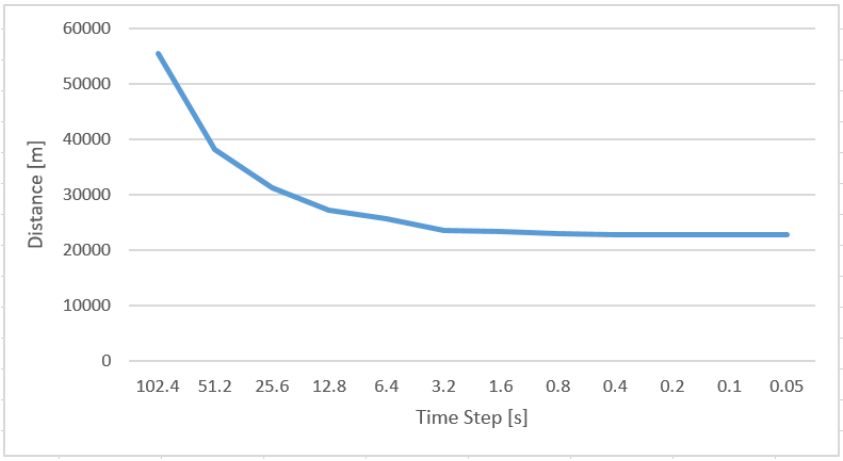

Figure 4.1: Convergence of the distance x from $x(t = 1000s)$ with relation to the time step chosen for the initial state $x = [-10000; -20000; -8000; 6; 6; 3]^T$.

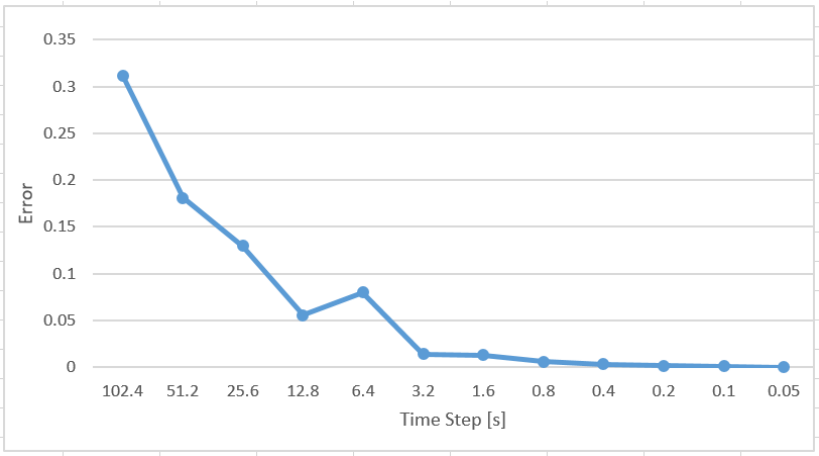

Figure 4.2: Convergence of the relative error with relation to the time step chosen for the initial state $x = [-10000; -20000; -8000; 6; 6; 3]^T$.

The weighting matrices Q and R are defined as stated in chapter 3 and go as displayed below:

$$Q = \begin{bmatrix} 1 & 0 & 0 & 0 & 0 & 0 \\ 0 & 1 & 0 & 0 & 0 & 0 \\ 0 & 0 & 1 & 0 & 0 & 0 \\ 0 & 0 & 0 & 1 & 0 & 0 \\ 0 & 0 & 0 & 0 & 1 & 0 \\ 0 & 0 & 0 & 0 & 0 & 1 \end{bmatrix} \quad (4.18)$$

$$R = \begin{bmatrix} 1 & 0 & 0 \\ 0 & 1 & 0 \\ 0 & 0 & 1 \end{bmatrix} \quad (4.19)$$

The matrices $U_i (i = x, y, z)$ were introduced in order to limit the control forces applied by the thrust engines so as to more accurately describe the reality of the problem were technological limitations weigh in the behaviour of the chaser spacecraft, opposite to the phenomenon to be seen in figures 4.3 and 4.4 where the lack of limitations led to an unrealistic representation

of the behaviour to be expected from the mission with the chaser reaching the target within a absurdly small time frame owning to the fact that the chaser spacecraft's propulsion system is capable to exert the amount of thrust necessary to reach the target spacecraft.

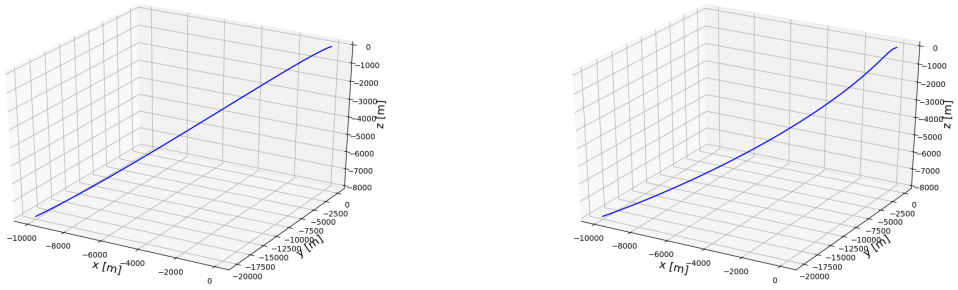

(a) LQR controller (b) H_∞ controller

Figure 4.3: Rendezvous trajectory performed by the chaser spacecraft to reach the target spacecraft with LQR controller (a) and H_∞ controller (b) for the initial state $x = [-10000; -20000; -8000; 6; 6; 3]^T$ without input constraints.

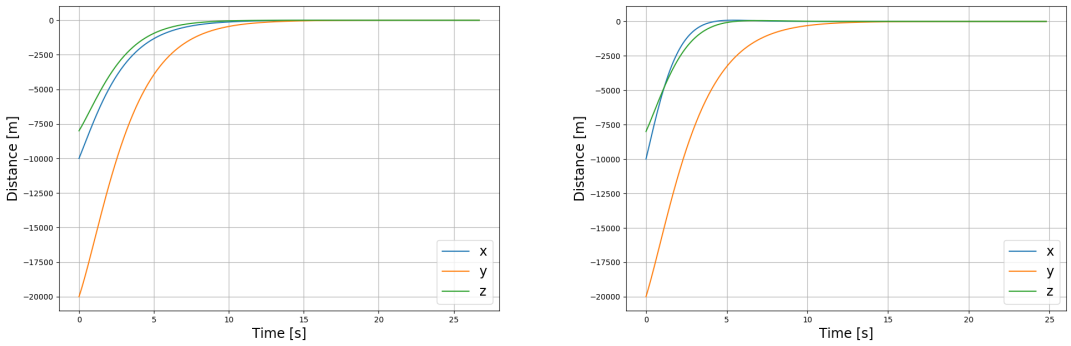

(a) LQR controller (b) H_∞ controller

Figure 4.4: Relative positions components x, y and z with LQR controller (a) and H_∞ controller (b) for the initial state $x = [-10000; -20000; -8000; 6; 6; 3]^T$ without input constraints.

The results in relation to figures 4.3 and 4.4 were obtained through manipulation of matrices 4.18 and 4.19. The more the diagonal of matrix 4.18 increases the higher the output of the propulsive engine thrust generated and, therefore, the fastest the rendezvous became. The simulation stopped at around 20 seconds of rendezvous on the grounds that the computational values became immensely large and the the programming language $Python^{TM}$ was no longer capable of computing any further.

The following figures 4.5, 4.6 and 4.7 represent the propulsive control components history and as can be observed along with all six figures, there is a peak generated immediately at the start of the rendezvous with abnormally high values, which sustains the statement that without physical limitations the chaser spacecraft could theoretically reach the target spacecraft in any time desired. It is also important to note that when contrasting figures 4.5(a), 4.6(a) and 4.7(a) with 4.5(b), 4.6(b) and 4.7(b), the propulsive thrusts generated through the robust H_∞ controller present higher maximum values in all three components, which goes along with the fact that the H_∞ controller takes in consideration the worst possible case and responds in

accordance with it in order to attenuate the disturbances present in the controlled outputs, which means that the H_∞ controller is much less likely to be perturbed when compared to the LQR controller.

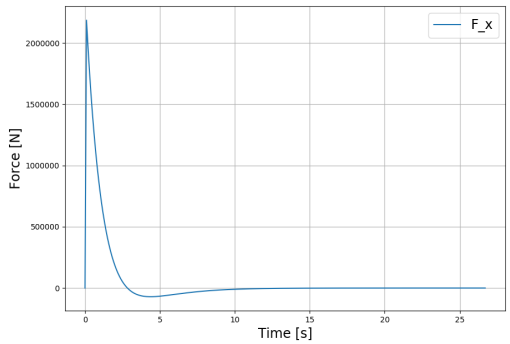

(a) LQR controller

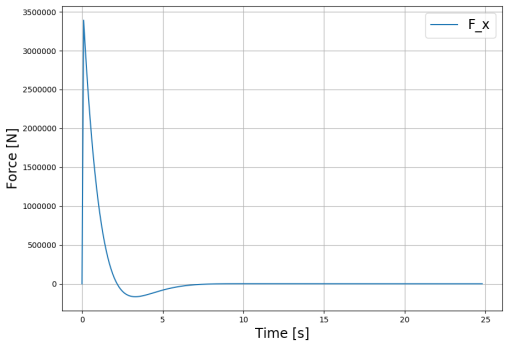

(b) H_∞ controller

Figure 4.5: Propulsive thrust component along the direction x with LQR controller (a) and H_∞ controller (b) for the initial state $x = [-10000; -20000; -8000; 6; 6; 3]^T$.

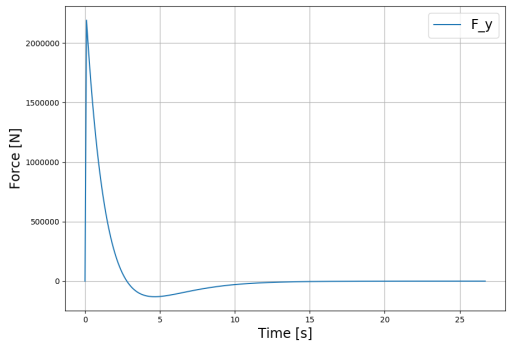

(a) LQR controller

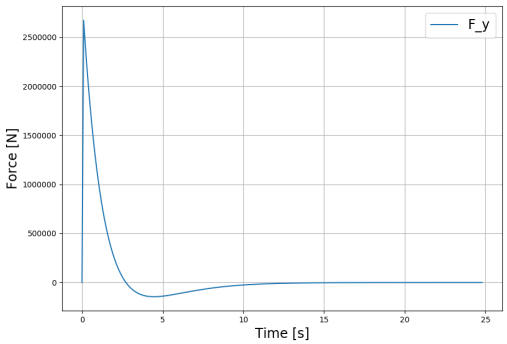

(b) H_∞ controller

Figure 4.6: Propulsive thrust component along the direction y with LQR controller (a) and H_∞ controller (b) for the initial state $x = [-10000; -20000; -8000; 6; 6; 3]^T$.

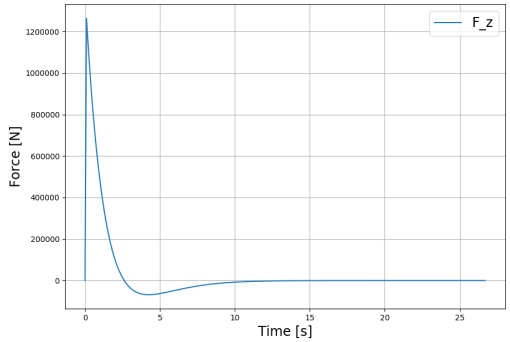

(a) LQR controller

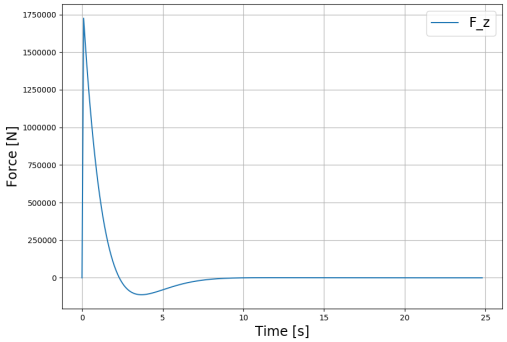

(b) H_∞ controller

Figure 4.7: Propulsive thrust component along the direction z with LQR controller (a) and H_∞ controller (b) for the initial state $x = [-10000; -20000; -8000; 6; 6; 3]^T$.

Notwithstanding the many benefits in theory from not having physical limitations, it is still not possible from current standards and with that in mind the input constraints $U_x = [1,0,0]^T[1,0,0]$, $U_y = [0,1,0]^T[0,1,0]$ and $U_z = [0,0,1]^T[0,0,1]]$ were implemented and defined as:

$$|f_i| = |U_i u(t)| \leq u_{i,max}(i = x, y, z) \quad (4.20)$$

where $u_{i,max}$ is the maximum control force that the thrusters can produce along the i-axis, meaning that the propulsive control thrusts must not exceed the maximum values assigned as $40N$, $40N$ and $20N$ for the control thrusts along the x, y and z axis respectively. The control input limitations, as described above, are applied to all case studies through the course of the present dissertation.

A first simulation for the initial state $x = [-1000; -2000; -800; 6; 6; 3]^T$ with both controllers confirms the validity of the statements mentioned, as can be seen in figures 4.8(a) and 4.8(b).

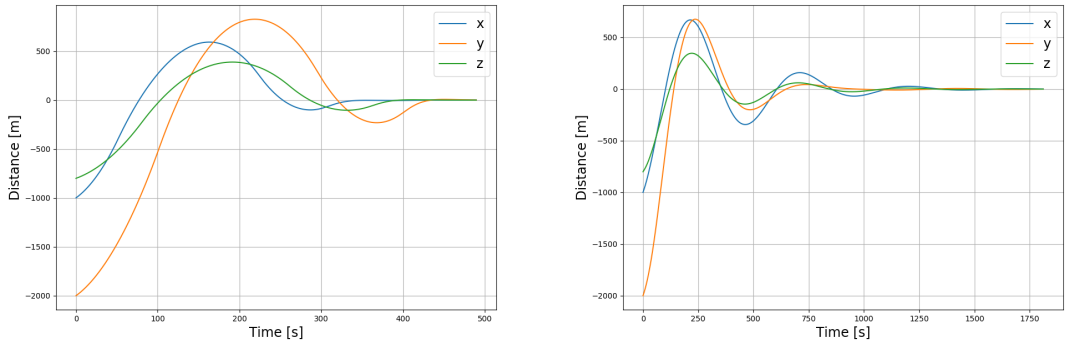

(a) LQR controller (b) H_∞ controller

Figure 4.8: Relative positions x, y and z with LQR controller (a) and H_∞ controller (b) for the initial state $x = [-1000; -2000; -800; 6; 6; 3]^T$.

Through analysis of figures 4.8(a) and 4.8(b), it is possible to observe that the system behaves as expected and the controller LQR as well as the controller H_∞ achieve rendezvous, confirming that the system is indeed stable, controllable and observable as was to be expected. The rendezvous obtained through the LQR controller occurs around the $500s$ mark with some attenuation of the movement as can be seen in the relative position y, with the initial state never being surpassed. The same phenomenon can also be seen with the robust controller H_∞ by achieving rendezvous near the $1500s$ mark with also a good decrease of the system's oscillations amplitude with the downside of having more oscillations when compared to the LQR case. We can conclude that in both cases the chaser spacecraft meets the target spacecraft with success for the case where the chaser begins the mission at a position relatively close to the target.

Interesting results can also be seen when studying a case where the chaser starts at a position considerably further than the previous case. Assuming a initial position $x = [-10000; -20000; -8000; 6; 6; 3]^T$, we obtain the results shown in figures 4.9 and 4.10.

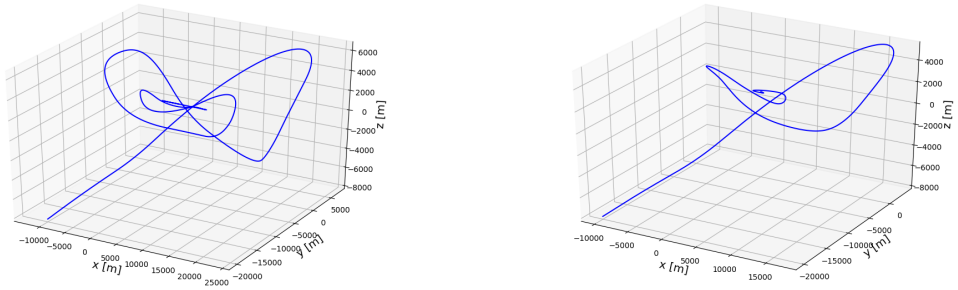

(a) LQR controller (b) H_∞ controller

Figure 4.9: Rendezvous trajectory performed by the chaser spacecraft to reach the target spacecraft with LQR controller (a) and H_∞ controller (b) for the initial state $x = [-10000; -20000; -8000; 6; 6; 3]^T$.

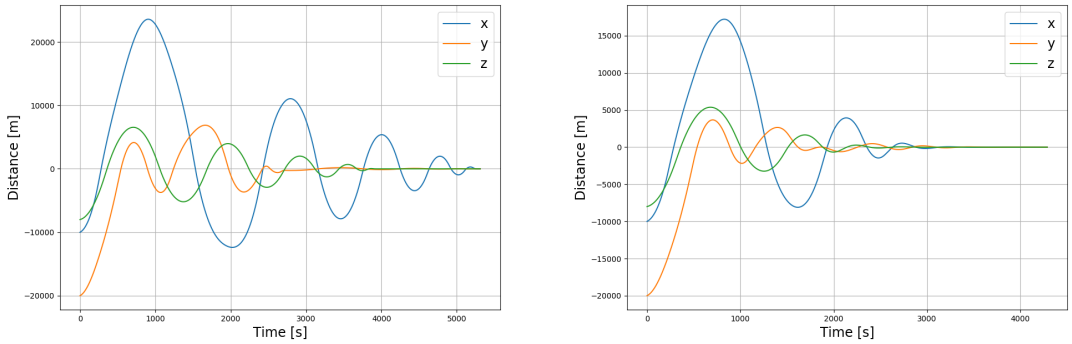

(a) LQR controller (b) H_∞ controller

Figure 4.10: Relative positions components x, y and z with LQR controller (a) and H_∞ controller (b) for the initial state $x = [-10000; -20000; -8000; 6; 6; 3]^T$.

It is clear to see through figures 4.10(a) and 4.10(b) that both the LQR controller and the H_∞ controller are able to guide the chaser until it reaches the target even though the trajectory is not direct and optimal as is recommended to perform the rendezvous mission. We can also note, through figures 4.9 and 4.10 that the LQR controller starts to show some difficulty in dampening the frequency of the oscillations when compared to the H_∞ controller, which can complete its mission in a considerably smaller time frame whilst having notably smaller amplitude for each oscillation as well as a minor number of oscillations until the chaser reaches the target. These disparities between the results obtained for both controllers translates to a much more direct route until the chaser spacecraft approaches its target.

Through analysis of figures 4.8 and 4.10 it is possible to conclude that while the LQR controller shows faster times of rendezvous for smaller trajectories, due to the fact that its linear nature makes it go straight to the target, it also demonstrates fewer depletion of the oscillations amplitude for greater distances. In contrast, the H_∞ controller presents better overall conditions for the mission, concluding rendezvous at approximately $4000s$ opposite to the LQR case, whilst showing considerably more dampening of the oscillations amplitude and frequency, which could lead to the mission benefiting from lower fuel usage and less risk of actuators saturation.

4.3 Optimization and Detailed Analysis

The results displayed previously are still far away from being the desired optimal approach to the rendezvous problem with the rendezvous time and the fuel usage being two rather important features that are to be subject to improvement in most rendezvous studies and projects in order to increase the success rate and efficiency of each rendezvous mission.
Bryson's method described in chapter 3 yields good results by working with the constants η_i and λ_i for the purpose of optimizing the mission.
For correct use of Bryson's method there is the requirement of ascertain the maximum allowed values for the state and control, $x_{i,max}$ and $u_{i,max}$, respectively. These parameters are intimately dependent of the control surfaces physical properties and, as such, its deliberation is limited to the technology available. For the purpose of this dissertation, the maximum state values, $x_{i,max}$, were set as the initial state parameters, x_0 and the maximum control values, $u_{i,max}$, were fixed at the propulsive control thrusts, $40N$, $40N$ and $20N$ mentioned previously.
Starting with the state weighting matrix, $Q \in \mathbb{R}^{6X6}$, it is possible to alter the convergence rate of the relative motion states as well as the smoothness of the rendezvous trajectory, by carefully selecting the optimal values for $\eta_i (i = 1, 2, 3, 4, 5, 6)$. Through an iteration process of trial and error and having in consideration the condition mentioned in chapter 3, $\forall_i\ \eta_i \geq 1$, it was possible to obtain the satisfactory results of $\eta = [114200000; 354200000; 76300000; 1164000; 581800; 231000]^T$ for the LQR case and $\eta = [94500000; 388000000; 7130000; 54670000; 35200000; 10220000]^T$ for the H_∞ case respectively.
Together with the maximum state values for the initial case $x = [-10000; -20000; -8000; 6; 6; 3]^T$, we obtain the following state weighting matrix, Q, for the LQR and H_∞ case respectively:

$$Q = \begin{bmatrix} \frac{114200000}{(-10000)^2} & 0 & 0 & 0 & 0 & 0 \\ 0 & \frac{354200000}{(-20000)^2} & 0 & 0 & 0 & 0 \\ 0 & 0 & \frac{76300000}{(-8000)^2} & 0 & 0 & 0 \\ 0 & 0 & 0 & \frac{1164000}{(6)^2} & 0 & 0 \\ 0 & 0 & 0 & 0 & \frac{581800}{(6)^2} & 0 \\ 0 & 0 & 0 & 0 & 0 & \frac{231000}{(3)^2} \end{bmatrix} \tag{4.21}$$

$$Q = \begin{bmatrix} \frac{94500000}{(-10000)^2} & 0 & 0 & 0 & 0 & 0 \\ 0 & \frac{388000000}{(-20000)^2} & 0 & 0 & 0 & 0 \\ 0 & 0 & \frac{7130000}{(-8000)^2} & 0 & 0 & 0 \\ 0 & 0 & 0 & \frac{54670000}{(6)^2} & 0 & 0 \\ 0 & 0 & 0 & 0 & \frac{35200000}{(6)^2} & 0 \\ 0 & 0 & 0 & 0 & 0 & \frac{10220000}{(3)^2} \end{bmatrix} \tag{4.22}$$

The subsequent results were obtained:

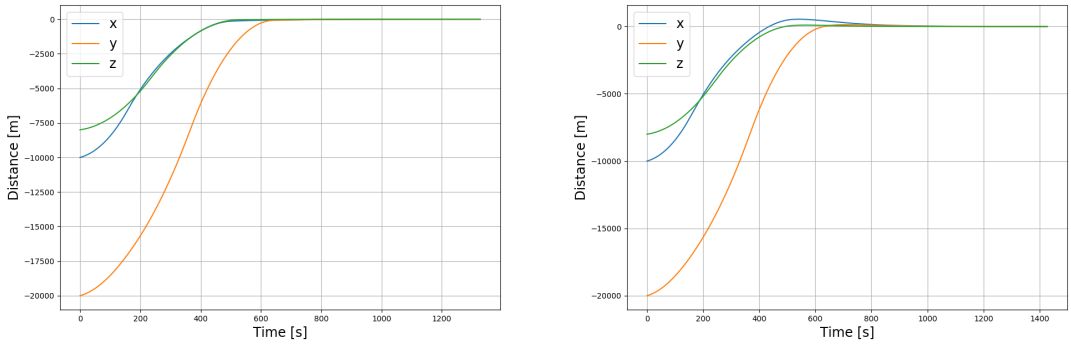

(a) LQR controller (b) H_∞ controller

Figure 4.11: Relative positions components x, y and z with LQR controller (a) and H_∞ controller (b) for the initial state $x = [-10000; -20000; -8000; 6; 6; 3]^T$ with optimal state weighting matrix, Q.

As it is possible to see through figures 4.11(a) and 4.11(b), the LQR controller as well as the robust H_∞ controller respond well to the alterations performed to the state weighting matrix showing in both cases a much more smooth transaction between the initial state, t_0, until the final state, t_f. Considerably lower times until rendezvous were obtained when compared to the case prior to the use of Bryson's method depicted in figures 4.10(a) and 4.10(b). Furthermore, a great improvement is seen for both cases in relation to the amplitude of each oscillation, with the initial state values no longer being surpassed for the entirety of the mission along with benefiting from considerably less oscillations to achieve rendezvous.

Lastly, rearranging the λ_i parameters in the control weighting matrix, $R \in \mathbb{R}^{3X3}$, which governs the fuel cost of the chase vehicle, it is possible to optimize the rendezvous to achieve fastest rendezvous, lower fuel cost or a compromise between both qualities, having in consideration the condition delineated previously as $\forall_i \; 0 < \lambda_i \leq 1$.

Contrary to the state weighting matrix, we have a much more linear response in the control weighting matrix as is portrayed in the set of figures displayed next:

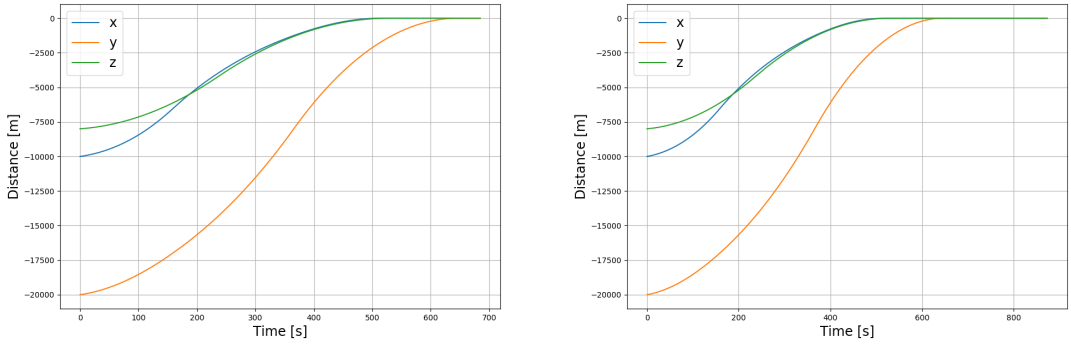

(a) LQR controller (b) H_∞ controller

Figure 4.12: Relative positions components x, y and z with LQR controller (a) and H_∞ controller (b) for the initial state $x = [-10000; -20000; -8000; 6; 6; 3]^T$ with $\lambda_i = 0.2$.

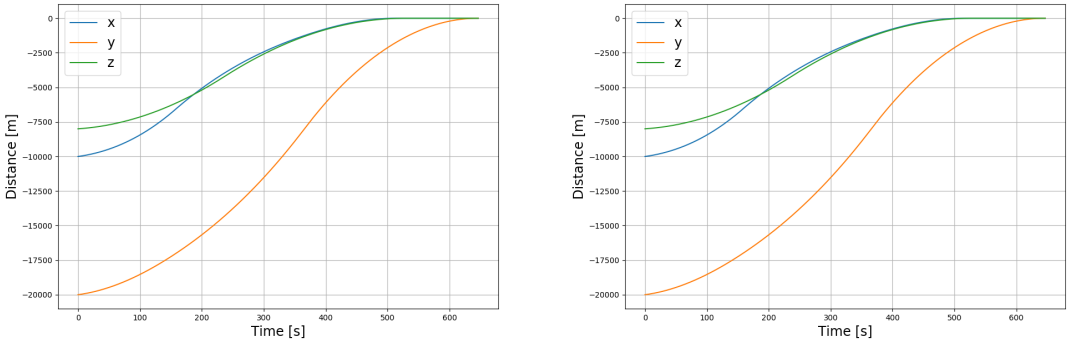

(a) LQR controller

(b) H_∞ controller

Figure 4.13: Relative positions components x, y and z with LQR controller (a) and H_∞ controller (b) for the initial state $x = [-10000; -20000; -8000; 6; 6; 3]^T$ with $\lambda_i = 1$.

It is possible to observe through figures A.1 and 4.13 that as λ_i increases from a value greater than 0.1 until it reaches the maximum value of 1, the time response of the system decreases, hence the time necessary for the chaser spacecraft to reach the target spacecraft is the lowest for $\lambda_i = 1$ and the greatest for $\lambda_i \approx 0.1$. This information is better portrayed through the additional figures displayed in appendix A. For the purpose of this dissertation, the constant λ_i will be set as 1, as is seen in matrix A.5, through all case studies in order to focus the optimization for faster response times.

$$R = \begin{bmatrix} \frac{1}{(40)^2} & 0 & 0 \\ 0 & \frac{1}{(40)^2} & 0 \\ 0 & 0 & \frac{1}{(20)^2}0 \end{bmatrix} \quad (4.23)$$

A more detailed and thorough analysis is now possible to perform with all the parameters determined. Continuing with the initial state, $x = [-10000; -20000; -8000; 6; 6; 3]^T$ with $\lambda_i = 1$, and employing the matrices 4.6, 4.11, 4.12, 4.13, 4.21, 4.22 and A.5 it is possible to solve the Algebraic Riccati Equations for the LQR and H_∞ controller described in chapter 3. The solution for the Algebraic Riccati Equation for the LQR and H_∞ controller are displayed in 4.24 and 4.25.

$$P = \begin{bmatrix} 20.0 \cdot 10^0 & -1.819 \cdot 10^0 & 0.00 \cdot 10^0 & 200 \cdot 10^0 & 4.60 \cdot 10^0 & 0.00 \cdot 10^0 \\ -1.819 \cdot 10^0 & 200 \cdot 10^0 & 0.00 \cdot 10^0 & -4.60 \cdot 10^0 & 199.9 \cdot 10^0 & 0.00 \cdot 10^0 \\ 0.00 \cdot 10^0 & 0.00 \cdot 10^0 & 200 \cdot 10^0 & 0.00 \cdot 10^0 & 0.00 \cdot 10^0 & 199.9 \cdot 10^0 \\ 20.0 \cdot 10^0 & -4.60 \cdot 10^0 & 0.00 \cdot 10^0 & 4.01 \cdot 10^3 & 18.15 \cdot 10^{-3} & 0.00 \cdot 10^0 \\ 4.60 \cdot 10^0 & 1.999 \cdot 10^0 & 0.00 \cdot 10^0 & 18.15 \cdot 10^{-3} & 4.00 \cdot 10^3 & 0.00 \cdot 10^0 \\ 0.00 \cdot 10^0 & 0.00 \cdot *10^0 & 199.9 \cdot 10^0 & 0.00 \cdot 10^0 & 0.00 \cdot 10^0 & 4.00 \cdot 10^3 \end{bmatrix} \quad (4.24)$$

$$P = \begin{bmatrix} 39.6 \cdot 10^0 & -2.63 \cdot 10^{-3} & 0.00 \cdot 10^0 & 770 \cdot 10^0 & 34.4 \cdot 10^0 & 0.00 \cdot 10^0 \\ -2.63 \cdot 10^{-3} & 39.6 \cdot 10^0 & 0.00 \cdot 10^0 & -34.4 \cdot 10^0 & 767 \cdot 10^0 & 0.00 \cdot 10^0 \\ 0.00 \cdot 10^0 & 0.00 \cdot 10^0 & 39.5 \cdot 10^0 & 0.00 \cdot 10^0 & 0.00 \cdot 10^0 & 767 \cdot 10^0 \\ 770 \cdot 10^0 & -34.4 \cdot 10^0 & 0.00 \cdot 10^0 & 29.8 \cdot 10^3 & 993 \cdot 10^{-3} & 0.00 \cdot 10^0 \\ 34.4 \cdot 10^0 & 767 \cdot 10^0 & 0.00 \cdot 10^0 & 993 \cdot 10^{-3} & 29.8 \cdot 10^3 & 0.00 \cdot 10^0 \\ 0.00 \cdot 10^0 & 0.00 \cdot 10^0 & 767 \cdot 10^0 & 0.00 \cdot 10^0 & 0.00 \cdot 10^0 & 29.8 \cdot 10^3 \end{bmatrix} \quad (4.25)$$

Both solutions to the Algebraic Riccati Equation are obtained through the use of the command solve_continous_are(A,B,Q,R) from $Python^{TM}$'s scipy.linalg library.

Therefore, implementing the equations acquired in chapter 3 to calculate the gain matrix, K, we have the following matrices 4.32 and 4.33, respectively:

$$K = \begin{bmatrix} 1.000 \cdot 10^{0} & -23.0 \cdot 10^{-3} & 0.00 \cdot 10^{0} & 20.0 \cdot 10^{0} & 90.7 \cdot 10^{-6} & 0.00 \cdot 10^{0} \\ 230 \cdot 10^{-3} & 1.000 \cdot 10^{0} & 0.00 \cdot 10^{0} & 90.7 \cdot 10^{-6} & 20.0 \cdot 10^{0} & 0.00 \cdot 10^{0} \\ 0.00 \cdot 10^{0} & 0.00 \cdot 10^{0} & 1.000 \cdot 10^{0} & 0.00 \cdot 10^{0} & 0.00 \cdot 10^{0} & 20.0 \cdot 10^{0} \end{bmatrix} \quad (4.26)$$

$$K = \begin{bmatrix} 36.6 \cdot 10^{-3} & -1.633 \cdot 10^{-3} & 0.00 \cdot 10^{0} & 1.418 \cdot 10^{0} & 47.2 \cdot 10^{-6} & 0.00 \cdot 10^{0} \\ 1.633 \cdot 10^{-3} & 36.4 \cdot 10^{-3} & 0.00 \cdot 10^{0} & 47.2 \cdot 10^{-6} & 1.416 \cdot 10^{0} & 0.00 \cdot 10^{0} \\ 0.00 \cdot 10^{0} & 0.00 \cdot 10^{0} & 36.4 \cdot 10^{-3} & 0.00 \cdot 10^{0} & 0.00 \cdot 10^{0} & 1.416 \cdot 10^{0} \end{bmatrix} \quad (4.27)$$

All the simulation results presented bellow are obtained from a simulation system built on the two-body problem.

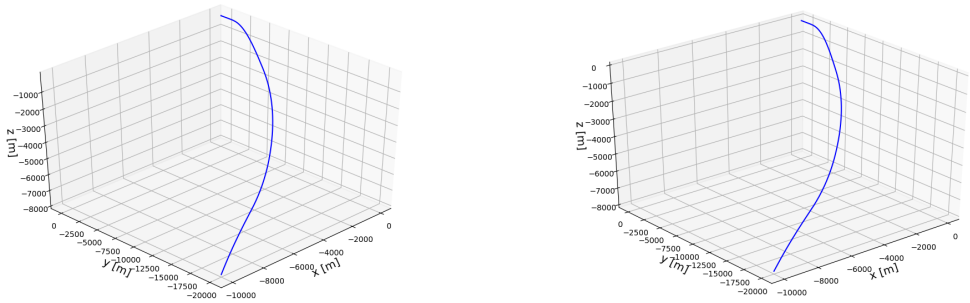

(a) LQR controller (b) H_{∞} controller

Figure 4.14: Rendezvous trajectory performed by the chaser spacecraft to reach the target spacecraft with LQR controller (a) and H_{∞} controller (b) for the initial state $x = [-10000; -20000; -8000; 6; 6; 3]^{T}$.

It is evident to see when analysing figures 4.9 and 4.14, that a much more smooth and direct trajectory to the target was obtained. The LQR controller along with the H_{∞} controller responded well to the optimization process obtaining a rather similar rendezvous trajectory as can be observed with figures 4.14(a) and 4.14(b).

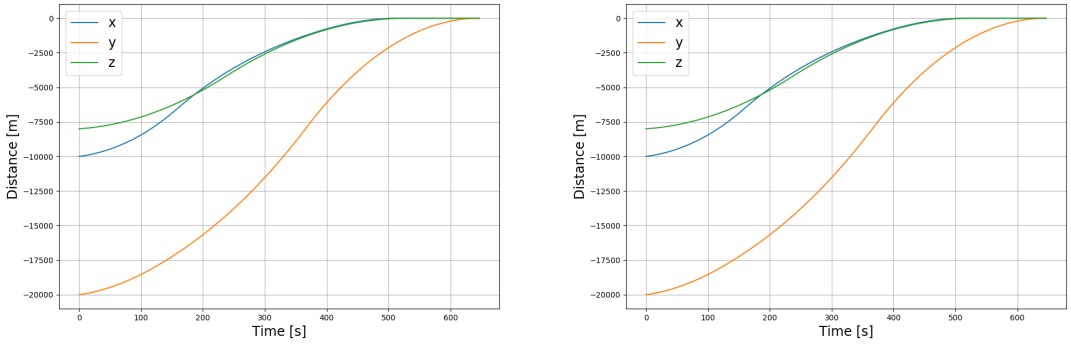

(a) LQR controller (b) H_∞ controller

Figure 4.15: Relative positions components x, y and z with LQR controller (a) and H_∞ controller (b) for the initial state $x = [-10000; -20000; -8000; 6; 6; 3]^T$.

Figures 4.15(a) and 4.15(b) show the rendezvous trajectory segregated along the directions x, y and z for the LQR and H_∞ controller, respectively. The similarity between the results obtained for both cases, is once more evident and no clear benefit can be seen from the use of one control method opposite to the other.

Figures 4.16, 4.17 and 4.18 serve as evidence that all relative position components converge asymptotically to zero. The disturbances were greatly attenuated and all position components approached the target through a smooth course with no oscillations.

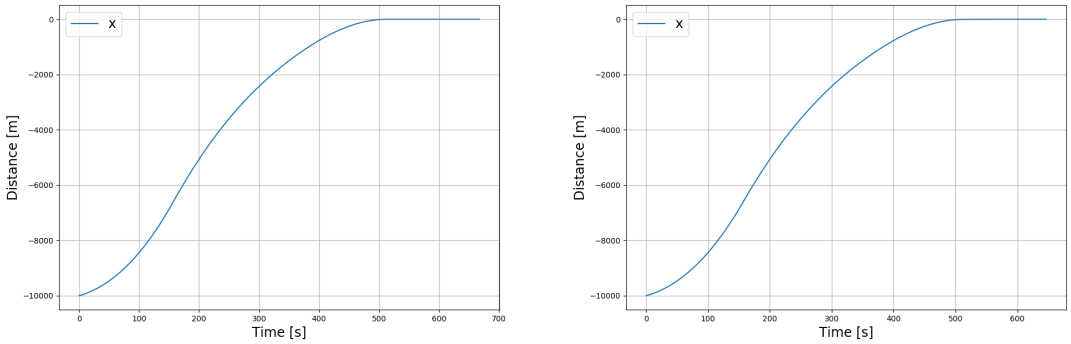

(a) LQR controller (b) H_∞ controller

Figure 4.16: Relative position component x with LQR controller (a) and H_∞ controller (b) for the initial state $x = [-10000; -20000; -8000; 6; 6; 3]^T$.

The velocity components of the state of the chaser spacecraft are portrayed with figures 4.19 to 4.25.

Through figure 4.19 we note that that the velocity component, u, increases for both cases from an initial positive value and then it starts decreasing until it reaches approximately zero. Both controllers present closely the same behaviour notwithstanding that some disparity can be observed in the zones of transaction.

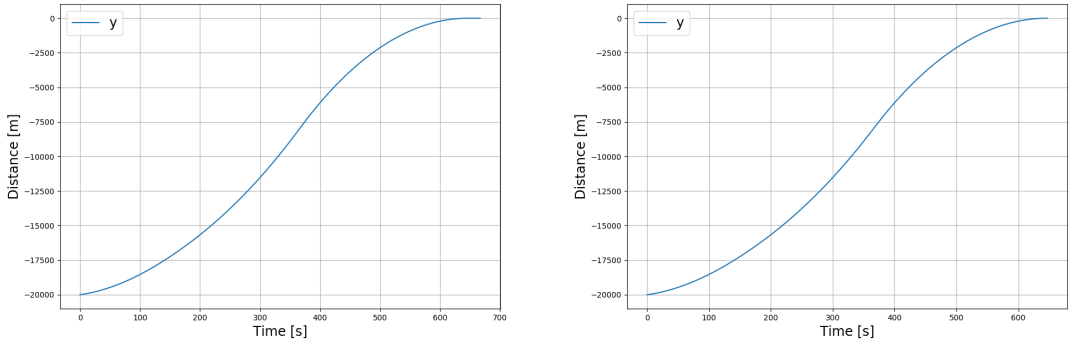

(a) LQR controller (b) H_∞ controller

Figure 4.17: Relative position component y with LQR controller (a) and H_∞ controller (b) for the initial state $x = [-10000; -20000; -8000; 6; 6; 3]^T$.

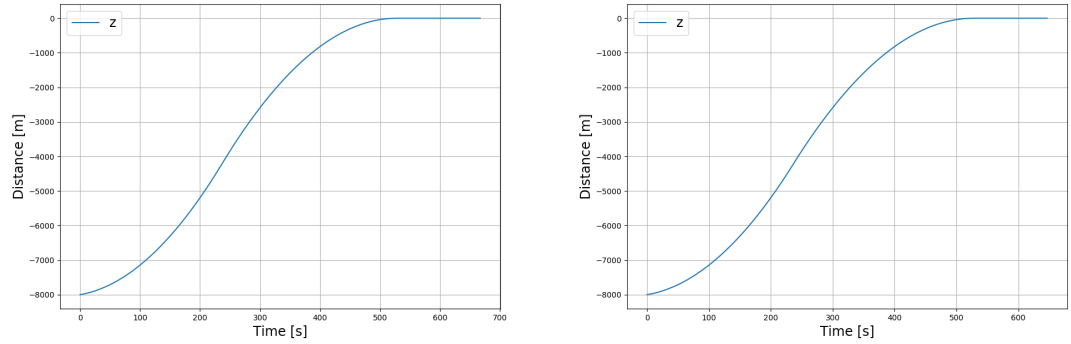

(a) LQR controller (b) H_∞ controller

Figure 4.18: Relative position component z with LQR controller (a) and H_∞ controller (b) for the initial state $x = [-10000; -20000; -8000; 6; 6; 3]^T$.

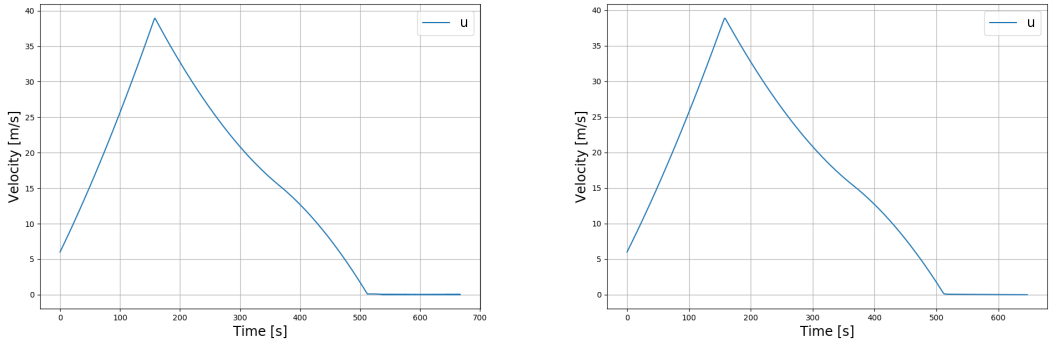

(a) LQR controller (b) H_∞ controller

Figure 4.19: Relative velocity component u with LQR controller (a) and H_∞ controller (b) for the initial state $x = [-10000; -20000; -8000; 6; 6; 3]^T$.

An enlargement of the transaction zones was performed to better analyse the phenomenons present. When paralleling figures 4.20(a) and 4.20(b) along with figures 4.21(a) and 4.21(b) we note that the LQR controller presents a more rough transaction from positive inclination to negative inclination when compared to the robust H_∞ controller. The transaction is specially

aggravated when the chaser spacecraft is nearing the target spacecraft, with the LQR controller denoting an up and down behaviour at a considerably fast pace that shows a great contrast with the smooth transaction generated with the robust H_∞ controller.

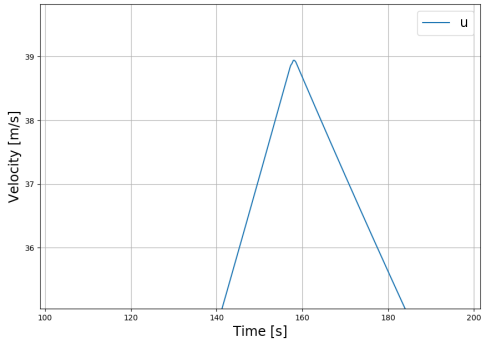

(a) LQR controller

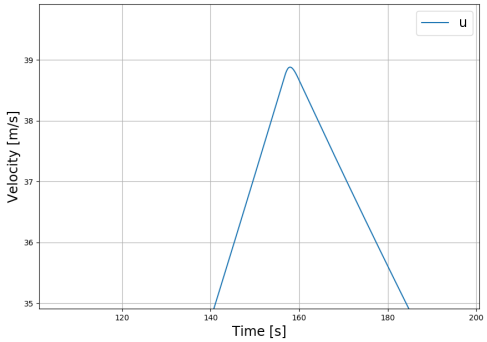

(b) H_∞ controller

Figure 4.20: Relative velocity component u shift from positive to negative tendency with LQR controller (a) and H_∞ controller (b) for the initial state $x = [-10000; -20000; -8000; 6; 6; 3]^T$.

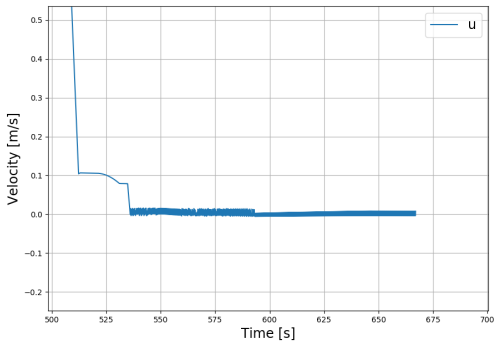

(a) LQR controller

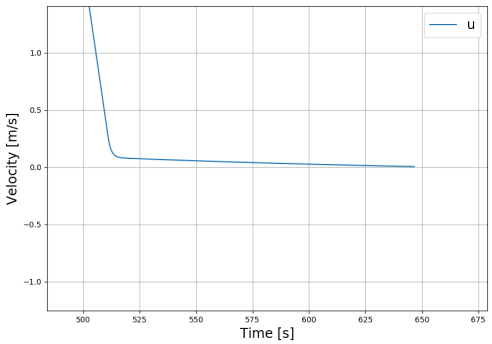

(b) H_∞ controller

Figure 4.21: Relative velocity component u transaction when reaching terminal phase with LQR controller (a) and H_∞ controller (b) for the initial state $x = [-10000; -20000; -8000; 6; 6; 3]^T$.

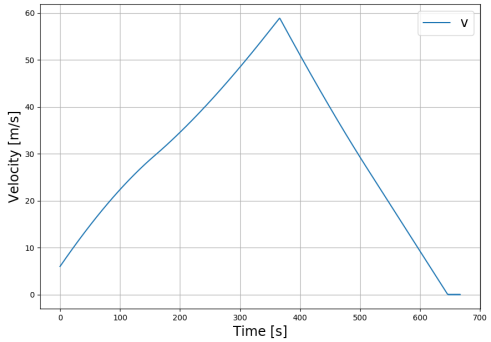

(a) LQR controller

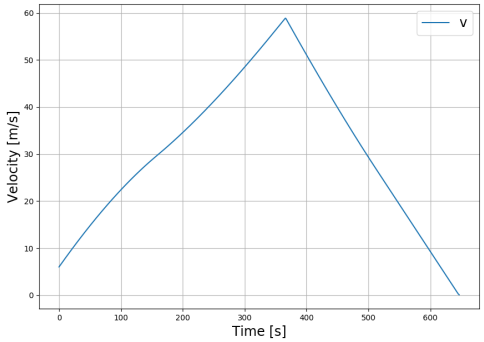

(b) H_∞ controller

Figure 4.22: Relative velocity component v with LQR controller (a) and H_∞ controller (b) for the initial state $x = [-10000; -20000; -8000; 6; 6; 3]^T$.

The same phenomenon is possible to perceive throughout figures 4.22, 4.23, 4.24 and 4.25. A smooth increase is observed for both components, v and w, similar to the previously analysed velocity component, u, followed by a decrease in speed when the chaser spacecraft is nearing the target spacecraft. The approximation, once again, shows an erratic behaviour for the velocities components, v and w, obtained through the LQR controller, the v component showing considerably less up and down behaviour due to the fact that the simulations end as the velocity component, v, reaches zero as it was the last of the components to converge to the stable condition, which is to be expected for the reason that the position, y, of the initial state is the farthest from the target spacecraft.

When comparing figures 4.23(a) with 4.23(b) and 4.25(a) with 4.25(b) it is plain to see that the robust H_∞ controller generates greatly improved transactions with much superior behaviour.

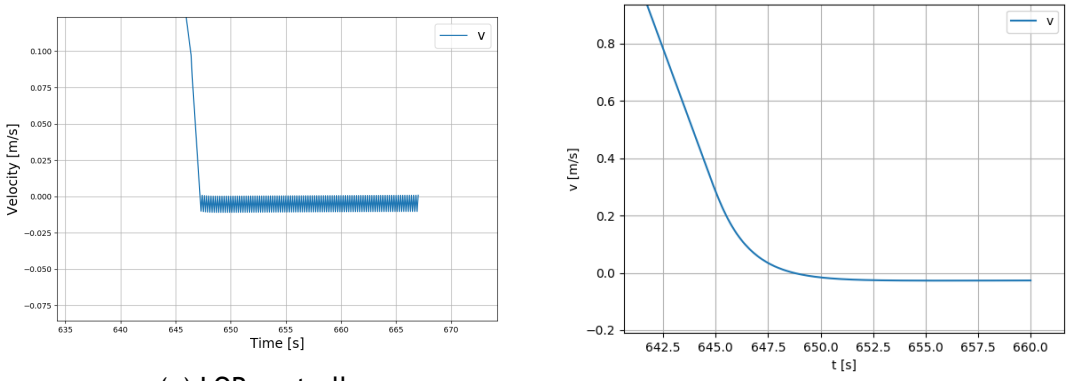

(a) LQR controller

(b) H_∞ controller

Figure 4.23: Relative velocity component v transaction when reaching terminal phase with LQR controller (a) and H_∞ controller (b) for the initial state $x = [-10000; -20000; -8000; 6; 6; 3]^T$.

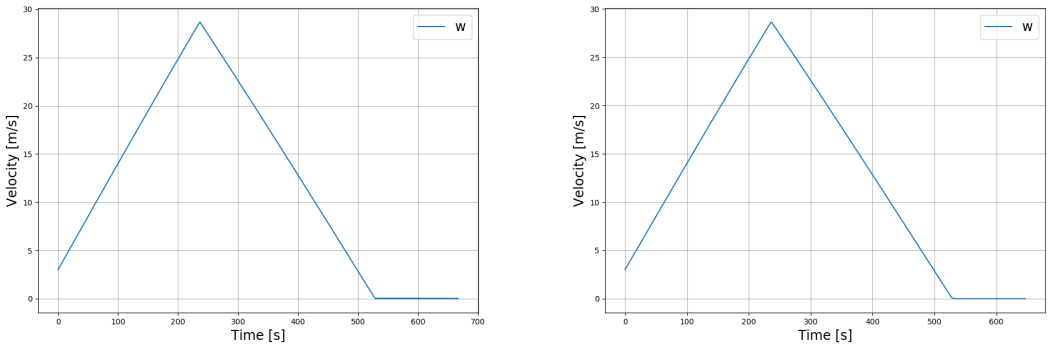

(a) LQR controller

(b) H_∞ controller

Figure 4.24: Relative velocity component w with LQR controller (a) and H_∞ controller (b) for the initial state $x = [-10000; -20000; -8000; 6; 6; 3]^T$.

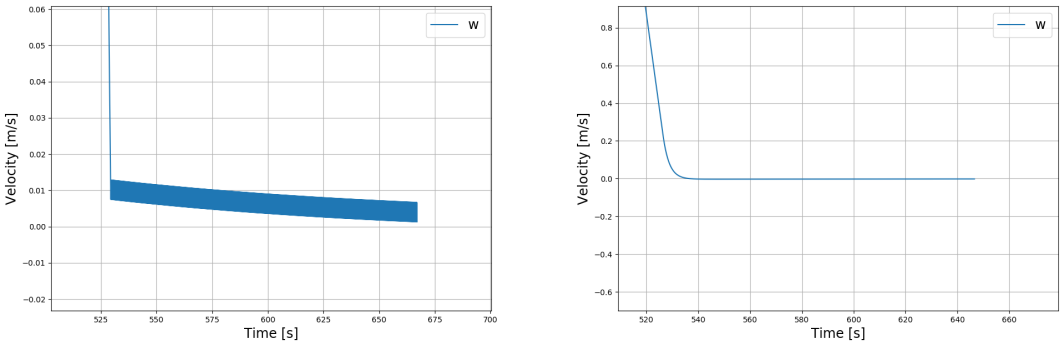

(a) LQR controller (b) H_∞ controller

Figure 4.25: Relative velocity component w transaction when reaching terminal phase with LQR controller (a) and H_∞ controller (b) for the initial state $x = [-10000; -20000; -8000; 6; 6; 3]^T$.

Figures 4.26, 4.27 and 4.28 elucidate on the phenomenons observed in the earlier figures. Through figure 4.26 we can understand the velocity behaviour displayed in figure 4.19, with the earlier increase in velocity, u, being related to the initial positive control thrust $(+40N)$ followed by a decrease in speed due to the change in control thrust to a negative value $(-40N)$. The odd behaviour depicted in figures 4.21(a) and 4.25(a) can be explained by observing figures 4.26(a) and 4.28(a) where the the control thrusts generated through the LQR controller present a large quantity of shifts from positive thrust to negative thrust elucidating on the phenomenon perceived in figures 4.19(a) and 4.24(a) where the velocity was subject to constant change between acceleration and deceleration. When analysing figures 4.26(b) and 4.28(b) we note that the behaviour described previously is not present which explains why there is a much more smooth velocity transactions as is perceived in figures 4.21(b) and 4.25(b) where there are no sharp turns present.

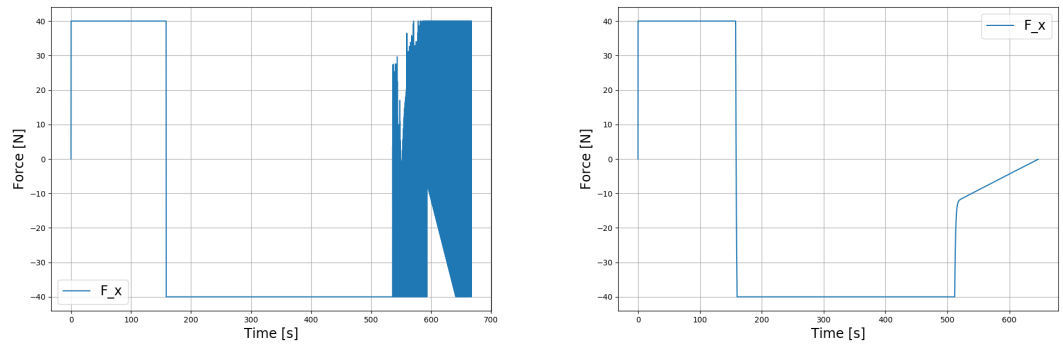

(a) LQR controller (b) H_∞ controller

Figure 4.26: Propulsive thrust component along the direction x with LQR controller (a) and H_∞ controller (b) for the initial state $x = [-10000; -20000; -8000; 6; 6; 3]^T$.

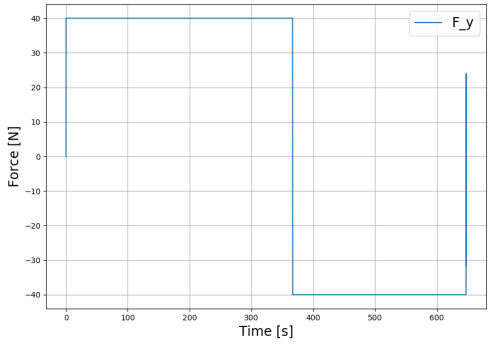

(a) LQR controller

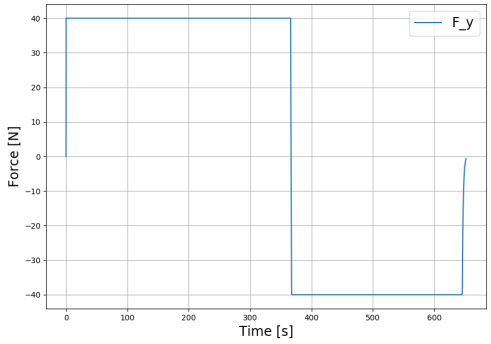

(b) H_∞ controller

Figure 4.27: Propulsive thrust component along the direction y with LQR controller (a) and H_∞ controller (b) for the initial state $x = [-10000; -20000; -8000; 6; 6; 3]^T$.

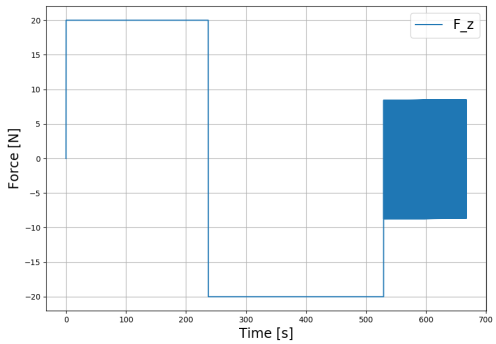

(a) LQR controller

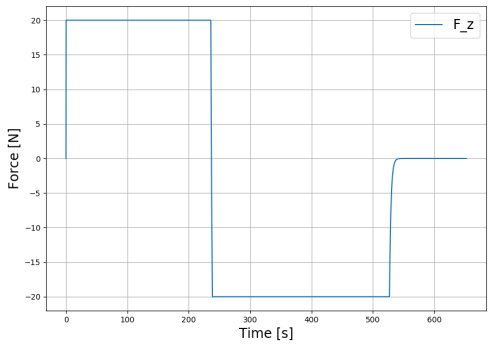

(b) H_∞ controller

Figure 4.28: Propulsive thrust component along the direction z with LQR controller (a) and H_∞ controller (b) for the initial state $x = [-10000; -20000; -8000; 6; 6; 3]^T$.

Two more case studies were analysed in order to compare to the earlier results in analysing the trajectory behaviour, velocity and control forces history when applying a LQR controller and a robust H_∞ controller with one being presented next and the other being present in appendix B. The initial state for this case study is $x = [-25000; 30000; 35000; 8; -7; -3]^T$ and by means of an initial simulation with the weighting matrices Q and R set as 4.18 and 4.19 it yield the results displayed in figures 4.29 and 4.30.

It is clear to note that there is a great disparity between the trajectory generated through the LQR controller in figure 4.29(a) when compared with the trajectory generated from the robust H_∞ controller in figure 4.29(b). Figure 4.29(a) illustrates a trajectory composed of sharp turns and erratic movement where figure 4.29(b) denotes a considerably more circular route from the chaser spacecraft to the target spacecraft.

Figure 4.30 augment the information by displaying the partitioning of the movement in three components x, y and z and giving information of the time for each instant location. When relating figure 4.30(a) with 4.30(b) it is clear to see that the H_∞ controller benefits from a lesser number of oscillations until each relative position component converges to zero, from smaller oscillation amplitude when compared to the LQR controller and from a significantly reduced time frame for the chaser spacecraft to reach the target spacecraft. Once more, Bryson's method is applied to generate the optimum weighting matrices Q and R and through an

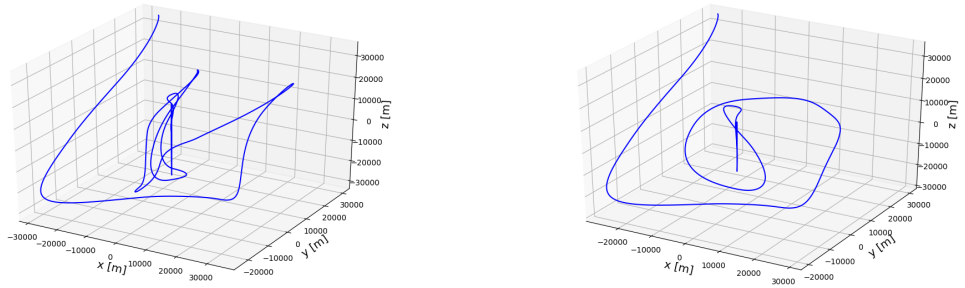

(a) LQR controller (b) H_∞ controller

Figure 4.29: Rendezvous trajectory performed by the chaser spacecraft to reach the target spacecraft with LQR controller (a) and H_∞ controller (b) for the initial state $x = [-25000; 30000; 35000; 8; -7; -3]^T$.

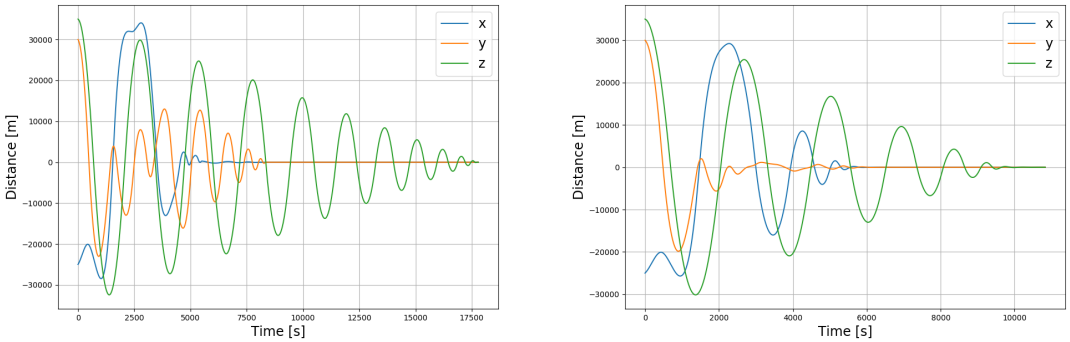

(a) LQR controller (b) H_∞ controller

Figure 4.30: Relative positions components x, y and z with LQR controller (a) and H_∞ controller (b) for the initial state $x = [-25000; 30000; 35000; 8; -7; -3]^T$.

iteration of trial and error yield the matrices 4.28 and 4.29. We note that for the initial the state $x = [-25000; 30000; 35000; 8; -7; -3]^T$, the weighting matrices 4.28 and 4.29 for optimal results presents higher values for $\eta_i (i = 1, 2, 3, 4, 5, 6)$ when compared with the weighting matrices 4.21 and 4.22 for the initial state $x = [-10000; -20000; -8000; 6; 6; 3]^T$ which is due to the increase in distance between the target and the chaser spacecraft.

$$Q = \begin{bmatrix} \frac{9831000000000}{(-25000)^2} & 0 & 0 & 0 & 0 & 0 \\ 0 & \frac{2139000000000}{(30000)^2} & 0 & 0 & 0 & 0 \\ 0 & 0 & \frac{13710000000}{(35000)^2} & 0 & 0 & 0 \\ 0 & 0 & 0 & \frac{17480000000}{(8)^2} & 0 & 0 \\ 0 & 0 & 0 & 0 & \frac{5550000000}{(-7)^2} & 0 \\ 0 & 0 & 0 & 0 & 0 & \frac{12550000}{(-3)^2} \end{bmatrix} \tag{4.28}$$

$$Q = \begin{bmatrix} \frac{3400000000}{(-25000)^2} & 0 & 0 & 0 & 0 & 0 \\ 0 & \frac{1080000000}{(30000)^2} & 0 & 0 & 0 & 0 \\ 0 & 0 & \frac{1080000000}{(35000)^2} & 0 & 0 & 0 \\ 0 & 0 & 0 & \frac{64100000}{(8)^2} & 0 & 0 \\ 0 & 0 & 0 & 0 & \frac{126700000}{(-7)^2} & 0 \\ 0 & 0 & 0 & 0 & 0 & \frac{60000000}{(-3)^2} \end{bmatrix} \tag{4.29}$$

The weighting matrix R is set as A.5 in the same vein as was mentioned previously and together with matrices 4.13, 4.11, 4.6, 4.12, 4.28 and 4.29 the solution to the algebraic riccati equation becomes 4.30 and 4.31 for the LQR controller and the H_∞ controller, respectively.

$$P = \begin{bmatrix} 20.0 \cdot 10^0 & -1.819 \cdot 10^0 & 0.00 \cdot 10^0 & 200 \cdot 10^0 & 4.60 \cdot 10^0 & 0.00 \cdot 10^0 \\ -1.819 \cdot 10^0 & 20.0 \cdot 10^0 & 0.00 \cdot 10^0 & -4.60 \cdot 10^0 & 199.9 \cdot 10^0 & 0.00 \cdot 10^0 \\ 0.00 \cdot 10^0 & 0.00 \cdot 10^0 & 20.0 \cdot 10^0 & 0.00 \cdot 10^0 & 0.00 \cdot 10^0 & 199.9 \cdot 10^0 \\ 200 \cdot 10^0 & -4.60 \cdot 10^0 & 0.00 \cdot 10^0 & 4.01 \cdot 10^3 & 18.15 \cdot 10^{-3} & 0.00 \cdot 10^0 \\ 4.60 \cdot 10^0 & 1.999 \cdot 10 & 0.00 \cdot 10^0 & 18.15 \cdot 10^{-3} & 4.00 \cdot 10^3 & 0.00 \cdot 10^0 \\ 0.00 \cdot 10^0 & 0.00 \cdot 10^0 & 199.9 \cdot 10^0 & 0.00 \cdot 10^0 & 0.00 \cdot 10^0 & 4.00 \cdot 10^3 \end{bmatrix} \tag{4.30}$$

$$P = \begin{bmatrix} 39.6 \cdot 10^0 & -2.63 \cdot 10^{-3} & 0.00 \cdot 10^0 & 770 \cdot 10^0 & 34.4 \cdot 10^0 & 0.00 \cdot 10^0 \\ -2.63 \cdot 10^{-3} & 39.6 \cdot 10^0 & 0.00 \cdot 10^0 & -34.4 \cdot 10^0 & 767 \cdot 10^0 & 0.00 \cdot 10^0 \\ 0.00 \cdot 10^0 & 0.00 \cdot 10^0 & 39.5 \cdot 10^0 & 0.00 \cdot 10^0 & 0.00 \cdot 10^0 & 767 \cdot 10^0 \\ 770 \cdot 10^0 & -34.4 \cdot 10^0 & 0.00 \cdot 10^0 & 29.8 \cdot 10^3 & 993 \cdot 10^{-3} & 0.00 \cdot 10^0 \\ 34.4 \cdot 10^0 & 767 \cdot 10^0 & 0.00 \cdot 10^0 & 993 \cdot 10^{-3} & 29.8 \cdot 10^3 & 0.00 \cdot 10^0 \\ 0.00 \cdot 10^0 & 0.00 \cdot 10^0 & 76.7 \cdot 10^0 & 0.00 \cdot 10^0 & 0.00 \cdot 10^0 & 29.8 \cdot 10^3 \end{bmatrix} \tag{4.31}$$

The equations mentioned in chapter 3 were employed to generate the following gain matrices, K, represented in matrices 4.32 and 4.33.

$$K = \begin{bmatrix} 1.000 \cdot 10^0 & -23.0 * 10^{-3} & 0.00 * 10^0 & 20.0 * 10^0 & 90.7 * 10^{-6} & 0.00 * 10^0 \\ 23.0 * 10^{-3} & 1.000 * 10^0 & 0.00 * 10^0 & 90.7 * 10^{-6} & 20.0 * 10^0 & 0.00 * 10^0 \\ 0.00 * 10^0 & 0.00 * 10^0 & 1.000 * 10^0 & 0.00 * 10^0 & 0.00 * 10^0 & 20.0 * 10^0 \end{bmatrix} \tag{4.32}$$

$$K = \begin{bmatrix} 36.6 * 10^{-3} & -1.633 * 10^{-3} & 0.00 * 10^0 & 1.418 * 10^0 & 47.2 * 10^{-6} & 0.00 * 10^0 \\ 1.633 * 10^{-3} & 36.4 * 10^{-3} & 0.00 \cdot 10^0 & 47.2 \cdot 10^{-6} & 1.416 \cdot 10^0 & 0.00 \cdot 10^0 \\ 0.00 \cdot 10^0 & 0.00 \cdot 10^0 & 36.4 \cdot 10^{-3} & 0.00 \cdot 10^0 & 0.00 \cdot 10^0 & 1.416 \cdot 10^0 \end{bmatrix} \tag{4.33}$$

All the simulation results are, once more, obtained from a simulation system based on the two-body problem.

The rendezvous trajectory displayed in figure 4.31 shows great improvement when compared with figure 4.29 with a much more direct route from the chaser spacecraft until the target spacecraft. The optimization process performed to the LQR and H_∞ controllers obtained rather similar trajectories as can be seen through figures 4.31(a) and 4.31(b). Figure 4.32 confirms the similarities perceived with figure 4.31 and also reveals that the trajectory generated with the H_∞ controller converges faster to zero when compared to the trajectory obtained through

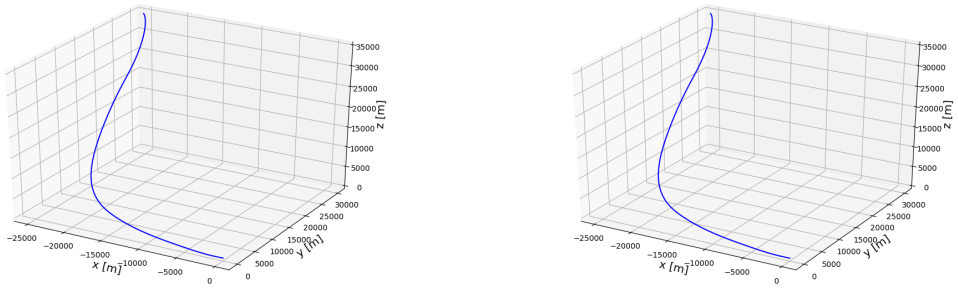

(a) LQR controller (b) H_∞ controller

Figure 4.31: Rendezvous trajectory performed by the chaser spacecraft to reach the target spacecraft with LQR controller (a) and H_∞ controller (b) for the initial state $x = [-25000; 30000; 35000; 8; -7; -3]^T$.

the LQR controller. The following figures 4.33, 4.34 and 4.35 provide a better overview of each movement separately and allow for better comparison between the LQR and H_∞ controller. Figure 4.33(a) 4.33(b) represent the movement performed by the chaser spacecraft on the x

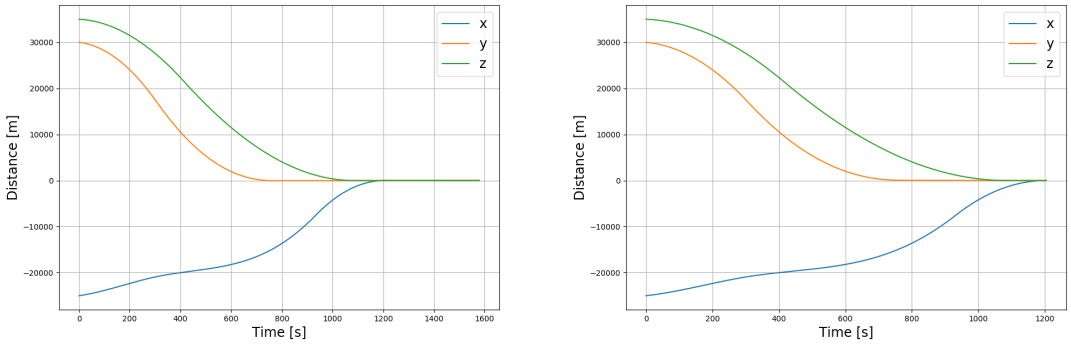

(a) LQR controller (b) H_∞ controller

Figure 4.32: Relative positions components x, y and z with LQR controller (a) and H_∞ controller (b) for the initial state $x = [-25000; 30000; 35000; 8; -7; -3]^T$.

direction until it reaches the target spacecraft. It can also be seen that both figures illustrate a a shift in concavity in the earlier stages until halfway and, following that, the trajectory stabilizes and converges to zero. The trajectory in figure 4.33(b) present a more subtle concavity change when compared to figure 4.33(a) which is due to the fact that the H_∞ method provides a more robust controller.

Figures 4.34 and 4.35 present similar conclusion as what was previously mentioned with figures 4.34(a) and 4.35(a) displaying almost similar results with figures 4.34(b) and 4.35(b) where the main difference is the convergence time, meaning that the movements along direction y and z obtained with the LQR controller converge to zero at a later time than the ones obtained through the H_∞ controller. The following figures 4.36, 4.37, 4.38, 4.39, 4.40 and 4.41 provide an outline of the velocity components behaviour and history with relation to time and also a closer view of the more problematic transactions perceived in the graphics obtained with the LQR controller.

Firstly, figure 4.36 presents the velocity component u history along the rendezvous time, with figure 4.36(a) being obtained with LQR controller and figure 4.36(b) through H_∞ controller. By

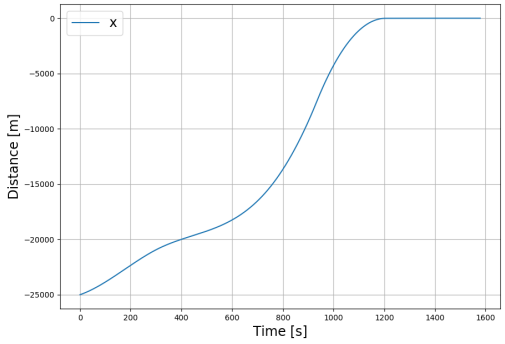

(a) LQR controller

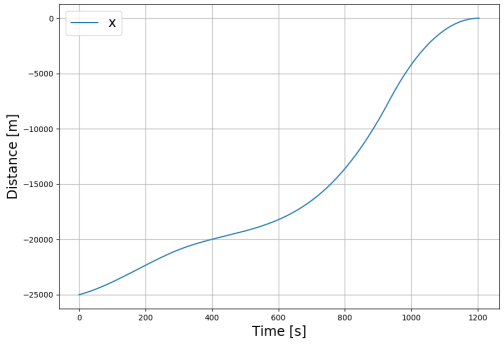

(b) H_∞ controller

Figure 4.33: Relative position component x with LQR controller (a) and H_∞ controller (b) for the initial state $x = [-25000; 30000; 35000; 8; -7; -3]^T$.

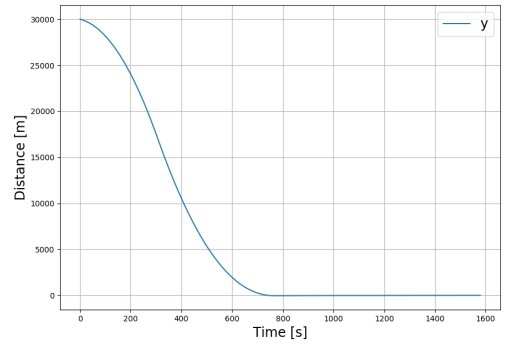

(a) LQR controller

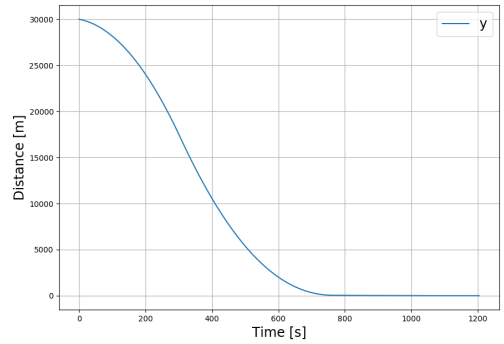

(b) H_∞ controller

Figure 4.34: Relative position component y with LQR controller (a) and H_∞ controller (b) for the initial state $x = [-25000; 30000; 35000; 8; -7; -3]^T$.

analysing the first 600 seconds it is possible to understand the behaviour portrayed in figure 4.33. Furthermore, the positive velocity, u, as well as the apparent positive acceleration in the earlier stages of rendezvous goes along with the fact that the initial position, x, has negative value, so the chaser spacecraft increases the position component, x, in order to reach the target spacecraft. Figure 4.36(a) shows close resemblance with figure 4.36(b) despite the fact that in figure 4.36(a) there appears to be some irregularities when the velocity, u, reaches its maximum value and then suffer a deceleration until it reaches zero as well as when the chaser spacecraft is almost reaching the terminal phase with zero velocity, u, in contrast with figure 4.36(b) where smooth transactions are presented along the entirety of the rendezvous process.

A closer look is provided with figure 4.37(b) presenting the area where the velocity, u, reaches its maximum value and figure 4.37(b) offers a zoomed area of the terminal phase where the velocity, u, is almost zero. Through figure 4.37(a) we note a sharp transaction when the velocity, u, reaches its maximum value and figure 4.37(b) also denotes a sharp decrease in velocity until almost zero followed by an odd behaviour of intense up and down through the terminal phase. The constant and very intense up and down behaviour presented in figure 4.37(b) would imply higher fuel cost and the possibility of being susceptible to external disturbances due to this behaviour not being under control. All these phenomenons occur only for the LQR controller case as can be seen in figure 4.36(b) where the velocity, u, starts nearing zero is subject to

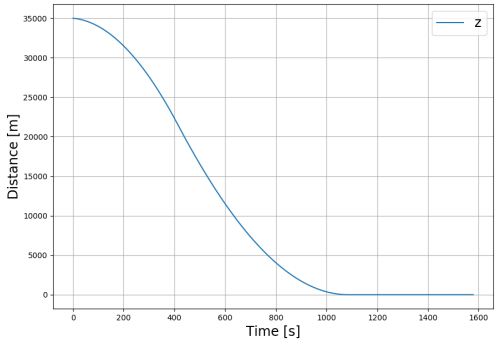

(a) LQR controller

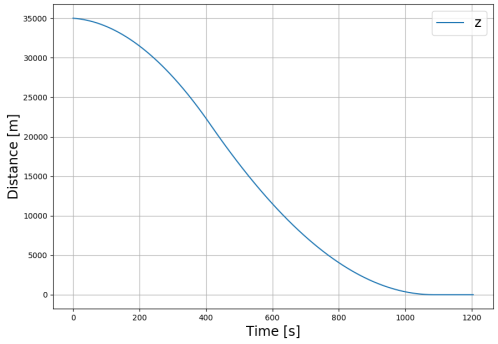

(b) H_∞ controller

Figure 4.35: Relative position component z with LQR controller (a) and H_∞ controller (b) for the initial state $x = [-25000; 30000; 35000; 8; -7; -3]^T$.

lower intensity decelerations providing a more smooth transaction to zero.

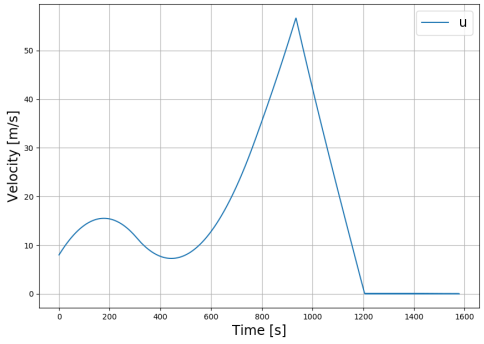

(a) LQR controller

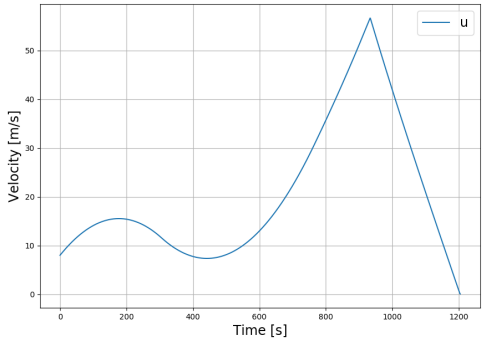

(b) H_∞ controller

Figure 4.36: Relative velocity component u with LQR controller (a) and H_∞ controller (b) for the initial state $x = [-25000; 30000; 35000; 8; -7; -3]^T$.

Figures 4.38, 4.39, 4.40 and 4.41 contribute with similar information as the previously provided. The position components, y and z, both have positive value and on that account the velocity components, v and w, are negative for the chaser to reach the target spacecraft and both components increase in module until they reach the module maximum for each velocity component succeeded by an acceleration with the aim of increasing the velocities components, v and w, from negative value until zero as can be seen in figures 4.38 and 4.40. The moments where the velocities components, v and w, present a change in behaviour and when the velocities reach near zero are, once again, amplified from figures 4.38(a) and 4.40(a) in order to provide a closer look to the odd behaviour denoted in the velocity components history provided through the LQR controller and are displayed in figures 4.39 and 4.41. Figure 4.39(a) and 4.41(a) present a non smooth transaction accompanied with the transaction from deceleration to acceleration as was perceived in figure 4.37(a) and figures 4.39(b) and 4.41(b) display the same abnormalities in the terminal phase as was observed in figure 4.37(b). The sharp transition in velocities and odd up and down behaviour when the velocities components, v and w, get near zero coupled with the same phenomenons perceived in figure 4.37(b) can explain why, even though, both controllers produce rather similar trajectories, there was a discrepancy in the

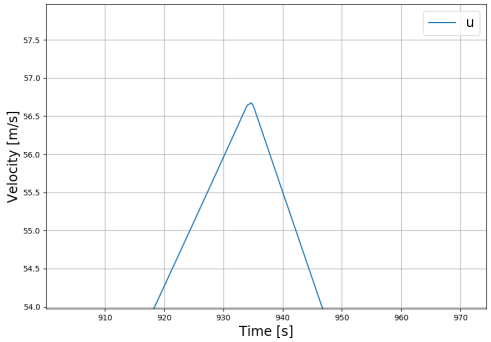

(a) Maximum value

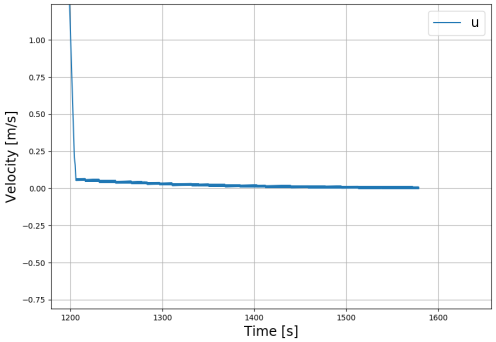

(b) Terminal phase

Figure 4.37: Zoomed area of velocity component v near maximum value(a) and for terminal phase (b) for the initial state $x = [-25000; 30000; 35000; 8; -7; -3]^T$ with LQR controller.

rendezvous time where the LQR controller generates a rendezvous time around the $1600s$ mark and the H_∞ controller makes the chaser reach the target spacecraft around the $1300s$ mark, meaning that the wasted movement perceived in figures 4.37(b), 4.39(b) and 4.41(b) increase the time necessary for the chaser to reach the target spacecraft.

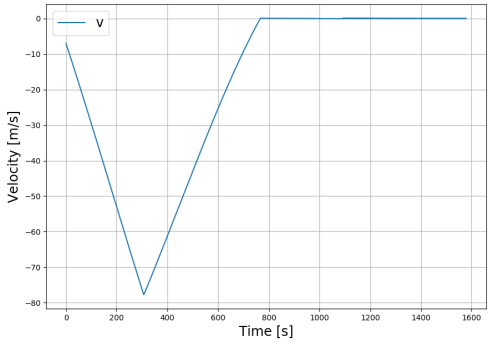

(a) LQR controller

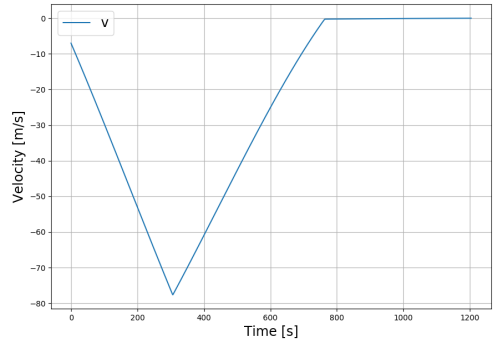

(b) H_∞ controller

Figure 4.38: Relative velocity component v with LQR controller (a) and H_∞ controller (b) for the initial state $x = [-25000; 30000; 35000; 8; -7; -3]^T$.

The succeeding figures 4.42, 4.43 and 4.44 complement the information formerly provided. Figure 4.42 relates with figure 4.36 and exposes why there is an increase in velocity until the $900s$ mark followed by a deceleration in order for the velocity component, u, converge to zero. The same information can be perceived when relating figures 4.43 and 4.44 with figures 4.38 and 4.40, where the initial deceleration denoted in the both figures 4.38 and 4.40 being related to the the negative control force ($-40N$) portrayed in figures 4.43 and 4.44, followed by a positive control force ($+40N$) that explains the acceleration displayed when the velocities components, v and w, reach the maximum in module value in figures 4.38 and 4.40. The difference in behaviour displayed by the velocity history represented in figures 4.36, 4.38 and 4.40 when comparing the LQR controller with the robust H_∞ controller is explained through figures 4.42, 4.43 and 4.44 with the erratic behaviour of constant accelerations followed by decelerations in the terminal phases represented in figures 4.36(a), 4.38(a) and 4.40(a) being related to the constant change in attitude seen in figures 4.42(a), 4.43(a) and 4.44(a) where the control force

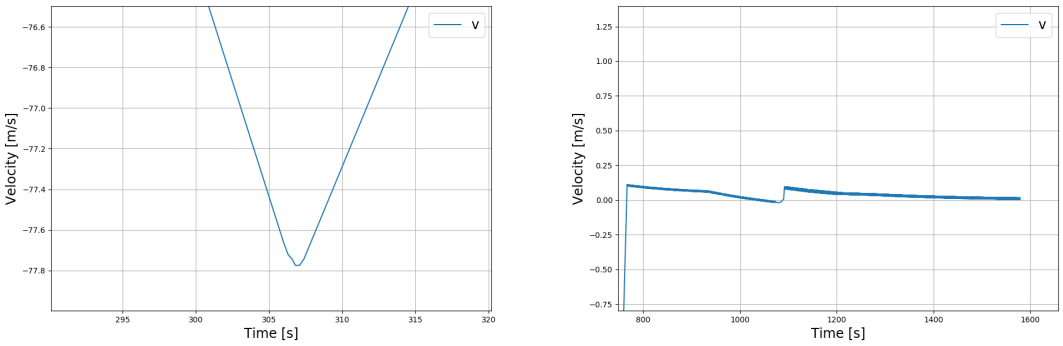

(a) Maximum value (b) Terminal phase

Figure 4.39: Zoomed area of velocity component v near maximum value(a) and for terminal phase (b) for the initial state $x = [-25000; 30000; 35000; 8; -7; -3]^T$ with LQR controller.

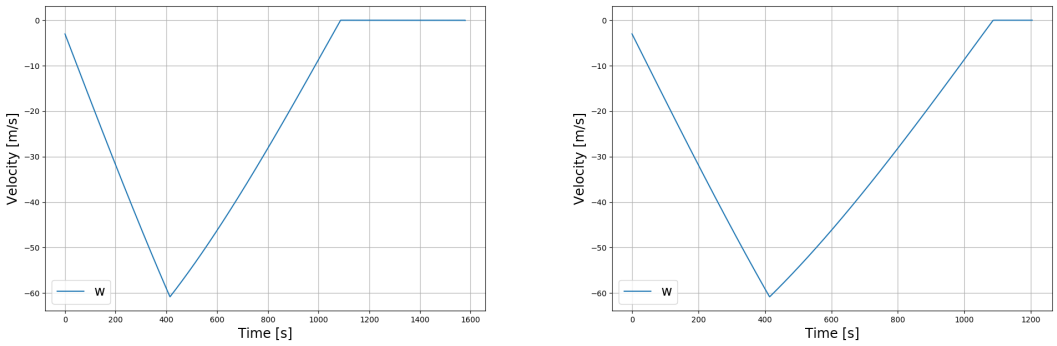

(a) LQR controller (b) H_∞ controller

Figure 4.40: Relative velocity component w with LQR controller (a) and H_∞ controller (b) for the initial state $x = [-25000; 30000; 35000; 8; -7; -3]^T$.

changes from positive ($+40N$) to negative ($-40N$) at each iteration opposite to what is seen in figures 4.42(b), 4.43(b) and 4.44(b) with the slow decrease in control force explaining the smooth convergence portrayed in figures 4.36(b), 4.38(b) and 4.40(b).

The results displayed in the current chapter confirms that the LQR controller along with the robust H_∞ controller can be used to solve the rendezvous problem between two different spacecraft . The LQR controller provides great results when the initial state presents close proximity between the chaser and target spacecraft, however, as the distance increases the LQR controller results pale in comparison with the H_∞ controller. The H_∞ controller presents a more robust control of the chaser state providing close to optimal results even as the distance between the chaser and target spacecraft increases, as well as better behaviour in the presence of uncertainties and perturbations by guaranteeing that in all situations the chaser always reaches the target spacecraft. It is important to note that all comparisons performed between the LQR controller and the H_∞ controller are performed resorting to different weighting matrices meaning that the optimal point to one control method is different than the other case and a comparison between both controllers is executed for different optimal points.

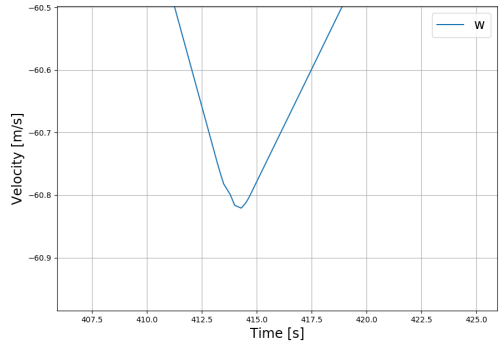

(a) Maximum value

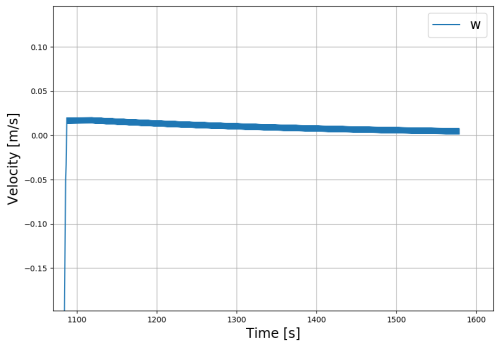

(b) Terminal phase

Figure 4.41: Zoomed area of velocity component v near maximum value(a) and for terminal phase (b) for the initial state $x = [-25000; 30000; 35000; 8; -7; -3]^T$ with LQR controller.

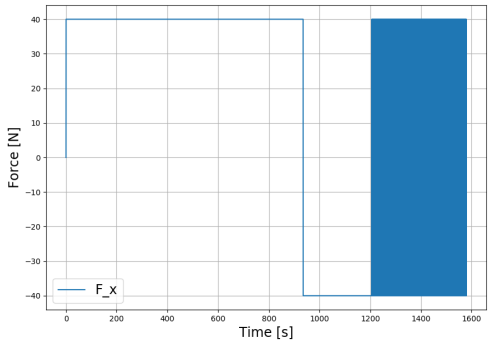

(a) LQR controller

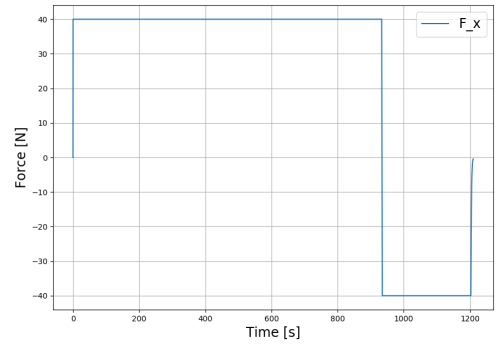

(b) H_∞ controller

Figure 4.42: Propulsive thrust component along the direction x with LQR controller (a) and H_∞ controller (b) for the initial state $x = [-25000; 30000; 35000; 8; -7; -3]^T$.

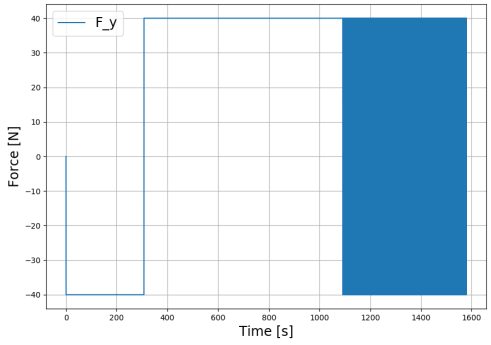

(a) LQR controller

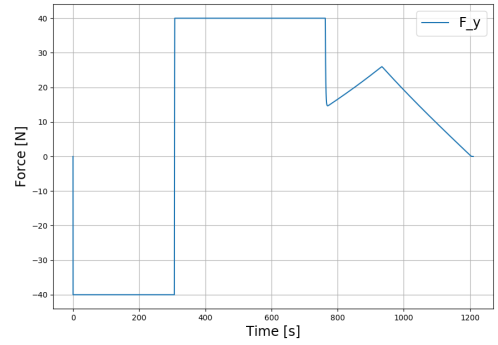

(b) H_∞ controller

Figure 4.43: Propulsive thrust component along the direction y with LQR controller (a) and H_∞ controller (b) for the initial state $x = [-25000; 30000; 35000; 8; -7; -3]^T$.

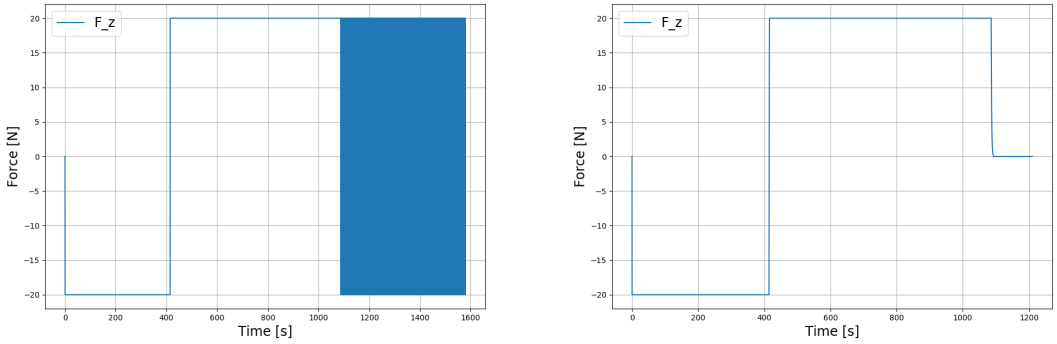

(a) LQR controller

(b) H_∞ controller

Figure 4.44: Propulsive thrust component along the direction z with LQR controller (a) and H_∞ controller (b) for the initial state $x = [-25000; 30000; 35000; 8; -7; -3]^T$.

Chapter 5

Concluding Remarks

A numerical study of the rendezvous between two different spacecraft was performed for this dissertation. The emphasis of the dissertation was to explore two different control methods, the LQR and the H_∞ controller, and compare the results obtained through each controller. Results for three different case study were obtained and thoroughly discussed. The methods and models applied throughout this dissertation were presented, explained and validated. The results obtained corroborate the methods and models employed in this dissertation to solve the rendezvous problem.

The LQR controller as well as the H_∞ controller were able to perform rendezvous for all the different examples studied in this dissertation as was to be expected with the results obtained through the LQR controller presenting good performance when the chaser spacecraft starts at a relatively close distance from the target spacecraft. As the distance between both spacecraft increases, the robust H_∞ controller, where the capacity to deal with perturbations and uncertainties becomes a key component of the rendezvous problem, exhibits better overall performance with shorter rendezvous duration and lower fuel usage. The main objective of presenting a robust controller to solve the rendezvous problem is accomplished in this dissertation with promising results.

The system where no limitations to the propulsive engines were employed provided interesting results. Both controllers were capable of generating a trajectory sending the chaser in an almost direct route in an incredibly small time frame, which was achieved due to the propulsive engines having the possibility of generating insurmountable force. It was also noted that the H_∞ controller was capable to produce more control force for the same trajectory produced by the LQR controller which is due the robust nature of the H_∞ controller of considering the worst case scenario and reacting accordingly which allows for the H_∞ controller to have better performance in the presence of perturbations and uncertainties.

A limitation to the maximum control force in module was employed in all three directions for the remaining simulations. The LQR controller presented less dampening of the system oscillations and faster rendezvous times when the initial distance between the different spacecraft was considerably close which resulted in trajectories with sharp turns and rough transactions whereas the H_∞ controller produced a more smooth trajectory to reach the target spacecraft. The increase in initial distance between the target and chaser spacecraft led to slightly different results with the LQR controller no longer being able to provide faster rendezvous and still suffering from less oscillation dampening and more susceptibility to the presence of perturbations and uncertainties when compared to the robust H_∞ controller.

The optimization process performed to both controllers provided satisfactory results with similar trajectories being obtained with the LQR controller as well as the H_∞ controller. The main difference perceived when comparing the results obtained with both controllers appears in the velocity state and the control force history of the chaser spacecraft. The results provided by the LQR controller displayed difficulties converging to zero in the terminal phase of the rendezvous with the appearance of erratic behaviour of sudden changes in attitude at each iteration whereas the results obtained through the H_∞ controller had a smooth transaction to

zero. This phenomenon is being provoked by the control force where in the LQR controller case appeared sudden changes from maximum positive force to maximum negative force at each iteration contrary to what is seen in the results provided by the H_∞ controller where the control force provided smooth convergence to zero to all velocities components. This difference could lead to the possibility of actuators saturation, increase in fuel consumption and deviation from the rendezvous trajectory in the presence of perturbations capable of amplifying the undesired oscillations, meaning that the robust H_∞ controller is the more well suited to solve the rendezvous problem.

The results obtained were quite satisfactory even though the optimization method to obtain the optimal weighting matrices is a process of trial and error, meaning that the existence of better suited results is not impossible, has this process is dependant on the designer experience. It is also worth to note that the technology improvement, namely the advancement in engine technology could provide better results by imposing a less restraining limit to the control forces. Overall, the robust H_∞ controller provided better performance when solving the rendezvous problem, being quite adequate to this dissertation thematic when compared to the LQR controller.

To further improve the work done for this dissertation many different approaches can be performed as this is a complex thematic subject to many different conditions that can be improved. The dynamic model employed to simulate the rendezvous problem can be modified to better describe rendezvous when the target spacecraft's orbit has higher eccentricities allowing the possibility of performing rendezvous with not only near circular orbits. A different optimization method to obtain optimal weighting matrices can be devised. Also, a study having in consideration other optimal condition parameters besides rendezvous time can also be performed to give better insight on the controllers performance.

Bibliography

[1] E. I. Butikov, "Orbital maneuvers and space rendezvous," in *Advances in Space Research*, vol. 56, no. 11. Elsevier, 2015, pp. 2582–2594.

[2] H. Hu and T. Straube, "Orion GN&C overview and architecture," in *AIAA Guidance, Navigation and Control Conference and Exhibit*, 2007, p. 6678.

[3] D. Zimpfer, P. Kachmar, and S. Tuohy, "Autonomous rendezvous, capture and in-space assembly: past, present and future," in *1st Space exploration conference: continuing the voyage of discovery*, 2005, p. 2523.

[4] Y. Luo, J. Zhang, and G. Tang, "Survey of orbital dynamics and control of space rendezvous," in *Chinese Journal of Aeronautics*, vol. 27, no. 1. Elsevier, 2014, pp. 1–11.

[5] C. D'Souza, C. Hannak, P. Spehar, F. Clark, and M. Jackson, "Orion rendezvous, proximity operations and docking design and analysis," in *AIAA Guidance, Navigation and Control Conference and Exhibit*, 2007, p. 6683.

[6] O. OLSZEWSKI, "Automated terminal guidance for a shuttle rendezvous to space station freedom," in *Guidance, Navigation and Control Conference*, 1990, p. 3356.

[7] Z. Ma, O. Ma, and B. N. Shashikanth, "Optimal control for spacecraft to rendezvous with a tumbling satellite in a close range," in *Intelligent Robots and Systems, 2006 IEEE/RSJ International Conference on*. IEEE, 2006, pp. 4109–4114.

[8] R. Bevilacqua, M. Romano, and O. Yakimenko, "Online generation of quasi-optimal spacecraft rendezvous trajectories," in *Acta Astronautica*, vol. 64, no. 2-3. Elsevier, 2009, pp. 345–358.

[9] A. Miele, M. Weeks, and M. Ciarcia, "Optimal trajectories for spacecraft rendezvous," in *Journal of optimization theory and applications*, vol. 132, no. 3. Springer, 2007, pp. 353–376.

[10] A. Miele, M. Ciarcià, and M. Weeks, "Guidance trajectories for spacecraft rendezvous," in *Journal of optimization theory and applications*, vol. 132, no. 3. Springer, 2007, pp. 377–400.

[11] D. Arzelier, F. Bréhard, N. Deak, M. Joldes, C. Louembet, A. Rondepierre, and R. Serra, "Linearized impulsive fixed-time fuel-optimal space rendezvous: A new numerical approach," in *IFAC-PapersOnLine*, vol. 49, no. 17. Elsevier, 2016, pp. 373–378.

[12] J.-U. Park, K.-H. Choi, and S. Lee, "Orbital rendezvous using two-step sliding mode control," in *Aerospace science and technology*, vol. 3, no. 4. Elsevier, 1999, pp. 239–245.

[13] C. Tournes, Y. Shtessel, and D. Foreman, "Automatic space rendezvous and docking using second order sliding mode control," in *Sliding Mode Control*. InTech, 2011.

[14] G. Zhang and D. Zhou, "A second-order solution to the two-point boundary value problem for rendezvous in eccentric orbits," in *Celestial Mechanics and Dynamical Astronomy*, vol. 107, no. 3. Springer, 2010, pp. 319–336.

[15] G. Zhang, D. Wang, X. Cao, and Z. Sun, "Tangent orbital rendezvous using linear relative motion with perturbations," in *Mathematical Problems in Engineering*, vol. 2013. Hindawi, 2013.

[16] M. Claeys, D. Arzelier, D. Henrion, and J.-B. Lasserre, "Measures and lmi for impulsive optimal control with applications to space rendezvous problems," in *American Control Conference (ACC), 2012*. IEEE, 2012, pp. 161–166.

[17] J. Sullivan, A. Koenig, and S. D'Amico, "Improved maneuver-free approach to angles-only navigation for space rendezvous," in *26th AAS/AIAA Space Flight Mechanics Meeting, Napa, CA*, 2016.

[18] D. Lee and H. Pernicka, "Optimal control for proximity operations and docking," in *International Journal Aeronautical and Space Sciences*, vol. 11, no. 3. Lee Daero; Pernicka Henry, 2010, pp. 206–220.

[19] P. Lu and X. Liu, "Autonomous trajectory planning for rendezvous and proximity operations by conic optimization," in *Journal of Guidance, Control, and Dynamics*, vol. 36, no. 2. American Institute of Aeronautics and Astronautics, 2013, pp. 375–389.

[20] J. Zhang and G. Parks, "Multi-objective optimization for multiphase orbital rendezvous missions," in *Journal of Guidance, Control, and Dynamics*, vol. 36, no. 2. American Institute of Aeronautics and Astronautics, 2013, pp. 622–629.

[21] E. Lancaster and R. Blanchard, *A unified form of Lambert's theorem*. National Aeronautics and Space Administration, 1969.

[22] D. Izzo, "Revisiting lambert's problem," in *Celestial Mechanics and Dynamical Astronomy*, vol. 121, no. 1. Springer, 2015, pp. 1–15.

[23] R. H. Battin, "Lambert's problem revisited," in *AIAA Journal*, vol. 15, no. 5, 1977, pp. 707–713.

[24] S. Lee and J. Cochran, "Orbital maneuvers via feedback linearization and bang-bang control," in *Journal of guidance, control, and dynamics*, vol. 20, no. 1, 1997, pp. 104–110.

[25] P. P. Khargonekar, I. R. Petersen, and M. A. Rotea, "h_∞ optimal control with state-feedback," in *IEEE Transactions on Automatic Control*, vol. 33, no. 8. IEEE, 1988, pp. 786–788.

[26] P. P. Khargonekar, I. R. Petersen, and K. Zhou, "Robust stabilization of uncertain linear systems: quadratic stabilizability and h/sup infinity/control theory," in *IEEE Transactions on Automatic Control*, vol. 35, no. 3. IEEE, 1990, pp. 356–361.

[27] Y. J. Wang, L. S. Shieh, and J. Sunkel, "Observer-based robust h_∞ control laws for uncertain linear systems," in *Journal of guidance, control, and dynamics*, vol. 15, no. 5, 1992, pp. 1125–1133.

[28] H. Gao, X. Yang, and P. Shi, "Multi-objective robust h_∞ control of spacecraft rendezvous," in *IEEE Transactions on Control Systems Technology*, vol. 17, no. 4. IEEE, 2009, pp. 794–802.

[29] N. Wan, M. Liu, and H. R. Karimi, "Observer-based robust control for spacecraft rendezvous with thrust saturation," in *Abstract and Applied Analysis*, vol. 2014. Hindawi, 2014.

[30] R. R. Bate, D. D. Mueller, and J. E. White, *Fundamentals of astrodynamics*. Courier Corporation, 1971.

[31] R. H. Battin, *An Introduction to the Mathematics and Methods of Astrodynamics, revised edition*. American Institute of Aeronautics and Astronautics, 1999.

[32] W. Clohessy, "Terminal guidance system for satellite rendezvous," in *Journal of the Aerospace Sciences*, vol. 27, no. 9, 1960, pp. 653–658.

[33] N. Wan, M. Liu, and H. R. Karimi, "Robust tracking control for rendezvous in near-circular orbits," in *Mathematical Problems in Engineering*, vol. 2013. Hindawi, 2013.

[34] H. Kwakernaak and R. Sivan, *Linear optimal control systems*. Wiley-Interscience New York, 1972, vol. 1.

[35] D. A. Caughey, "Introduction to aircraft stability and control course notes for m&ae 5070," in *Sibley School of Mechanical & Aerospace Engineering, Cornell University, Ithaca, New York*, 2011, pp. 14 853–7501.

[36] K. Zhou, J. C. Doyle, K. Glover *et al.*, *Robust and optimal control*. Prentice hall New Jersey, 1996, vol. 40.

[37] A. M. Lyapunov, "The general problem of the stability of motion," in *International journal of control*, vol. 55, no. 3. Taylor & Francis, 1992, pp. 531–534.

[38] B. M. Fontenelle, "Técnica de controle robusto h_∞ aplicada a um sistema de posicionamento dinâmico," Ph.D. dissertation, Universidade Federal do Rio de Janeiro, 2011.

[39] J. C. Butcher, *Numerical methods for ordinary differential equations*. John Wiley & Sons, 2016.

Appendix A

Comparison between the effect produced by the control weighting matrix R for the initial state $x = [-10000; -20000; -8000; 6; 6; 3]^T$

A.1 $x = [-10000; -20000; -8000; 6; 6; 3]^T$

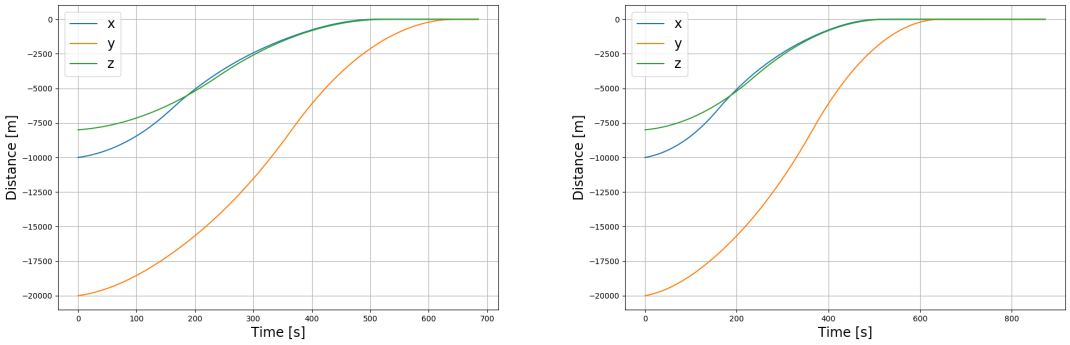

(a) LQR controller (b) H_∞ controller

Figure A.1: Relative positions components x, y and z with LQR controller (a) and H_∞ controller (b) for the initial state $x = [-10000; -20000; -8000; 6; 6; 3]^T$ with $\lambda_i = 0.3$.

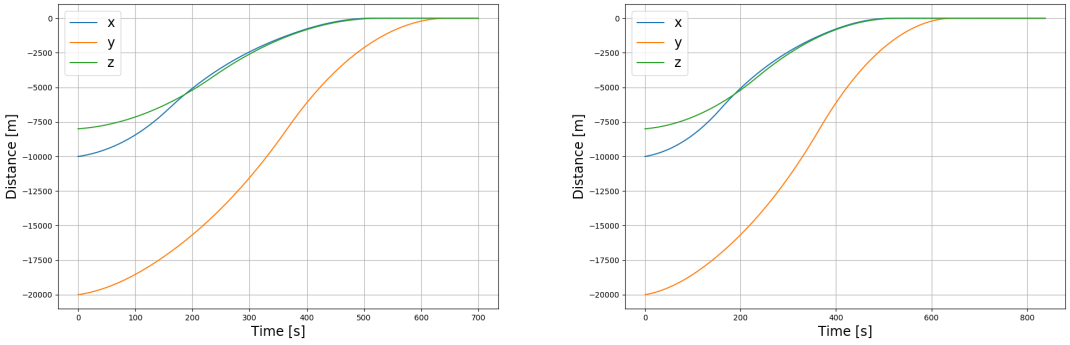

(a) LQR controller (b) H_∞ controller

Figure A.2: Relative positions components x, y and z with LQR controller (a) and H_∞ controller (b) for the initial state $x = [-10000; -20000; -8000; 6; 6; 3]^T$ with $\lambda_i = 0.4$.

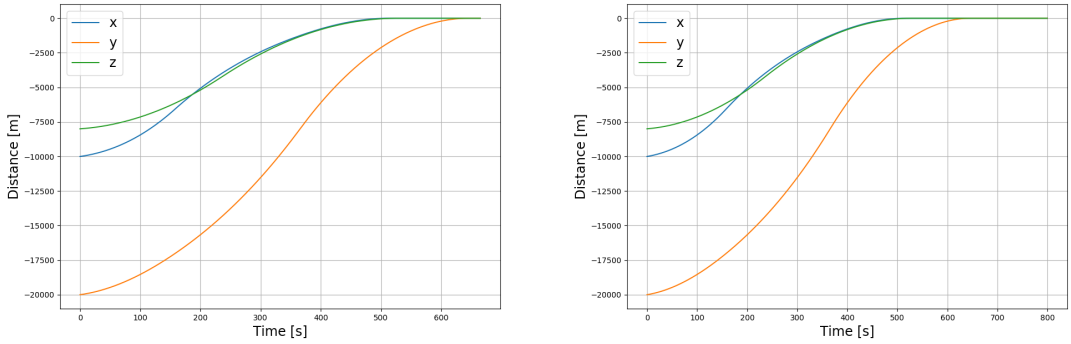

(a) LQR controller (b) H_∞ controller

Figure A.3: Relative positions components x, y and z with LQR controller (a) and H_∞ controller (b) for the initial state $x = [-10000; -20000; -8000; 6; 6; 3]^T$ with $\lambda_i = 0.6$.

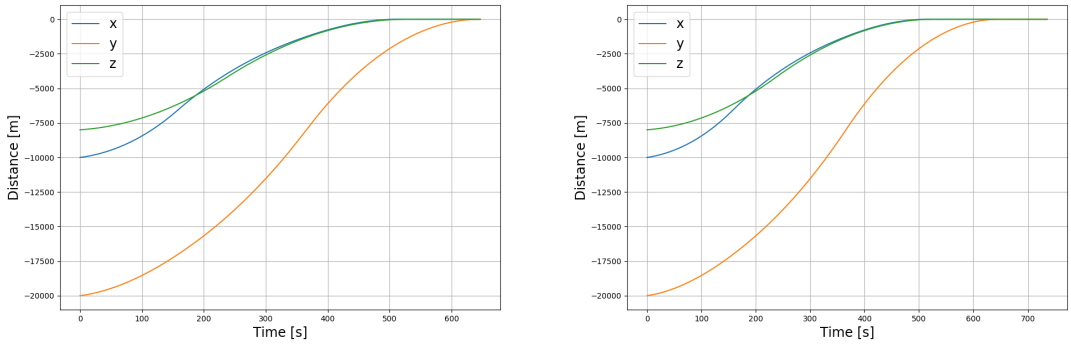

(a) LQR controller (b) H_∞ controller

Figure A.4: Relative positions components x, y and z with LQR controller (a) and H_∞ controller (b) for the initial state $x = [-10000; -20000; -8000; 6; 6; 3]^T$ with $\lambda_i = 0.8$.

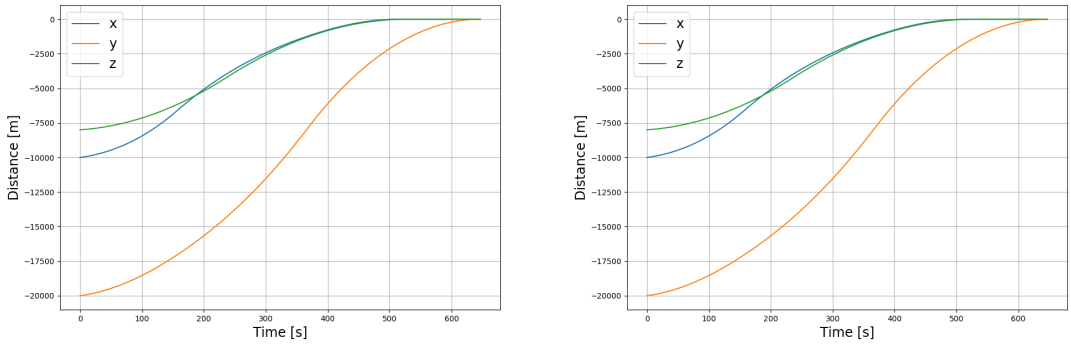

(a) LQR controller (b) H_∞ controller

Figure A.5: Relative positions components x, y and z with LQR controller (a) and H_∞ controller (b) for the initial state $x = [-10000; -20000; -8000; 6; 6; 3]^T$ with $\lambda_i = 1$.

Appendix B

Comparison between the the LQR controller and the H_∞ controller for the initial state $x = [5000; -6000; 7000; -3; 4; -1]^T$

B.1 $x = [5000; -6000; 7000; -3; 4; -1]^T$

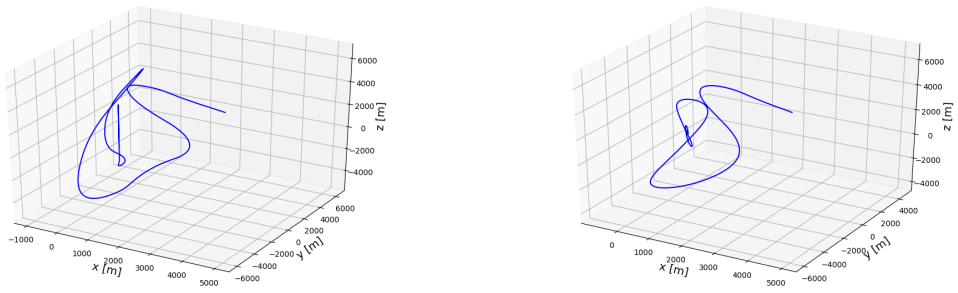

(a) LQR controller (b) H_∞ controller

Figure B.1: Rendezvous trajectory performed by the chaser spacecraft to reach the target spacecraft with LQR controller (a) and H_∞ controller (b) for the initial state $x = [5000; -6000; 7000; -3; 4; -1]^T$.

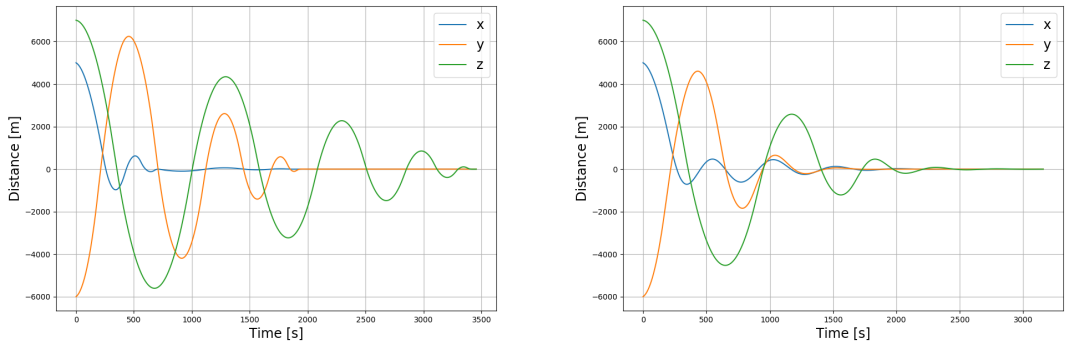

(a) LQR controller (b) H_∞ controller

Figure B.2: Relative positions components x, y and z with LQR controller (a) and H_∞ controller (b) for the initial state $x = [5000; -6000; 7000; -3; 4; -1]^T$.

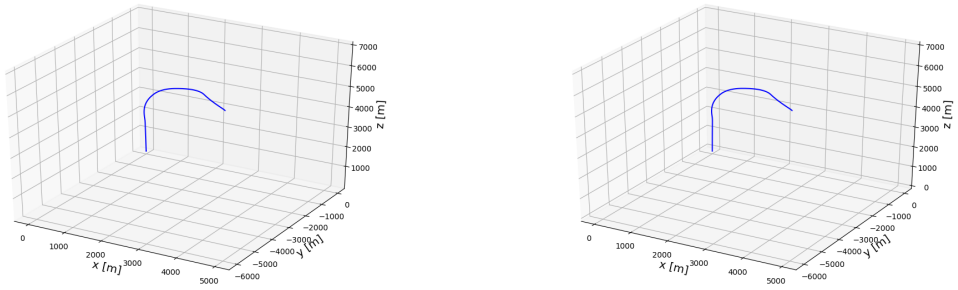

(a) LQR controller (b) H_∞ controller

Figure B.3: Rendezvous trajectory performed by the chaser spacecraft to reach the target spacecraft with LQR controller (a) and H_∞ controller (b) for the initial state $x = [5000; -6000; 7000; -3; 4; -1]^T$.

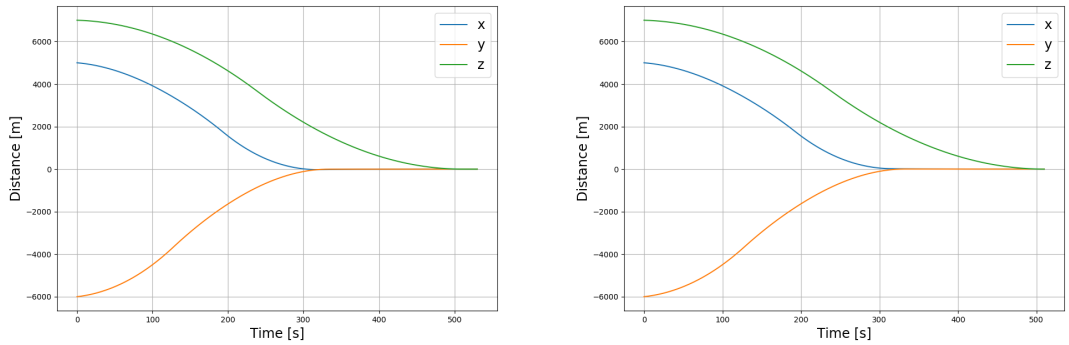

(a) LQR controller (b) H_∞ controller

Figure B.4: Relative positions components x, y and z with LQR controller (a) and H_∞ controller (b) for the initial state $x = [5000; -6000; 7000; -3; 4; -1]^T$.

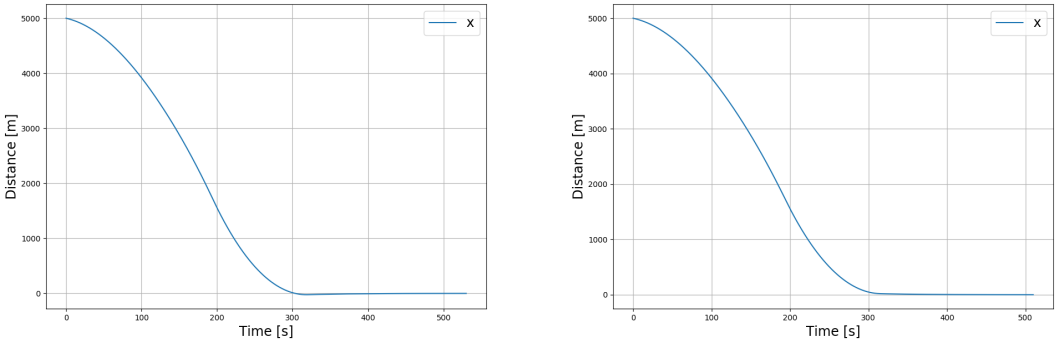

(a) LQR controller (b) H_∞ controller

Figure B.5: Relative position component x with LQR controller (a) and H_∞ controller (b) for the initial state $x = [5000; -6000; 7000; -3; 4; -1]^T$.

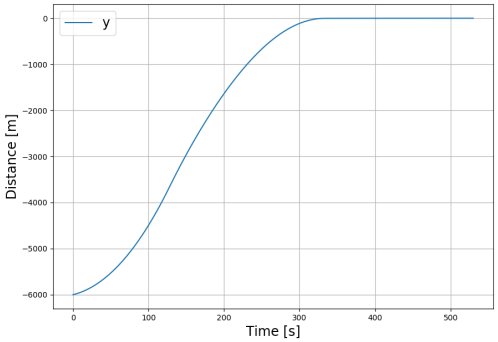

(a) LQR controller

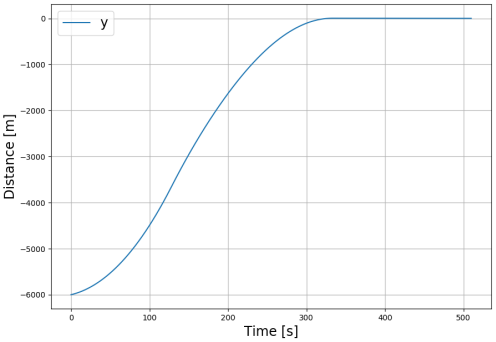

(b) H_∞ controller

Figure B.6: Relative position component y with LQR controller (a) and H_∞ controller (b) for the initial state $x = [5000; -6000; 7000; -3; 4; -1]^T$.

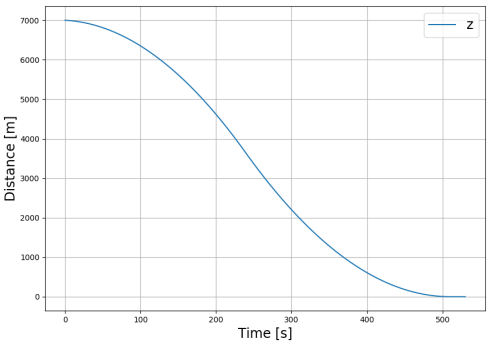

(a) LQR controller

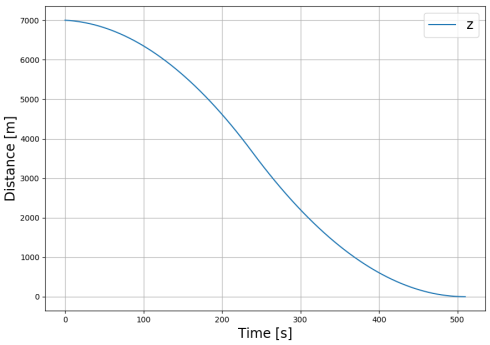

(b) H_∞ controller

Figure B.7: Relative position component z with LQR controller (a) and H_∞ controller (b) for the initial state $x = [5000; -6000; 7000; -3; 4; -1]^T$.

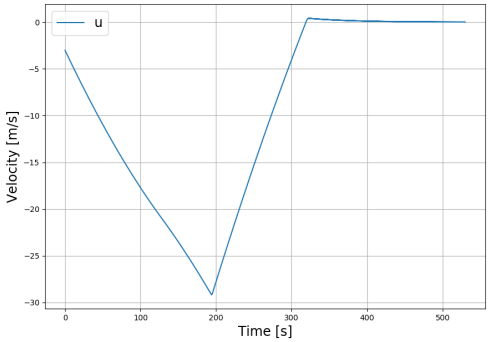

(a) LQR controller

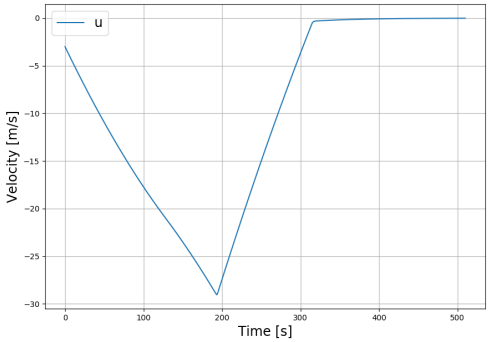

(b) H_∞ controller

Figure B.8: Relative velocity component u with LQR controller (a) and H_∞ controller (b) for the initial state $x = [5000; -6000; 7000; -3; 4; -1]^T$.

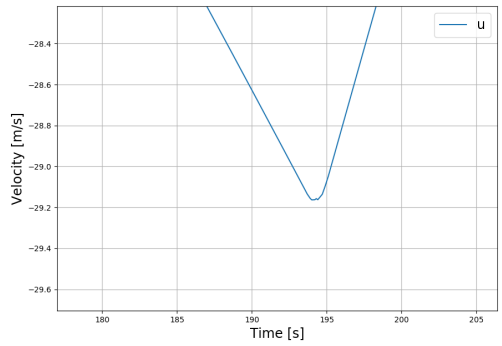

(a) Maximum value

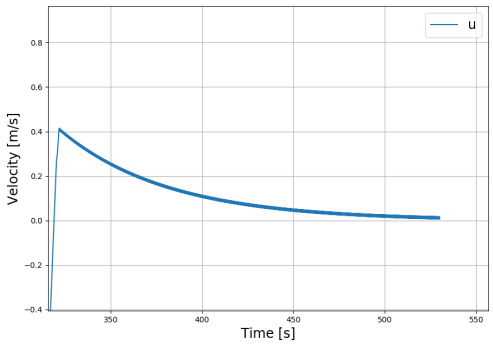

(b) Terminal phase

Figure B.9: Zoomed area of velocity component v near maximum value(a) and for terminal phase (b) for the initial state $x = [5000; -6000; 7000; -3; 4; -1]^T$ with LQR controller.

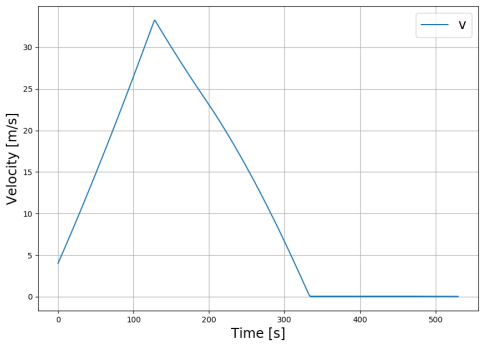

(a) LQR controller

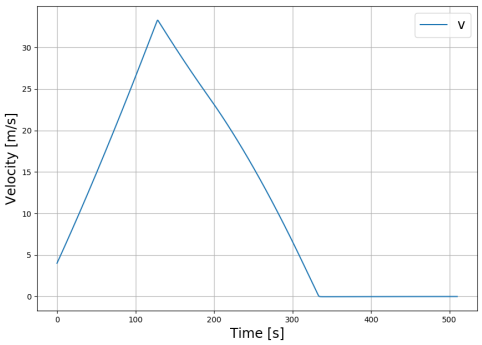

(b) H_∞ controller

Figure B.10: Relative velocity component v with LQR controller (a) and H_∞ controller (b) for the initial state $x = [5000; -6000; 7000; -3; 4; -1]^T$.

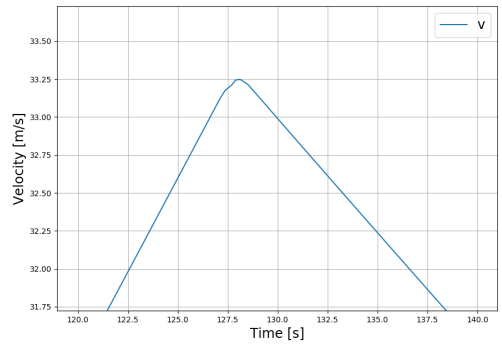

(a) Maximum value

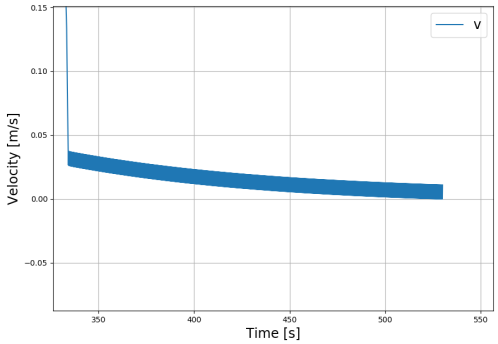

(b) Terminal phase

Figure B.11: Zoomed area of velocity component v near maximum value(a) and for terminal phase (b) for the initial state $x = [5000; -6000; 7000; -3; 4; -1]^T$ with LQR controller.

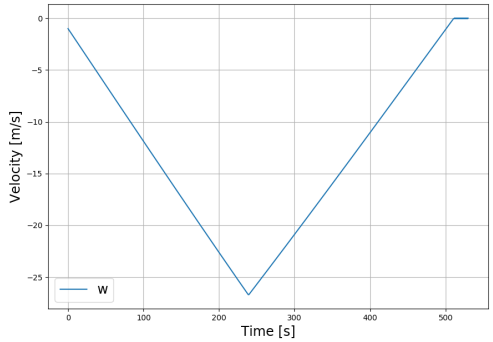

(a) LQR controller

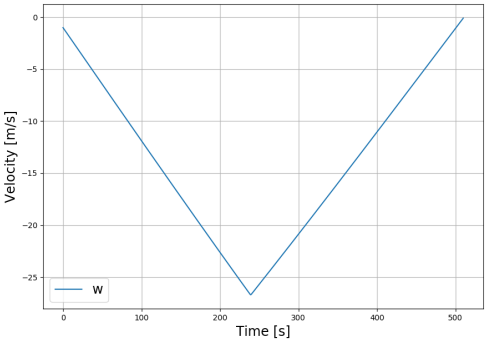

(b) H_∞ controller

Figure B.12: Relative velocity component w with LQR controller (a) and H_∞ controller (b) for the initial state $x = [5000; -6000; 7000; -3; 4; -1]^T$.

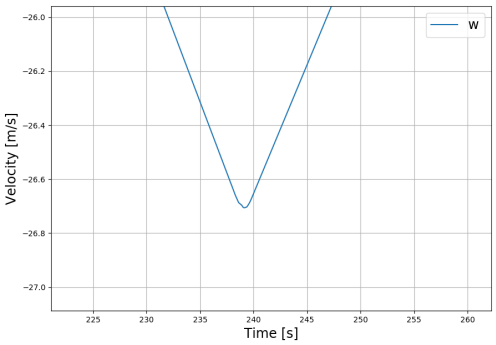

(a) Maximum value

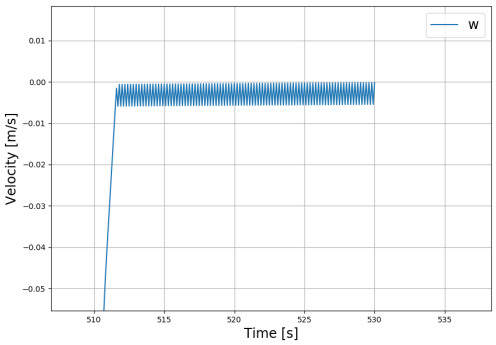

(b) Terminal phase

Figure B.13: Zoomed area of velocity component v near maximum value(a) and for terminal phase (b) for the initial state $x = [5000; -6000; 7000; -3; 4; -1]^T$ with LQR controller.

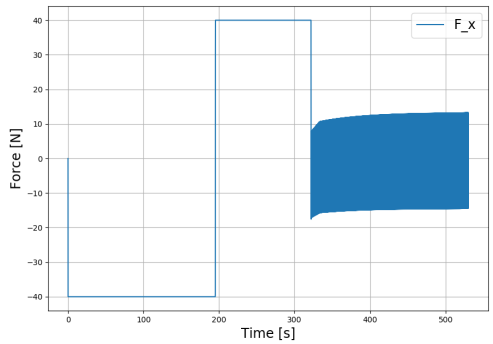

(a) LQR controller

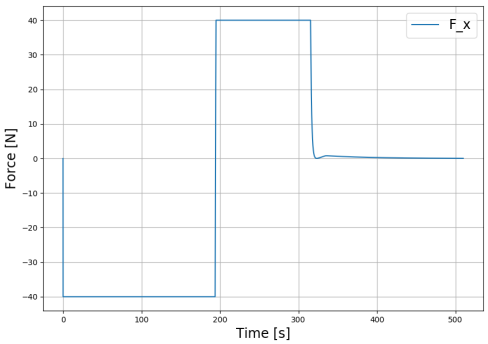

(b) H_∞ controller

Figure B.14: Propulsive thrust component along the direction x with LQR controller (a) and H_∞ controller (b) for the initial state $x = [5000; -6000; 7000; -3; 4; -1]^T$.

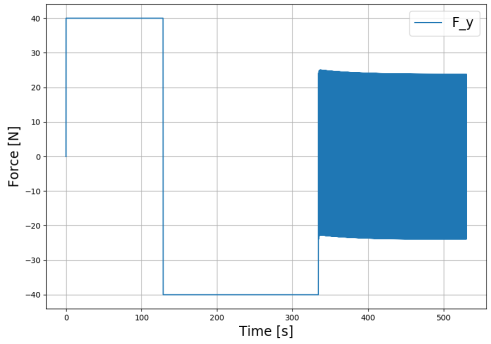

(a) LQR controller

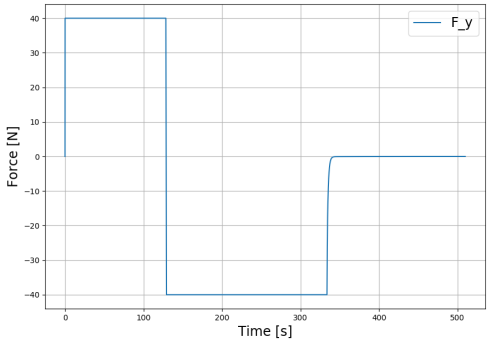

(b) H_∞ controller

Figure B.15: Propulsive thrust component along the direction y with LQR controller (a) and H_∞ controller (b) for the initial state $x = [5000; -6000; 7000; -3; 4; -1]^T$.

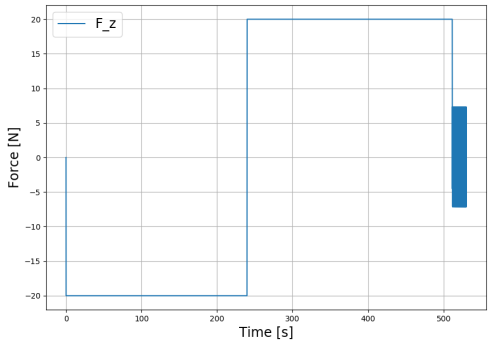

(a) LQR controller

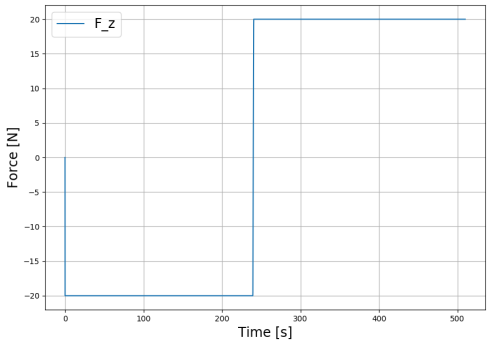

(b) H_∞ controller

Figure B.16: Propulsive thrust component along the direction z with LQR controller (a) and H_∞ controller (b) for the initial state $x = [5000; -6000; 7000; -3; 4; -1]^T$.

Appendix C

P. Barros, K. Bousson

Abstract – *The efficient and safe execution of a rendezvous maneuver is a critical section of many space exploration mission. This paper describes the formulation and numerical investigation of a robust optimal control method for thrust-limited rendezvous in near-circular orbital rendezvous. A dynamic linear model, derived from the two-body problem, treating the non-circularity of the target as parameters uncertainties is implemented as the control plant to accurately describe the physical motion of the spacecraft performing rendezvous. An optimal robust H_∞ controller is developed based on this model.*

Keywords: *Orbital Rendezvous; H_∞ robust controller, Near-circular orbit;*

Nomenclature

ARE	Algebraic Riccati Equations
C-W	Clohessy-Wiltshire equations
LEO	Low Earth Orbit
LVLH	Local Vertical, Local Horizontal
RODC	Rendezvous Orbital Dynamics and Control
RVD	Rendezvous and Docking Technology
A	State Matrix
B	Control Matrix
C	Output Matrix
F	Control force input
J	Performance Index
K	Gain Matrix
M	Mean anomaly
P	Algebraic Riccati equation solution
Q	State weighting matrix
R	Control weighting matrix
a	Acceleration
e	Eccentricity
m	Mass
n	Mean motion
u	Control vector
x(t)	State vector
y(t)	Measured Variables
x	Position along x-axis
y	Position along y-axis
z	Position along z-axis
$\dot{x}$	Velocity along x-axis
$\dot{y}$	Velocity along y-axis
$\dot{z}$	Velocity along z-axis
$\ddot{x}$	Acceleration along x-axis
$\ddot{y}$	Acceleration along y-axis
$\ddot{z}$	Acceleration along z-axis
γ	Disturbance attenuation

I. Introduction

Space exploration has been a dream of humanity for the past century with men trying to soar through the skies and conquer space.

Starting with the Gemini and Apollo programs, which developed the initial concepts for rendezvous and docking technology (RVD) until the most recent programs of the H-II transfer vehicle from Japan and the Shenzou spaceship from China we can clearly see that all these programs relied heavily on Rendezvous Orbital Dynamics and Control (RODC) as a key technology of RVD, with more than half a century of study and research, and yet, it is still a long way to go until it becomes a completely autonomous and independent procedure.

Many procedures such as crew exchange, spacecraft intercepting, repairing and maintenance, saving, docking, large structure assembling and satellite networking are examples of several procedures that are heavily dependent on RODC as a primary factor which determines the success of the mission. Douglas Zimpfer [1], Luo Yazhong [2] and Christopher D'Souza [3] provided technical and historical perspectives on autonomous rendezvous and capture missions, exposing the technology future requirements.

Even though a circular orbit could provide many benefits to the rendezvous mission, the reality is that it is near impossible to achieve and maintain it throughout the course of the mission, which led to most of the rendezvous missions being performed in near circular orbits.

One of the most important aspects in devising a rendezvous mission is the adoption of a proper and accurate plant model before designing a rendezvous controller.

Clohessy and Wiltshire developed [4] the most widely used plant model for the study of orbital rendezvous that is known as the C-W equations. This linear model is very concise, however, these equations are only adequate for rendezvous in circular orbits.

For this paper, a linearized model for rendezvous in near circular orbits, based on the C-W equations, is employed as the control plant.

II. Dynamic Model and Problem Formulation

The current section is dedicated to present a dynamic model for rendezvous in near-circular orbits.

Assuming that two spacecraft are dozens of kilometres away from the planet Earth are relatively close to each other, allowing the relative motion to be described in a target-centred orbital coordinate system. Both spacecraft are only influenced by a central gravitational force and the vehicle that approaches the other by orbital manoeuvring is known as the chaser spacecraft and the latter is denoted as the target spacecraft and does not perform any type of manoeuvre. The propulsive thrusts of the active chaser spacecraft are independent and continous along each axis.

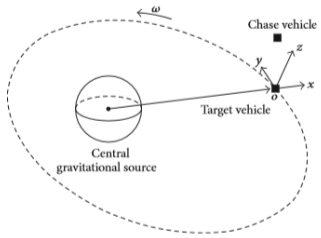

Fig. 1. Relative cartesian coordinate system for spacecraft rendezvous (LVLH type).

The coordinate system employed is of the Local Vertical, Local Horizontal type (LVLH) located in the target's center of mass, with the x-axis, also known as the R-bar, being directed radially outward along the local vertical, the y-axis, also called V-bar, along the direction of motion or velocity direction and the z-axis normal to the reference orbit plane and completes the right handed system as can be seen in Figure 1.

Clohessy and Whiltshre developed a set of linear dynamic equations, based on Kepler's and the Gravitational law, to effectively describe the relative motion between two different spacecraft as presented next [4]:

$$\begin{cases} \ddot{x} - 2n\dot{y} - 3n^2x = a_x \\ \ddot{y} + 2n\dot{x} = a_y \\ \ddot{z} + n^2z = a_z \end{cases} \quad (1)$$

where x, y and z represent the relative position components, the $\dot{x}$, $\dot{y}$ and $\dot{z}$ compose the relative velocity components and the $\ddot{x}$, $\ddot{y}$ and $\ddot{z}$ are the components of the relative acceleration; n is the mean motion of the target spacecraft and $a_i (i$ = x, y, z) being the i^{th} component of the thrust acceleration.

The thrusts components can be described relating to the chaser spacecraft mass and control force as follows:

$$\begin{cases} a_x = \dfrac{1}{m}F_x \\ a_y = \dfrac{1}{m}F_y \\ a_z = \dfrac{1}{m}F_z \end{cases} \quad (2)$$

where m is the mass of the chaser spacecraft and $F_i\ (i = x, y, z)$ is the i^{th} component of the control input force acting on the relative motion dynamics.

The addition of uncertain parameters in the C-W equations accomplishes a more accurate description of the dynamics present in the rendezvous problem. The resultant equation go as follows:

$$\begin{cases} \ddot{x} - 2n\dot{y} - 3n^2x + [-10en^2\cos(M)\,x + 2en^2\sin(M)\,y - 4encos(M)\dot{y}] = a_x \\ \ddot{y} + 2n\dot{x} + [-2en^2\sin(M)\,x - en^2\cos(M)\,y + 4encos(M)\dot{x}] = a_y \\ \ddot{z} + n^2z + [3en^2\cos(M)\,z] = a_z \end{cases} \quad (3)$$

where e is the eccentricity of the target orbit and $M = n(t - t_p)$ is the mean anomaly with t_p being the time of periapsis passage. In these equations the dot superscript denotes derivative with relation to the actual time, t, which ranges in the interval $0 \leq t \leq t_f$, t_f being the time when rendezvous is achieved.

By forming the state vector as $x(t) = [x, y, z, \dot{x}, \dot{y}, \dot{z}]^T$ containing the position and velocity states of the chaser spacecraft, the input vector as $u(t) = [F_x(t), F_x(t), F_x(t)]^T$ and rewriting the system of equation 3 into a matrix form, the relative motion model for rendezvous in near circular orbit yields the following:

$$\dot{x} = \big(A + \Delta A(t)\big)x(t) + Bu(t) \quad (4)$$

where,

$$A = \begin{bmatrix} 0 & 0 & 0 & 1 & 0 & 0 \\ 0 & 0 & 0 & 0 & 1 & 0 \\ 0 & 0 & 0 & 0 & 0 & 1 \\ 3n^2 & 0 & 0 & 0 & 2n & 0 \\ 0 & 0 & 0 & -2n & 0 & 0 \\ 0 & 0 & -n^2 & 0 & 0 & 0 \end{bmatrix} \quad (5)$$

$$B = \frac{1}{m}\begin{bmatrix} 0 & 0 & 0 \\ 0 & 0 & 0 \\ 0 & 0 & 0 \\ 1 & 0 & 0 \\ 0 & 1 & 0 \\ 0 & 0 & 1 \end{bmatrix} \quad (6)$$

$$\Delta A(t) = \begin{bmatrix} 0 & 0 & 0 & 0 & 0 & 0 \\ 0 & 0 & 0 & 0 & 0 & 0 \\ 0 & 0 & 0 & 0 & 0 & 0 \\ 10en^2\cos(M) & -2n^2\sin(M) & 0 & 0 & -4encos(M) & 0 \\ 2en^2\sin(M) & en^2\cos(M) & 0 & -4encos(M) & 0 & 0 \\ 0 & 0 & -3en^2\cos(M) & 0 & 0 & 0 \end{bmatrix} \quad (7)$$

The uncertain matrix ΔA [5] is bounded by the presence of the mean motion and the *cos(M)* as $n \in [n_{min}\,;\, n_{max}]$ and *cos(M)* $\in [-1;\ 1]$, so $\|\Delta A\| \leq \alpha$ where α is positive and can be determined by the mean anomaly, *M*. By adding the norm-bounded matrix ΔA, which determines the shape of the target orbit, it is possible to more accurately represent the rendezvous problem, seeing as it contains the target orbit's eccentricity. Normal plant models for elliptical orbits are, usually, nonlinear in contrast to the plant model presented in the current paper which is a linearized model, making it more designer friendly and easier to implement. Most of the rendezvous mission, the current case study included, are accomplished in near circular orbits, implying that this control plant is practical and precise enough to represent the regular spacecraft rendezvous of the present paper.

It is necessary to also chose a control input vector *u(t)* that can minimize a quadratic performance index *J* defined by:

$$J = \int_0^\infty [x^T(t)Qx(t) + u^T(t)Ru(t)]\,dt \quad (8)$$

where the state weighting matrix Q $\in \mathbb{R}^{nxn}$ is a positive symmetric matrix related to the convergence rate of the relative motion states and the smoothness of the rendezvous trajectory, and the control weighting matrix R $\in \mathbb{R}^{mxm}$ is a positive symmetric matrix related to the fuel cost of the chaser spacecraft. The minimum quadratic cost means an optimal compromise among the weighting matrix Q and the weighting matrix R.

The weight of both these matrices should not be chosen arbitrarily as they have great effect on the performance of the controller. That being said, the weighting matrices final values should be carefully evaluated through simulation and iteration. One method to obtain fairly good results is the modifies version of Bryson's method that relates the weighting matrices diagonal with the maximum acceptable value for each state as can be seen bellow:

$$Q = \begin{bmatrix} \frac{\eta_1}{u_{1,max}^2} & 0 & \dots & 0 \\ 0 & \frac{\eta_2}{u_{2,max}^2} & \dots & 0 \\ \vdots & \vdots & \ddots & \vdots \\ 0 & 0 & \dots & \frac{\eta_n}{u_{n,max}^2} \end{bmatrix} \quad (9)$$

$$R = \begin{bmatrix} \frac{\lambda_1}{u_{1,max}^2} & 0 & \dots & 0 \\ 0 & \frac{\lambda_2}{u_{2,max}^2} & \dots & 0 \\ \vdots & \vdots & \ddots & \vdots \\ 0 & 0 & \dots & \frac{\lambda_n}{u_{n,max}^2} \end{bmatrix} \quad (10)$$

with $\forall_i\, \eta_i \geq 1$ and $\forall_i\, 0 \leq \lambda_i \leq 1$. Adjusting these matrices improves the overall performance of the control plant.

Matrices $U_i = (i = x, y, z)$ are introduced for the purpose of limiting the control forces and are defined as

$$|f_i| = U_i u(t) \leq u_{i,max} \ \ (i = x, y, z) \quad (11)$$

where $u_{i,max}$ is the maximum control force on the i^{th} direction.

III. H_∞ Robust Control

In the present section a H_∞ controller with input saturation for autonomous rendezvous in near-circular orbits is presented.

The H_∞ norm, is essentially, a measure of the worst possible performance for many classes of input signals, which means that its minimization implies the attenuation of the relation between inputs and outputs of the system. In other words, it is the attenuation of the disturbances in the controlled outputs, making the main focus of an H_∞ robust control to find the gain matrix *K* that minimizes the closed-loop transfer function $||T||_\infty$.

Consider the following linear dynamic system:

$$\begin{aligned} \dot{x}(t) &= Ax(t) + Bu(t) + Dw(t) \\ y(t) &= Cx(t) \\ x(t_0) &= x_0 \end{aligned} \quad (12)$$

where x_0 is given but arbitrary, $w \in \mathbb{R}^p$ and *D* is a matrix of appropriate size. The matrix *A* is a time varying matrix which contains uncertain parameters and the measured state is assumed to be available for feedback which means that the measured output is the state *x(t)*. The main objective being to find a control function, *u(t)*, defined on the interval $[t_0,\ T]$, *T* defining the time of rendezvous, which can be a function of the state *x(t)* such that the state

x(t) is driven close enough to the target at a predefined time *T*.

A static state feedback disturbance attenuation is employed in order for the norm, γ, to minimize the disturbances affecting the plant state. This disturbance attenuation is easier to design and implement whilst having lower times of computation. The H_∞ controller has a control vector that can be described as a linear function of the state vector as follows:

$$u = -Kx \tag{13}$$

with $K \in \mathbb{R}^{m.n}$

The main objective of the controller lies in finding the matrix *K* that minimizes the performance index *J* with the controller defined in equation.

Let,

$$\gamma := \inf\{\left|\left|\mathrm{T}\right|\right|_\infty : K \in S\} \tag{14}$$

where

$$S = \{K \in \mathbb{R}^{m.m} : A - BK \; is \; a \; stability \; matrix\} \tag{15}$$

The disturbance attenuation described previously with the plant states available for feedback, allows the norm of the closed-loop transfer function to be reduced as desired to the H_∞ optimum control using state feedback.

Let *P* be a positive definite solution of the Algebraic Ricatti Equation (ARE) [6].

$$PA + A^T P - \frac{1}{\varepsilon} PBR^{-1}B^T P + \frac{1}{\gamma} PDD^T + \frac{1}{\gamma} C^T C + \varepsilon Q = 0 \tag{16}$$

with disturbance attenuation, γ, constant for some $\varepsilon > 0$, where:

$$K = \frac{R^{-1}B^T P}{2\varepsilon} \tag{17}$$

The matrix *P* is the solution to the ARE, which is a control systems synthesis well suited to system analysis and plays a central role in H_∞ optimal control.

Then, through equations 13 and 17 we obtain the control function as:

$$u = -\frac{R^{-1}B^T Px}{2\varepsilon} \tag{18}$$

IV. Simulation Results

This section displays an example to elucidate on the capabilities and advantages of a robust H_∞ control for rendezvous in near-circular orbits.

The example used for the purpose of demonstration is assumed to be moving on a Low Earth Orbit (LEO) with eccentricity $e = 0.01$, gravitational constant parameter $\mu = 3.99 \cdot 10^{14}\, m^3 s^{-2}$ and mean motion $n = 1.130 \cdot 10^{-3}\, rad \cdot s^{-1}$. The chaser spacecraft mass $m = 200\, Kg$ and the maximum control thrusts are set as 40 N, 40 N and 20 N along the axis x, y and z respectively.

The initial state for this example is $x(0) = [-10000;\ -20000;\ -8000; 6; 6; 3\ ]^T$ and the following weighting matrices Q and R are obtained through trial and error, employing the modified version of Bryson's method.

$$Q = \begin{bmatrix} \frac{94500000}{(-10000)^2} & 0 & 0 & 0 & 0 & 0 \\ 0 & \frac{388000000}{(-20000)^2} & 0 & 0 & 0 & 0 \\ 0 & 0 & \frac{7130000}{(-8000)^2} & 0 & 0 & 0 \\ 0 & 0 & 0 & \frac{54670000}{(6)^2} & 0 & 0 \\ 0 & 0 & 0 & 0 & \frac{581800}{(6)^2} & 0 \\ 0 & 0 & 0 & 0 & 0 & \frac{231000}{(3)^2} \end{bmatrix} \tag{19}$$

$$R = \begin{bmatrix} \frac{1}{40^2} & 0 & 0 \\ 0 & \frac{1}{40^2} & 0 \\ 0 & 0 & \frac{1}{20^2} \end{bmatrix} \quad (20)$$

For this example, the velocities states are not capable of direct measurement, so the output matrix is set as:

$$C = \begin{bmatrix} 1 & 0 & 0 & 0 & 0 & 0 \\ 0 & 1 & 0 & 0 & 0 & 0 \\ 0 & 0 & 1 & 0 & 0 & 0 \end{bmatrix} \quad (21)$$

All the results presented below are obtained from a simulation system built based on the two-body problem.

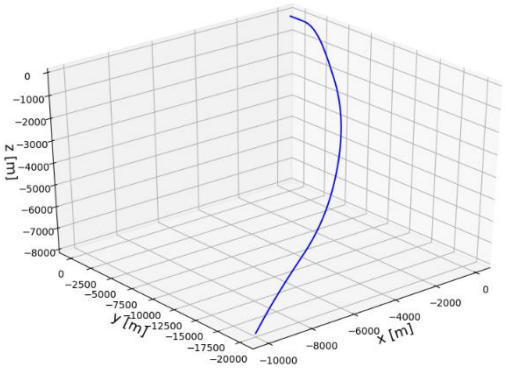

Fig. 2. Rendezvous trajectory performed by the chaser spacecraft.

From Figure 2 it is possible to see that through the H_∞ robust controller the chaser spacecraft performs rendezvous resorting to a smooth trajectory until it reaches the target.

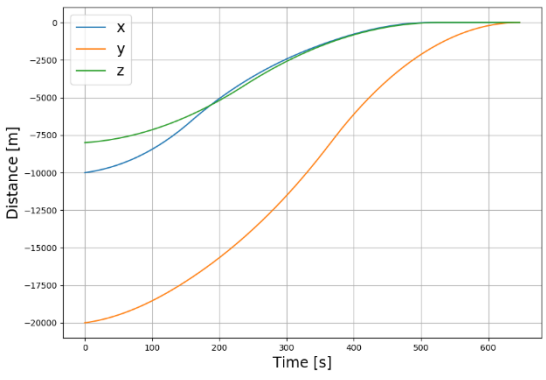

Fig. 3. Relative positions components x, y and z along each axis.

Through Figure 3, it can be perceived that all position components converge asymptotically to zero in a considerably low time frame.

Figures 4, 5 and 6 display the relative velocity history throughout the entire mission. It is possible to see that all

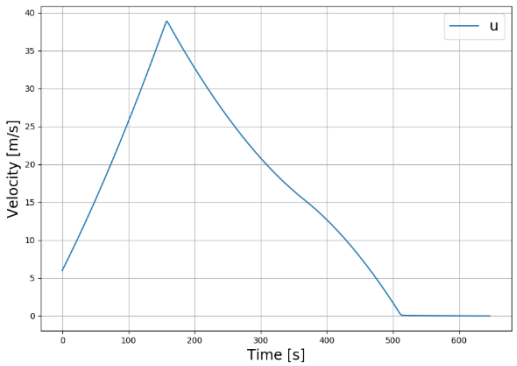

components go through a period of acceleration for the chaser spacecraft to reach the target spacecraft, followed by a period of deceleration in order to the relative velocity of the chaser spacecraft to become zero meaning that the chaser spacecraft will remain in the same relative position in relation with the target spacecraft.

Fig. 4. Relative velocity component u along x-axis.

Fig. 5. Relative velocity component v along y-axis.

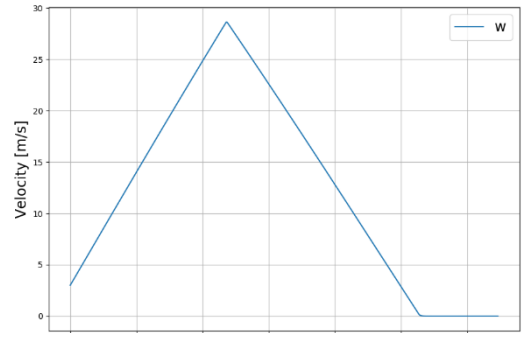

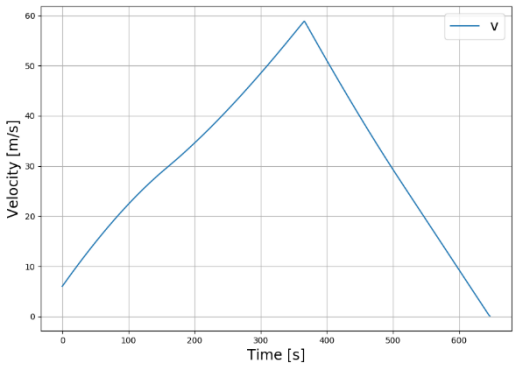

Fig. 6. Relative velocity component w along z-axis.

The Figures 7, 8 and 9 present the control force input along the three direction x-axis, y-axis and z-axis, respectively. The results presented go in accordance with Figures 4, 5 and 6 with the acceleration portrayed in the earlier stage being related to the positive control force and the following deceleration being related to the negative control force. The thrusts along each axis respect the boundary given previously.

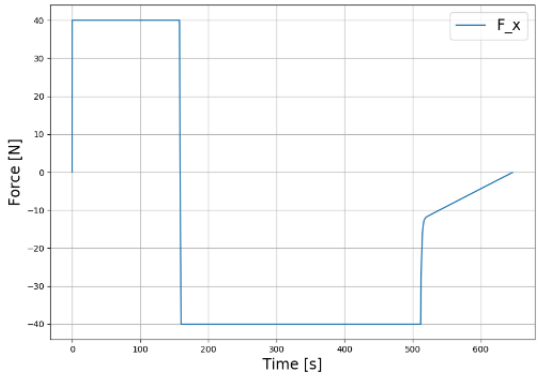

Fig. 7. Propulsive thrust component along the x-axis.

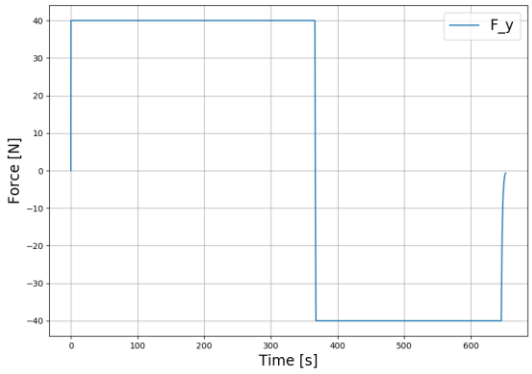

Fig. 8. Propulsive thrust component along the y-axis.

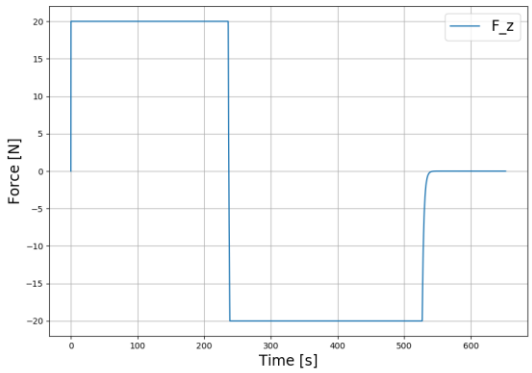

Fig. 9. Propulsive thrust component along the z-axis.

V. Conclusion

A numerical study of the rendezvous between two spacecraft is performed for this study. The emphasis of this paper is to explore the benefits of a robust H_∞ controller to control and guide a chaser spacecraft performing orbital rendezvous with a target spacecraft. The models and methods applied in this paper are presented, explained and validated. The example provided corroborates the methods and models employed to solve the rendezvous problem.

The H_∞ controller is able to perform rendezvous for the example presented, as was to be expected, with the results obtained presenting good performance dealing well with the presence of uncertain parameters in the plant adopted. The results present overall good performance with a short time frame duration, meaning that the main objective of the current study is achieved.

The optimization process performed to the robust H_∞ controller provided satisfactory results with a smooth trajectory being obtained for the rendezvous mission. All state components converge asymptotically and smoothly to zero.

The illustrative example verifies the effectiveness and advantages of the control method proposed to solve the rendezvous in near-circular orbits problem.

References

[1] D.Zimpfer, P.Kachmar, and S. Tuohy "Autonomous rendezvous, capture and in-space assembly: past, present and future" 1st Space Exploration conference: continuing the voyage discovery, 2005, p. 2523.

[2] Y. Luo, J. Zhang, and G. Tang, "Survey of orbital dynamics and control of space rendezvous", Chinese Journal of Aeronautics, vol. 27, no. 1, 2014, pp. 1-11.

[3] C. D'Souza, C. Hannak, P. Spehar, F. Clark, and M. Jackson, "Orion Rendezvous, proximity operations and docking design and analysis", AIAA Guidance, Navigation and Control Conference and Exhibit, 2007, p.6683.

[4] W. Clohessy, "Terminal guidance system for satellite rendezvous", Journal of the Aerospace Sciences, vol. 27, no. 9, 1960, pp. 653-658.

[5] N. Wan, M. Liu, and H. R. Karimi, "Observer-based robust control for spacecraft rendezvous with thrust saturation", Abstract and Applied Analysis, vol. 2014. Hindawi, 2014.

[6] P. P. Khargonekar, I. R. Petersen, and K. Zhou, "HH_∞ control laws for uncertain linear systems", Journal of guidance, control and dynamics, vol. 15, no. 5, 1992, pp. 1125-1133.

Authors' information

Department of Aerospace Science
University of Beira Interior 6201-001 Covilhã, Portugal